Spring 2020

The Manufacturing and Characterization of Pseudo-Woven Carbon Fiber Composite Architectures for Enhanced Damage Tolerance

Cyrus Vakili Rad

THE MANUFACTURING AND CHARACTERIZATION OF PSEUDO-WOVEN CARBON FIBER COMPOSITE ARCHITECTURES FOR ENHANCED DAMAGE TOLERANCE

by

Cyrus Vakili Rad

Bachelor of Science
University of South Carolina, 2016

Submitted in Partial Fulfillment of the Requirements

For the Degree of Master of Science in

Mechanical Engineering

College of Engineering and Computing

University of South Carolina

2020

Accepted by:

Subramani Sockalingam, Director of Thesis

Zafer Gurdal, Reader

Cheryl L. Addy, Vice Provost and Dean of the Graduate School

ACKNOWLEDGEMENTS

I would like to thank the University of South Carolina's Department of Mechanical Engineering and the McNair Center for the opportunity to work and learn about my passions. I would also like to thank my advisor, Dr. Subramani Sockalingam for his support, knowledge, and patience throughout the pursuit of my degree. I would also like to thank SC Space Grant Consortium, Office of Research, The Boeing Company, and The Department of Mechanical Engineering University of South Carolina who helped to provide financial support throughout. I would like to take the opportunity thank NASA Langley Research Center and NASA Glenn Research Center for assisting with the manufacturing and testing of the high velocity impact testing in this study. Lastly, I would like to thank my research colleagues Julie Roark, Robert Bass, Emily Kaufmann, and Joseph Lafond-Favières for helping with everything along the way and my friends and family for being far too supportive of me, I couldn't have done it without you.

.

ABSTRACT

Traditional unidirectional carbon fiber reinforced polymer matrix composites exhibit brittle failure, limited toughness, and poor damage tolerance often resulting in the overdesign of composite systems. This work focuses on the automated fiber placement (AFP) manufacturing and characterization of a new family of pseudo-woven (PW) laminate architectures aimed to enhance impact resistance and damage tolerance. The PW laminate architecture uses a specialized *in situ* AFP process implementing tow skips to produce its laminate architecture. This results in a heterogeneous architecture possessing spatially variable in-plane material properties unlike traditional laminated composites. This heterogeneity is associated with topological variations in the fiber orientations resulting in numerous interfaces and an expanded design space. The composite laminates are produced using carbon fiber-reinforced epoxy slit tapes in a gantry-based AFP machine. The PW laminate architectures manufactured in this work are experimentally characterized for warpage, uniaxial tension, low velocity impact, and high velocity impact response.

Experimental results indicate that a 4 ply PW laminate architecture can realize warpage reductions of up to 58% compared with traditional asymmetrical laminates. This is attributed to the spatial variations in the stacking sequence resulting in variations in the **B** matrix components of the ABD matrix. Uniaxial tension experiments indicate that 4-ply PW laminate architectures exhibit similar strength compared to traditional composites consisting of the same fiber angles. However, they exhibit an increased strain to failure and a more complex progressive failure including multiple mesoscale cracking and crack

deflection at the interfaces compared to traditional layups. A comparison between an 8 ply PW and a quasi-isotropic $[45, 90, -45, 0]_s$ control layup shows a variation in average strength, average strain to failure and average stiffness between the PW and control configuration as 2.9 %, 0.9% and 2.6% respectively.

PW subassemblies are combined with traditional layups for which PW subassemblies can be on the outer or inner surfaces to reduce manufacturing time compared to a fully PW architecture. Two 24 ply hybrid configurations, the first with PW laminates on the inside , P1 – TWT, and the second with PW laminates on the outer surfaces, P2 – WTW, are manufactured. A 24 ply quasi-isotropic $[45, 90, -45, 0]_{3s}$ control laminate is also manufactured.

Low velocity impact experiments are performed using an instrumented drop tower according to ASTM D7136 at 30 and 50 J energy levels. For a 30 J impact the P2 -WTW configuration absorbs 15-20% more energy than other configurations. Surface level damage inspection shows the P2 – WTW configuration exhibiting a smaller damage area than both the P1 - TWT and P3 - Control configurations at 30 and 55 J impact energies.

High velocity impact experiments are performed according to ASTM D8101 using a single stage gas gun while digital image correlation (DIC) and high-speed video are employed to evaluate the laminate's response. The impact velocities are in the range of 250 to 400 ft/s. Experimental results show that the hybridized configuration, P1 – TWT, show a V_{50} 8.5% greater than the control configuration. Results suggest that the P2 – WTW absorbs the most energy for all impact velocities; average normalized energies absorbed with respect to impact energy for P1 – TWT, P2 – WTW, and P3 Control are 0.85, 0.91, and 0.86 respectively. Experimental results also indicate reduction in back face damage

and back face deflection for the hybridized laminates compared to the control layups. Results obtained from impact testing suggest that the incorporation of PW laminates into a laminate may improve impact properties with respect to surface level damaged area, energy absorption, and V_{50}.

TABLE OF CONTENTS

LIST OF TABLES

LIST OF FIGURES

LIST OF ABBREVIATIONS

AFP ..... Automated Fiber Placement

ASTM ..... American Society for Testing and Materials

ASYM ..... Asymmetric

ATL ..... Automated Tape Laying

CFRP ..... Carbon Fiber Reinforced Polymer

Cont ..... Control

DIC ..... Digital Image Correlation

FPF ..... First Ply Failure

FRP ..... Fiber Reinforced Polymer

IBO ..... Interband Offset

PW ..... Pseudo-woven

QI ..... Quasi-isotropic

RTM ..... Resin Transfer Molding

TWT ..... Traditional Weave Traditional

UD ..... Unidirectional

VARTM ..... Vacuum Assisted Resin Transfer Molding

WTW ..... Weave Traditional Weave

CHAPTER 1

INTRODUCTION

1.1 PREAMBLE

Composites make up the world around us, they appear naturally as wood, bone, and stone to name a few examples. The concept of naturally occurring composites has been adopted by man to create derivatives that are widely used today, reinforced concrete, carbon fiber, and fiber glass as examples. Composite materials are broken down into two components, matrix and reinforcement. These two components are combined to achieve a system with improved functional or structural properties not attainable by the constituents alone. These structures have become prevalent in today's world because of the benefits that they offer from increased strength to improvements in damage tolerance. Modern advanced composites, like carbon fiber and glass fiber composites, can offer a tensile strength 4 to 6 times greater than that of steel or aluminum while being 30 – 45 % lighter than aluminum structures designed to meet the same functional requirements. The use of advanced composites in today's aircraft has the potential to reduce the overall weight of the aircraft by 20% increasing the airplanes efficiency and reducing its carbon footprint. In an article with the British broadcasting channel the head of Airbus' Research division stated that reducing the weight of an aircraft by 1 kilogram could reduce the costs over the lifetime of an aircraft by $1M. This is possible while allowing for the streamlining of complex part production resulting in reduced assembly complexity due to the elimination of traditionally

joined features. The combination of these benefits results in significant impacts in the overall production and design of components. The benefits of composite materials have affected us for the better, enabling a better quality of life allowing for the creation of vehicles that go farther, perform better, while improving safety.

While these materials have many areas where they perform better than conventional materials there are tradeoffs. Composite materials can experience brittle failure, low damage tolerance and resistance, and make damage difficult to identify making damage tolerance a key focus in many designs. This often results in the overdesign of composite components diluting the benefits of the material system. The severity of these tradeoffs can be partially mitigated through the use of different fiber architectures. Fiber architecture refers to the structure of the composite on the ply level where ply level is defined here as a discrete z position. This thesis aims to investigate the behavior of a novel pseudo-woven (PW) fiber architecture.

1.2 AFP PROCESS DESCRIPTION

Manufacturing of advanced composite components are done with a variety of manufacturing techniques which will be summarized to provide a scope on manufacturing methods. Manufacturing of advanced composites is done with fiber reinforced polymer (FRP) composites, the manufacturing techniques are broken down into two categories, manual and automated. First the manual methods for manufacturing will be discussed. Hand or manual layup starts from cutting layers from a roll of FRP then using those layers to build up a composite component for the specified design. Hand layup can use either preimpregnated material or dry material.

The manual layup process for prepreg material is less involved than that of dry fiber because the resin is already infused into the material eliminating any calculations needed to achieve a specific volume fraction of matrix to fiber. The layers are built to match the stacking sequence determined in the design and then put under vacuum to remove air bubbles that may have gotten trapped in the part, this process is called debulking. After the part has been debulked it is put into an autoclave where pressure and temperature work in tandem to reduce void content in the composite part.

The manual layup process for dry fiber is more involved because the resin must be infused into the system unlike prepreg materials. There are several ways to do this, the simplest being wet layup. Wet layup is a process in which dry layers are placed individually, and resin is painted on to infuse each layer. The next dry layer is then placed and more resin is painted on. This process repeats until the whole panel has been created. Vacuum assisted resin transfer molding (VARTM) and Resin transfer molding (RTM) are other methods which rely on resin being drawn or pushed into the system after the dry plies have been laid up. Consequent oven curing may be required to produce the desired mechanical properties

Automated systems are used for composites where variation in fiber angle can cause discrepancies in the part design when accumulated over the entire part. The automation of the layup process streamlines the entire process, reducing time needed to layup a part as well as increase overall part quality. Reduction of manufacturing time without sacrificing quality is seeing increasing demand in the aerospace industry where new aircrafts like the Airbus A350 and Boeing 787 are 50 % composite by weight. Automation is paramount to achieve a high rate of production for large aerospace structures

without sacrificing part quality. Automated fiber placement (AFP) is one method that is being used as a method to automate composite layup. In essence the process of automated fiber placement is similar to a 3D printer in that it stacks material onto the substrate building up a part. With slight variations which will be discussed below.

The system relies upon the use of composite tows which are small bands of composite material typically varying from ¼ to ½ of an inch. These tows or slit tapes are placed at angles determined by the user and laid by the machine's head as seen in Figure 1.1. The tows are laid as the machine applies heat and pressure ensuring that the material has enough tack to stick to the substrate. Typically, between 8-32 tows are laid at the same time in what is called a pass or course.

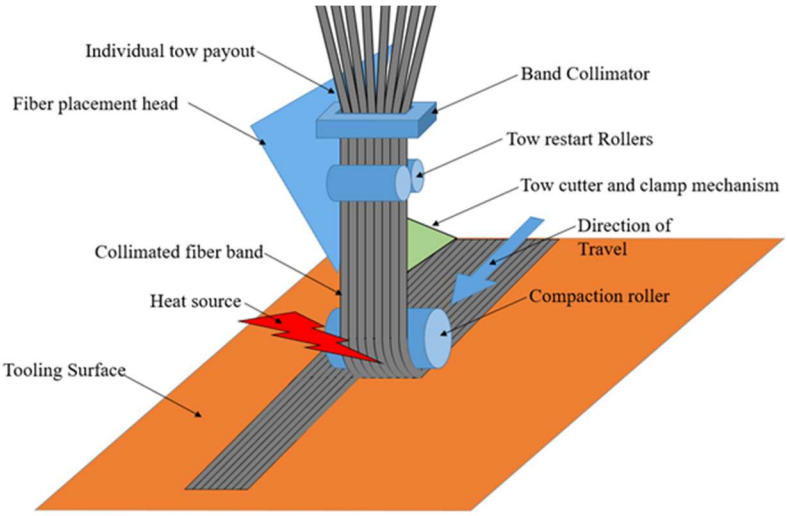

Figure 1.1 A general schematic of the AFP head [1]

For the case of referring to the motion of the machine it is called a pass. When talking about the material itself it would be referred to as a band. The AFP will lay down one band of material in that pass and then go to the subsequent course. This concept is visualized in Figure 1.2 where the orange box represents the next course where a pass will be made. The closeness of these material bands can be controlled using a parameter called

interband offset (IBO). This parameter is optimized for different material types, the materials respond differently under the compression applied by the AFP head and spread different amounts. The panels presented in this thesis utilized an IBO of 0.15 mm allowing for expansion during the layup process without producing overlap between bands.

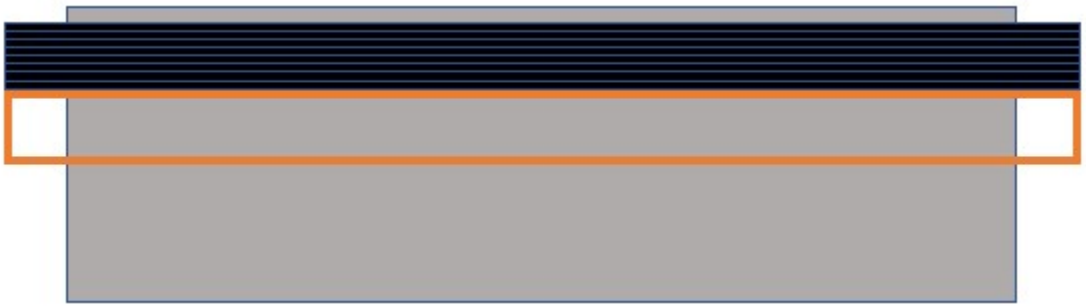

Figure 1.2 A depiction of a subsequent course to be laid.

Tows can be made from a variety of fiber reinforced polymers (FRP) depending upon the project's desires. Tows can be made from thermoset preimpregnated materials, dry fiber, and thermoplastic materials. Thermoset preimpregnated materials are currently the most widely used material type for AFP manufacturing because of their ease of use compared with the alternatives. They have high tack making them easy to layup on to a variety of surfaces without the need for high capacity heating equipment. The manufacturing of panels for these experiments was done using thermoset preimpregnated carbon fiber tows

1.3 OBJECTIVE

To explore and understand the development, manufacturing, and experimental characterization of pseudo-woven laminates to produce a more damage tolerant architecture while maintaining the strength of traditionally manufactured composite laminates. In this work the tensile, Low velocity impact, and High velocity impact

properties of PW laminates is experimentally characterized and compared with traditionally manufactured laminates.

1.4 THESIS OUTLINE

The points listed above will be discussed in different chapters in the work of this thesis. The chapters and their content are as follows:

Chapter 2	A literature review on different types of laminate architectures
Chapter 3	Manufacturing of Pseudo-woven laminat
Chapter 4	Warpage of Pseudo-woven Laminate
Chapter 5	Tensile Characterization
Chapter 6	Low Velocity Impact Characterization
Chapter 7	High velocity impact Characterizatio
Chapter 8	Conclusions and Future Wor

CHAPTER 2

LITERATURE REVIEW

2.1 THE CASE FOR ALTERNATIVE LAMINATE ARCHITECTURES

Traditionally, composite structures are made utilizing one or both of two material types, unidirectional and woven materials. These different material types are the fundamental building block of composite manufacturing with each holding their own benefits. Unidirectional materials, seen in Figure 2.2 A), are comprised of fibers oriented in the same direction, this leads to a high degree of material anisotropy where the material possesses high strength along the fiber orientation and little to none in the direction normal to the fibers. The material type's highly anisotropic nature can be utilized when building a composite structure that needs to be both lightweight and strong. Unidirectional fiber orientation allows for a composite structure to be strengthened only where the design dictates the need, allowing for weight savings while maintaining adequate strength. Unidirectional materials do suffer from drawbacks though, composite laminates made exclusively from unidirectional materials exhibit poor damage tolerance and damage resistance [2,3]. This caused by transverse loads that distribute throughout the laminate in an impact event. This can cause damage in a variety of mechanisms from matrix cracking to fiber failure. One of the most prevalent damage mode manifests as interply delamination for both high and low velocity impacts. This impact induced delamination spreads in a conical shape from the impact face through the thickness of the laminate resulting in barely

visible impact damage (BVID) as shown in Figure 2.1 on the surface of the laminate. BVID is the result of impact damage that isn't visible on the impact face. The damage shows itself on the backside, this is dangerous as it makes identification of composite damage difficult potentially allowing for damaged structures to pass inspection [4–7].

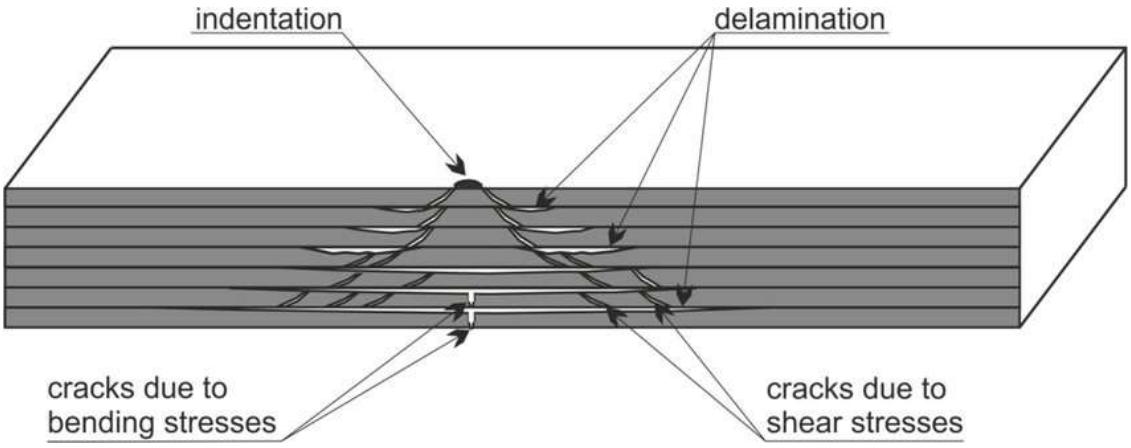

Figure 2.1 A schematic of impact induced damage modes experienced in an impact event.

Looking from a manufacturing perspective, unidirectional materials have a widespread application, this material - due to its unidirectional rigidity- can be used in automated manufacturing. This among other factors has led to the widespread adoption of this material type in the aerospace industry where large composite structures are often needed and manufacturing by hand is not practical or cost efficient. While unidirectional materials do have many benefits when used in automated manufacturing they are difficult to incorporate into geometries involving complex or curvatures. When laying a curved path wrinkles and puckers can form in the material due to the mismatch of curvatures on the edges of the material resulting in defects and a reduction in overall part quality [8].

Woven materials, shown in Figure 2.2 B), are more damage tolerant and resistant than their unidirectional counterparts and are often used for structures that could be subject

to damaging conditions [3]. Under dynamic loading conditions, woven materials have a higher ultimate strength than that of unidirectional materials making them a good choice for impact prone structures [9]. While they do possess properties that promote damage tolerance and resistance these materials possess less strength under quasi-static loading conditions than unidirectional materials while also being heavier.

In manufacturing, woven material systems are used for a variety of complex and simple geometries alike because they are easily conformable. The undulations in the fibers allow for the material to be easily manipulated locally to accommodate variations in substrate geometry There are a variety of different types of weaves that are best suited for different applications, satin weaves are often used in applications where drapability is sought after due to the material's pronounced trellising effect [10]. The usage of woven material's typically also allows for a more forgiving design experience because the material is more oriented than unidirectional materials, this means less work and a smaller barrier to entry for industry adoption. Currently, there are no ways to automate the layup of woven materials using automated fiber placement technologies because of the way that the material deforms when handled. When put under the tension required by AFP manufacturing the trellising effect becomes detrimental allowing for the manipulation of the material to the extent of it being unusable. Therefore woven materials have to be laid by hand which still presents a challenge due to material deformation in handling.

Figure 2.2 A) Unidirectional material B) Woven material

While each of these discreet material types have their own benefits there are many ways that these materials can be manipulated and combined to produce better performance. One simple and widely used ways to overcome the disadvantages of the individual material types is to hybridize the two structures. Studies have shown that the incorporation of unidirectional/woven hybrid structures results in a reduced damage footprint and higher residual compressive strength after an impact event [2]. Results from a study by Cantwell can be seen in Figure 2.3 where the plot on the left shows residual compressive strength of unidirectional laminates and the image on the right shows a mixed woven laminate. Often woven materials are used on the outsides of a laminate in order to protect the unidirectional plies that provide a vast majority of the stiffness and strength of the structure. In this configuration the woven plies are used as sacrificial layers to absorb damage, while they are relied upon very little for their structural contributions. The use of this hybrid architecture allows for a lightweight damage tolerant structure that possesses high strength when compared to a wholly woven laminate.

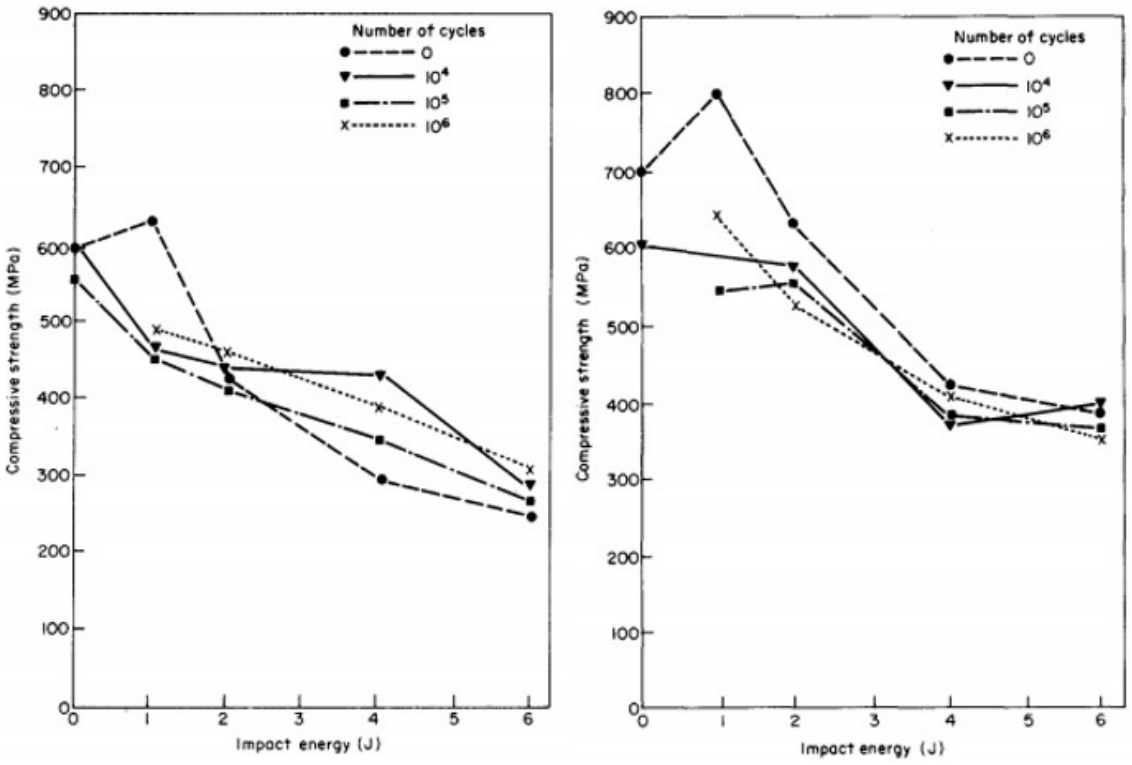

Figure 2.3 Residual compression tests performed at a variety of impact energies for unidirectional and mixed woven laminates [2].

While hybridized woven/unidirectional laminates work to increase damage tolerance while maintaining strength they can be improved upon. A lot of research is focused on producing strong, damage tolerant structures through a variety of approaches. A selected few that focus on the manipulation of the laminate architecture will be discussed below.

One of the dominating factors in mitigating impact damage is a composite laminate architectures ability to dissipate transverse loads introduced during an impact event [2,3,9,11–16]. Unidirectional and 2D fabric composite laminates possess poor out-of-plane properties compared to their in-plane properties. These out of plane properties can be enhanced through the introduction of fibers oriented in the thickness direction of the material. Orienting fibers in the z direction can be accomplished by weaving techniques

used in a family of laminates called 3D woven laminates shown in Figure 2.4. There are a variety of different 3D woven preforms that can be made all of which possess thickness oriented reinforcement which passes entirely through the thickness of the layer [17].

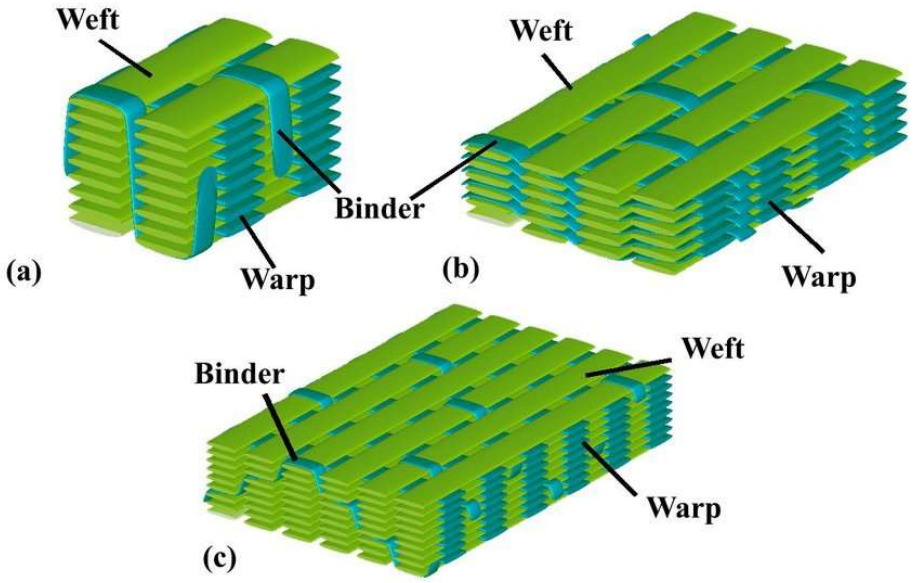

Figure 2.4 Schematics of 3D woven composites [17].

3D woven laminates have been shown to prevent delamination, resist crack propagation and increase impact toughness. Research has shown that after an impact event 3D woven laminates have a smaller damaged area than unidirectional cross plies or traditional 2D laminates. In Figure 2.5 the 3D woven laminates exhibit a smaller damage footprint for each tested impact energy. The effects become more pronounced as the impact energy increases as can be seen in Figure 2.5 where the 3D woven laminates demonstrate a vast departure from the 2D performance for each of their configurations [18]. They have also been shown to have a stepwise fracture under tensile loading and a higher failure strain than their 2D counterparts. 3D woven laminates have a critical damage below which there is no apparent degradation of compression strength. Unidirectional and 2D woven laminates do not exhibit similar behavior [18]. Although the utilization of the woven

laminate structure is not without its disadvantages, 3D woven laminate architecture reduces in-plane tensile strength and stiffness due to the reorientation of fibers compared to 2D fabrics [19,20]. However, the performance improvements in impact toughness are significant and should not be overlooked.

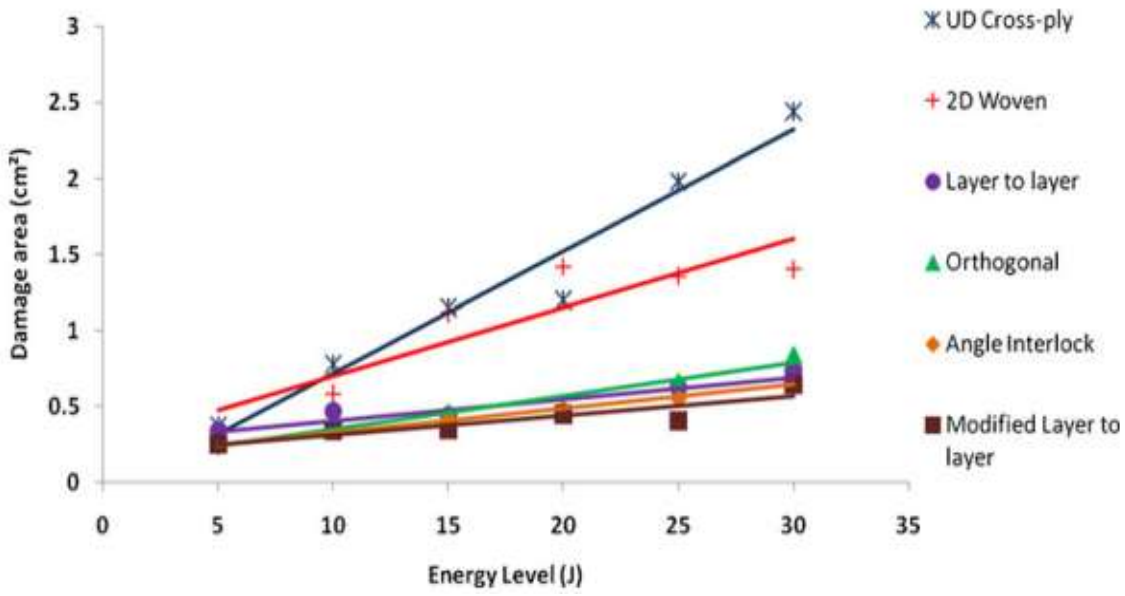

Figure 2.5 Damage area versus impact energy for a variety of laminate architectures.

Another laminate architecture to be discussed is a method focused on improving out of plane properties by placing pins into the laminate. These pins serve to arrest delamination growth in an impact event. The pins are placed using an ultrasonic gun to drive composite pins into the laminate to increase impact properties and damage resistance and damage tolerance by inhibiting delamination growth [21–24]. An example of the pins are shown in Figure 2.6. The Z laminate's effect on damage footprints are shown in Figure 2.7 where the pinned specimens show a reduction in the damage footprints at each respective impact energy.

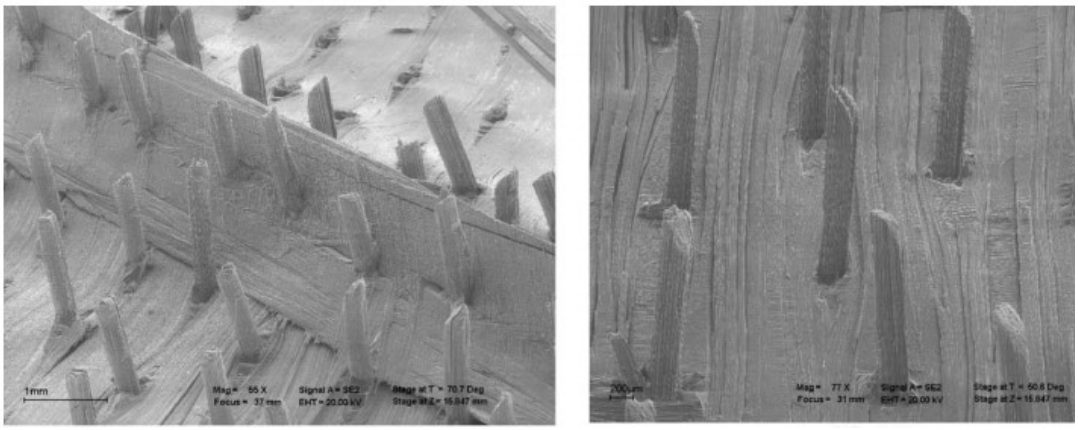

Figure 2.6 An electron micrograph of Z-pins on the fracture surface of a stiffened element [21].

Z pinning has been shown to reduce the elastic properties of the material, the extent of degradation experienced in the architecture's stiffness depends upon the density and diameter of the pins used. The reduction seen from pinning is generally under 10% [22] Tensile and compressive strength are also knocked down because of fiber breakage caused by the pinning process. Z pinning may be a viable method for increasing performance but the technique needs further large scale investigation to accurately determine its performance and effects on composite structures [21,22]

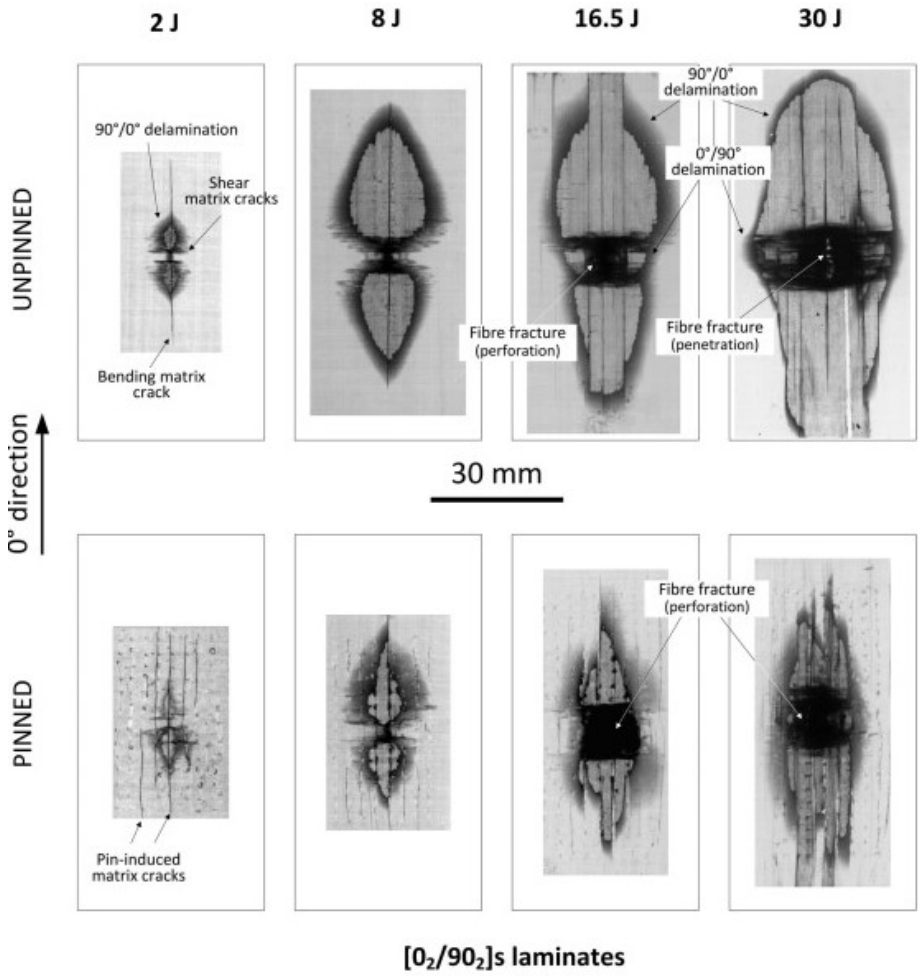

Figure 2.7 Delaminated specimens at different energy levels [18].

The delamination occurs between plies because of a mismatch in material properties which develop stresses at the interfaces A strategy for dealing with this mismatch of material properties is to reduce the difference in angle between unidirectional plies [25]. Helicoidal laminates utilize the effect of small mismatch angle between adjacent plies resulting in a spiraling or helicoidal laminate architecture, shown in Figure 2.8, to distribute transverse loads introduced in an impact event.

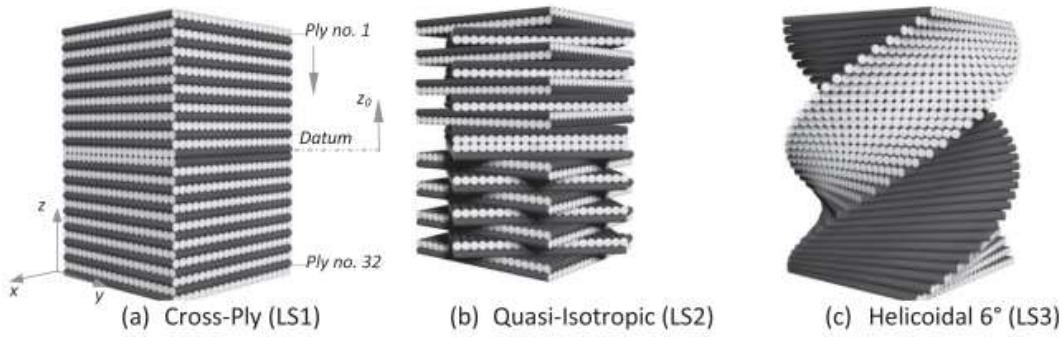

Figure 2.8 A representation of a helicoidal laminate architecture [26].

Cheng *et al.* has shown that a helicoidal structure with a 7.8° rotation per ply stacking sequence [0/7.8/…/180] results in an increase in the residual strength from the short-beam shear test [27]. The helicoidal laminate architecture has been reported in the literature to exhibit a greater damaged footprint than traditional quasi-isotropic laminates. Even though the footprint of damage is larger in the helicoidal laminates, the intensity of fiber damage is less pronounced. The helicoidal laminates are more prone than quasi-isotropic laminates to disperse energy in the form of delamination rather than fiber related damage as seen in Figure 2.9. Although the helicoidal laminate architectures have a greater extent of delamination the residual compression strength of the laminates is higher than traditional quasi-isotropic laminates due to the intensity of damage experienced during the impact event [28].

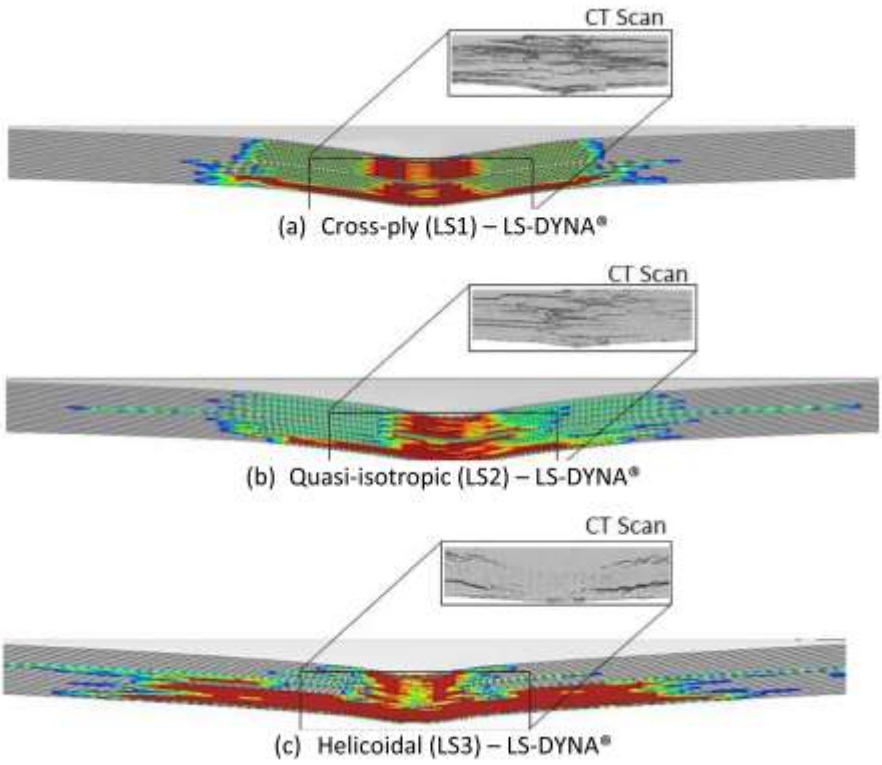

Figure 2.9 Delamination contours of different laminate architectures. Simulations are compared with CT scan data taken from experimental results [26].

Nagelsmidt et al. developed a type of laminate architecture at Delft University of Technology originally called AP-Ply which borrows concepts from 3D laminates and utilizing small carbon fiber tapes to create a semi-woven or also called a pseudo-woven (PW) structure, seen in Figure 2.10. This laminate architecture was shown to have increased damage tolerance while exhibiting similar uniaxial properties with traditionally manufactured unidirectional samples [29–31]. In instances of low velocity impact AP – Ply laminates have been shown to have a reduced damage footprint and increased residual strength compared with baseline traditionally manufactured laminates[29,32]. While this paper focused on the utilization of 1 – 2 skip tows in the manufacturing, the study seen in this work will expand upon that. The PW laminate architecture has been developed further and hybridized with unidirectional plies as well for impact resistant laminates. The PW

laminate developed by Nagelsmidt is the cornerstone of the work presented in this thesis. The structure of this laminate is complex and therefore it merits its own section before the characterization is discussed.

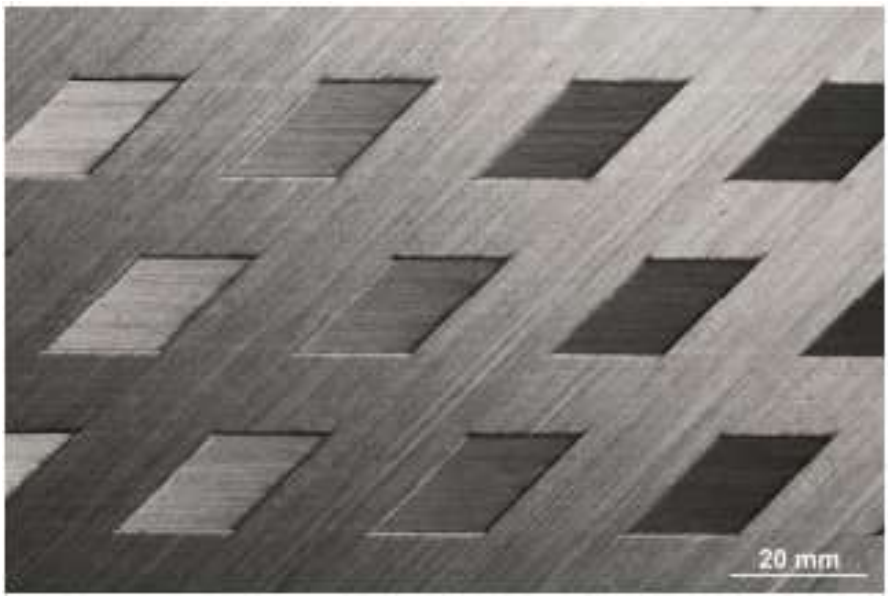

Figure 2.10 An example of Nagelsmidt's pseudo-woven laminate architecture [29,30].

CHAPTER 3

MANUFACTURING OF PSEUDO-WOVEN LAMINATE

3.1 ABSTRACT

PW laminates are manufactured through a fundamental change to the AFP manufacturing process, moving away from the ply-by-ply manufacturing concept where tows are laid adjacent to one another to a manufacturing technique that skips tows to make a pseudo-woven laminate architecture, discussed in detail in section 3.2. The difference between the laminates produced by the two skipping method and the traditional method is illustrated in Figure 3.1. The modified skip tow AFP process used in the manufacturing of the PW laminates allows for the creation of a woven-like architecture without the need for a loom. This pseudo-woven architecture, results in a complex laminate construction in which each tow can cross all plies multiple times. This manufacturing technique enables multifunctional tailoring by offering local control over stacking sequence.

Figure 3.1 Image of a PW laminate (b) graphical representation of PW laminate architecture.

3.2 PSEUDO-WOVEN LAMINATE MANUFACTURING

PW laminates are manufactured through a manipulation of the layup process typically used in AFP manufacturing. Traditionally AFP manufacturing utilizes full tow coverage when laying tows placing full bands resulting in the conventional laminate construction. When manufacturing a PW laminate, tows are intentionally skipped to produce gaps in the bands. The gaps produced during skipping are filled in the subsequent passes compounding to produce the woven-like architecture.

To understand the structure/architecture of the PW laminates, its manufacturing parameters and naming scheme are first discussed. The structure of a PW laminate is described using its AFP notation shown in Figure 3.2

$$[\theta^1,\theta^2,\theta^3,\theta^4,..\theta^m]_a[x000x000]_{n\,b}[w]_c[ds]_d$$

Figure 3.2 A generic example of AFP notation (a) directional set (b) tow mask (c) physical tow width (d) directional shift [1]

AFP notation is broken down into four parts to describe the architecture of a PW laminate. Figure 3.2 (a) denotes fiber orientations used in the laminate, called the directional set. The directional set provides the orientations used in the laminate and the

order in which orientations are laid. Using Figure 3.2 as an example, '$\theta^{1'}$ is laid, then '$\theta^{2'}$ to '$\theta^{m'}$, where 'm' is the number of fiber orientations in the laminate. The conventional definition of a ply is a layer of full coverage occupying a discrete Z position. Because of the apparent departure from conventional manufacturing for the PW laminates the authors have defined a ply as a completed directional set. The second grouping in Figure 1, subsection (b) represents the tow mask. This serves as a map of active, *x*, and inactive channels, *0*, of the AFP's head. The subscript *n* on the tow mask denotes the number of times the roller must pass over the domain to produce a panel of a specified width. For example, if a panel is sixteen tows wide then for this eight tow roller, n=2. The tow mask then is used to convey what channels are active and feed tows when the AFP's head makes its passes. Manipulation of this tow mask produces the woven-like architecture of the PW laminates. Figure 3.2 (c) represents the physical tow width, in this case 6.35 mm. It is possible for layups to have two adjacent active channels, where tow width is then defined as 12.7 mm.

Figure 3.2 (d) denotes directional shift, which takes effect after each directional set has been laid. Once a directional set has been laid, for a directional shift of *1*, the first fiber orientation in the previous directional set will shift to the end of the new set thus changing the directional set for the next ply. An example of directional shift is shown in Table 1, where column 'A' shows the effect of a directional shift of *1*, while column 'B' shows a shift of *0*. Note that the tow mask shifts irrespective of directional shift.

Table 3.1 An example of directional shift effect [1]

	A. Directional shift [1]		B. Directional shift [0]
A) Pass 1	$[\theta^1,\theta^2,\theta^3,\theta^4][x000x000]n[1/4"][1]$	B) Pass 1	$[\theta^1,\theta^2,\theta^3,\theta^4][x000x000]n[1/4"][0]$
A) Pass 2	$[\theta^2,\theta^3,\theta^4,\theta^1][0x000x00]n[1/4"][1]$	B) Pass 2	$[\theta^1,\theta^2,\theta^3,\theta^4][0x000x00]n[1/4"][0]$
A) Pass 3	$[\theta^3,\theta^4,\theta^1,\theta^2][00x000x0]n[1/4"][1]$	B) Pass 3	$[\theta^1,\theta^2,\theta^3,\theta^4][00x000x0]n[1/4"][0]$
A) Pass 4	$[\theta^4,\theta^3,\theta^2,\theta^1][000x000x]n[1/4"][1]$	B) Pass 4	$[\theta^1,\theta^2,\theta^3,\theta^4][000x000x]n[1/4"][0]$

Using the AFP notation, $[45, 90,-45,0][x000x000]_n[1/4"][0]$, the manufacturing of a PW panel used in the experiments is shown in Figure 3.3. In Figure 3.3(a) the first directional set is laid onto the tool. The next pass, shown in Figure 3.3 (b) is laid in the same order as the previous set except the active channel shifts over one space. This process repeats in Figure 3.3 (c) and Figure 3.3 (d) completing the PW laminate.

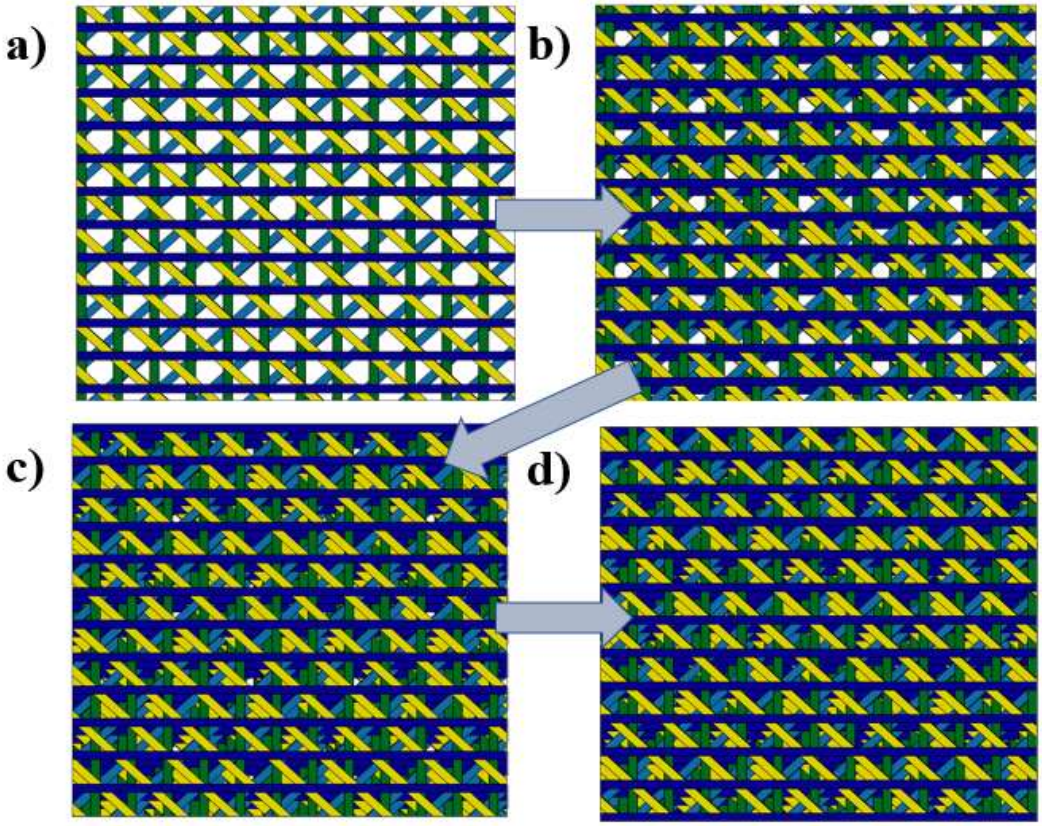

Figure 3.3 . A depiction of the manufacturing process a) Pass 1 b) Pass 2 c) Pass 3 d) Pass 4.

Figure 3.4 presents a visualization of the layup process for a PW laminate with an AFP notation of [0,45,90,-45][x000x000]$_2$[1/4"][1]. In Figure 3.4 (a) the first directional set is laid onto the tool; a directional shift of 1 then takes effect. The next pass, shown in Figure 3.4 (b), initiates with 45° tows followed by the 90°,-45°, 0° tows. This process repeats in Figure 3.4 (c) and Figure 3.4 (d). A ply book demonstrating the layup sequence layer by layer is shown in Appendix A.

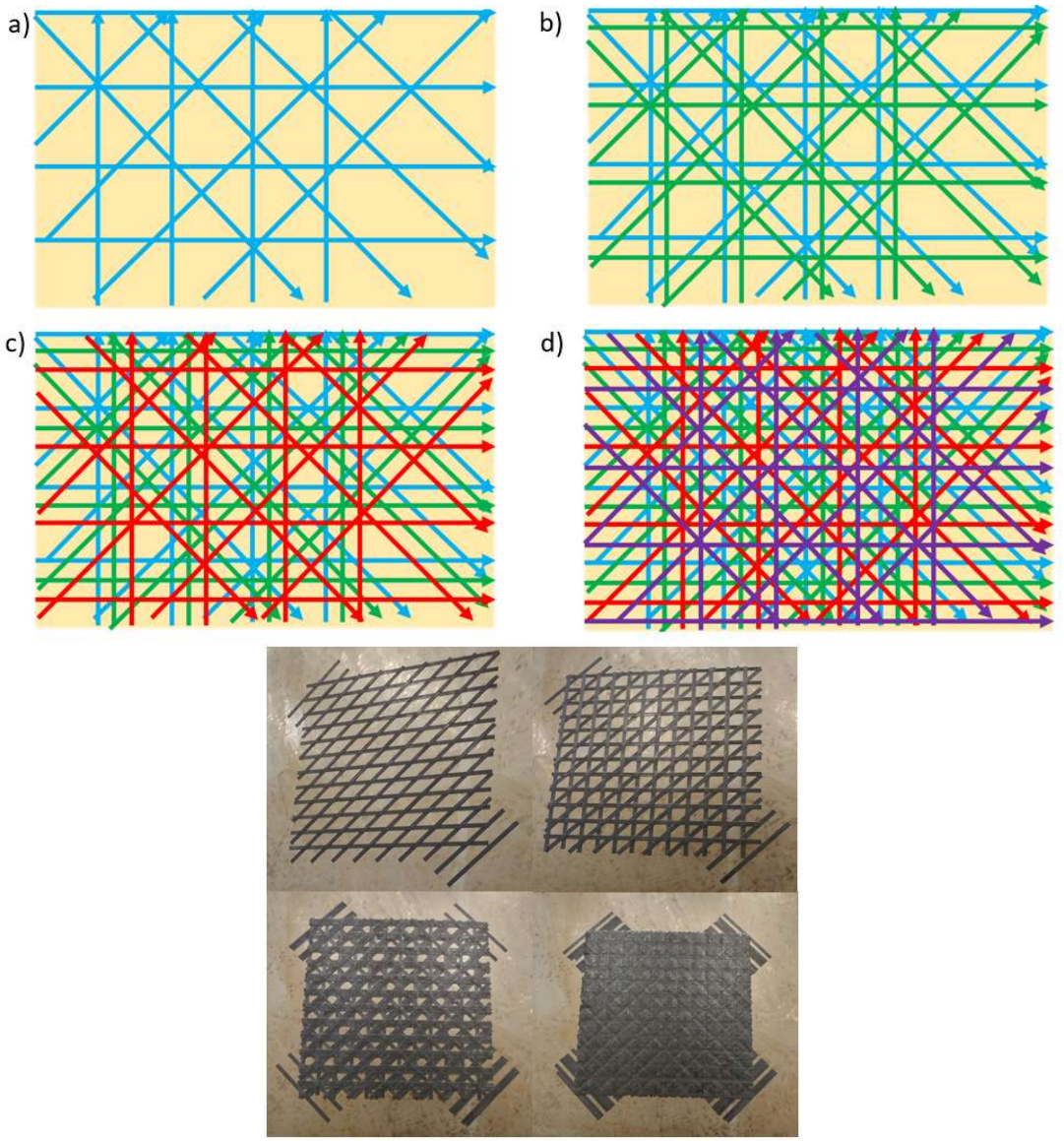

Figure 3.4 Visualization of the layup process (a) Pass 1 (b) Pass 2 (c) Pass 3 (d) Pass 4 (e) manufacturing.

CHAPTER 4

WARPAGE OF PSEUDO-WOVEN LAMINATES

4.1 ABSTRACT

The thermal and mechanical behavior is studied where the PW laminate lay-up pattern is represented with a sub cell approach utilizing 3D shell finite elements where the tows are deposited onto the regions mimicking the AFP course. Experimental results show that post-cure thermal warpage for the PW carbon/epoxy laminates are reduced, up to 58%, when compared to conventional asymmetric laminates while also exhibiting tensile properties comparable to traditional laminates of the same ply counts.

4.2 SPECIMEN MANUFACTURING

Warpage was quantified by comparing AFP manufactured panels listed in Table 4.1. The panels were manufactured using ¼ inch T-800SC-24K-10E carbon/epoxy tows from Toray and cured using an autoclave at 90 psi and 350 °F for 6 hours .

Table 4.1 Laminates manufactured on the AFP for warpage comparisons.

Laminate	AFP Notation		
3C	[0 60 120]	[xxxxxxxx]n	[1/4”][0]
4S-DS1-CS3	[0 45 90 -45]	[x000x000]n	[1/4"][1]
4C	[0 45 90 -45]	[xxxxxxxx]n	[1/4"][0]
5C	[0 72 144 216 288]	[xxxxxxxx]n	[1/4"][0]
6C	[0 30 60 90 120 150]	[xxxxxxxx]n	[1/4"][0]

4.3 EXPERIMENTAL METHODOLOGY

Panels were scanned using a Sense 3D scanner by 3D Systems with a manufacturer reported degree of accuracy of ± 1 mm [33]. To minimize distortion, panels are suspended vertically before being scanned. The ASCII file output by the scanner is used to generate a cloud of points fitted to a surface to generate the displacement field. The surface is fitted such that the panel’s center is aligned with the XY plane. Out of plane displacement is reported as the distance between the laminate surface and the closest corresponding coordinate on the XY plane. A representative example of a scanner generated displacement field is shown in Figure 4.1.

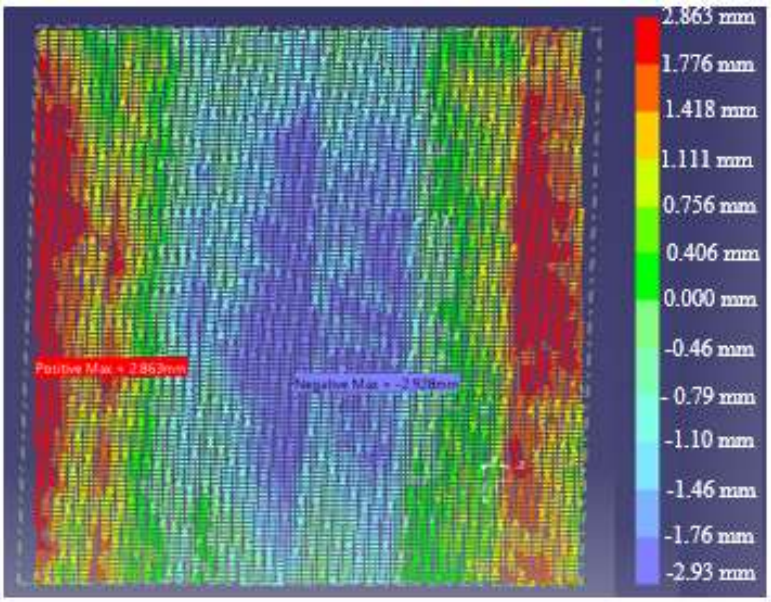

Figure 4.1 Out-of-plane displacement map of 4D-DS1-CS3. Maximum displacement: 2.863 mm, Minimum displacement: -2.928 mm.

4.4 RESULTS AND DISCUSSION

Soltani et al. [34,35] reported that factors that most effect out of plane deformation due to curing are layup symmetry, fabric type, and layup angle; the factor with the greatest effect being layup symmetry followed by fabric type. A harness weave used to create a 16 ply laminate shows a decrease in warpage (out of plane displacement) when compared to a 16 ply laminate made exclusively from non-crimp and unidirectional fibers.

The panels and their respective out-of-plane warpage maxima are shown below in Figure 4.2. In Figure 4.2, 3C, 4C, and 6C represent 5” x 5” conventional control samples where 3C is 3 ply, 4C is 4 ply, and 6C is 6 ply, and PW represents the 4 ply PW laminate called ‘4D-DS1-CS3’. The conventional control samples are laid using the same fiber angles as their PW laminate counterparts to allow for warpage comparison. All control samples shown here are manufactured with the same material and processes as the PW laminates. Figure 4.2 shows that the PW laminate’s out-of-plane displacement is smaller

than the 4 ply control by 58% as well as all of the other controls exhibiting a maximum displacement around 6 mm.

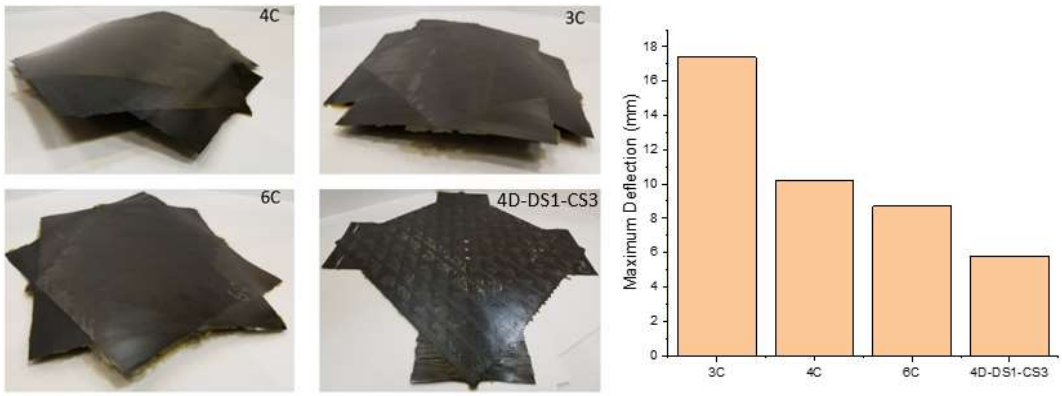

Figure 4.2 Warpage comparison between 3 conventional ply based laminates, 3C, 4C, and 6C, and a 4D-DS1-CS3 PW laminate.

4.5 SUMMARY AND CONCLUSION

Experimental results indicate these laminates show significantly reduced thermal warpage when compared to conventional asymmetric laminates of equal number plies. This reduction is likely due to the spatial variations in the effective stacking sequence, specifically the **B** matrix components. PW laminates when manufactured as asymmetric laminates have up to 58% less warpage than the conventional fiber architecture. This could enhance the usability of asymmetrical stacking sequences potentially dampening some of their adverse effects like warpage, atypical loading response, and complex failure

CHAPTER 5

TENSILE CHARACTERIZATION

5.1 ABSTRACT

In this study the manufacture and characterization of novel non-conventional composite laminates coined as PW laminates are presented. These carbon/epoxy laminates are manufactured using prepreg slit tape in an automated fiber placement (AFP) machine through tow skips. The AFP process allows for the tailoring of material architecture, resulting in woven-like structures without the need for a loom. These laminates are heterogeneous due to variation of fiber orientation and therefore, the material properties at a given section is a function of in-plane spatial coordinates. A variety of PW laminate configurations are manufactured for this study. Results suggest that PW laminates perform comparably to conventionally manufactured composite laminates possessing similar strength and similar and often higher strains compared to conventional laminates. These effects appear to diminish with increasing PW laminate thickness where stacked PW laminates are shown to have small percent differences between the average peak stress, average Eyy strain, average Exx strain and average stiffness of 2.9 %, 0.9%, 10.6% and 2.6% respectively with the exception of E_{xx} strains.

5.2 PSEUDO-WOVEN TENSILE CHARACTERIZATION USING EXTENSOMETER STRAINS

5.2.1 Tensile Characterization using Extensometer and Crosshead Derived Strains

A variety of PW laminates are manufactured with different fiber angles for this study. A comprehensive list of PW configurations manufactured using the AFP is shown in Table 5.1. The panels were manufactured and subjected to uniaxial tensile testing to understand the effects of manipulating: directional set, directional shift, and tow mask on tensile strength and strain. The laminates named in Table 5.1 except ASYM and QI are manufactured with ¼ inch T-800SC-24K-10E carbon/epoxy tows by Toray and are cured in an autoclave at 90 psi and 350° F for six hours.

Conventional laminates, 12″x12″, were manufactured with hand layup using AS4/8552 prepreg tape and cured at 90 psi and 350F for six hours. For this study two laminates are manufactured: a 4 ply asymmetric laminate with a stacking sequence of [0/45/90/-45] referred to as ASYM, and a quasi-isotropic 8 ply symmetric laminate with a stacking sequence of [0/45/90/-45]s referred to as QI. These laminates are to serve as the control for tensile behavior discussed in .

Table 5.1 A list of AFP notations for various Laminates

Laminate	AFP Notation		
3D-DS0-CS6	[0 60 120]	[xx000000]n	[1/4”][0]
3D-DS1-CS6	[0 60 120]	[xx000000]n	[1/4"][1]
4S-DS1-CS3	[0 45 90 -45]	[x000x000]n	[1/4"][1]
4D-DS0-CS6	[0 45 90 -45]	[xx000000]n	[1/4"][0]
4D-DS1-CS6	[0 45 90 -45]	[xx000000]n	[1/4"][1]
ASYM	[0 45 90 -45]	[xxxxxxxx]n	[1/4"][0]
5S-DS0-CS7	[0 72 144 216 288]	[x0000000]n	[1/4"][0]
5D-DS0-CS6	[0 72 144 216 288]	[xx000000]n	[1/4"][0]
6D-DS0-CS6	[0 30 60 90 120 150]	[xx000000]n	[1/4"][0]
QI	[0 45 90 -45]s	[xxxxxxxx]n	[1/4"][0]

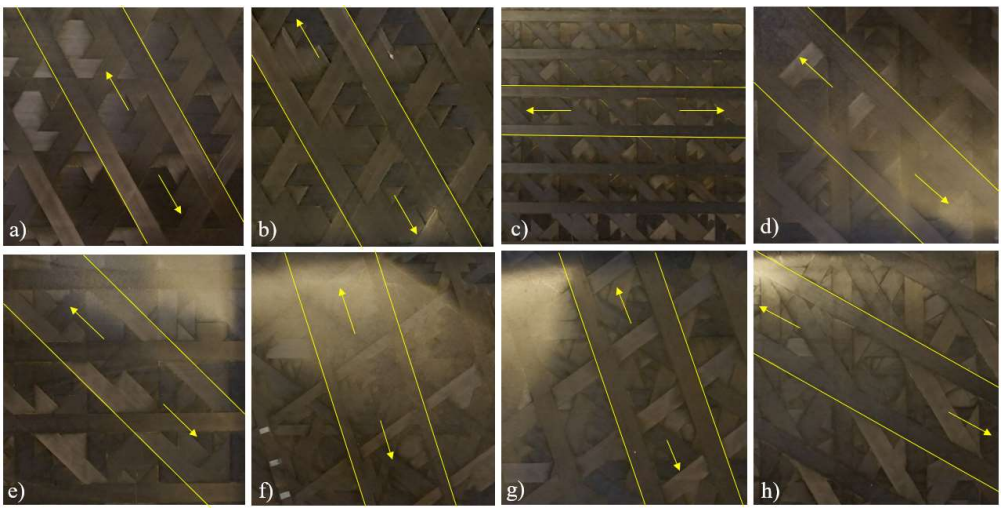

Figure 5.1 Sections of manufactured panels for each layup. Top row from left to right: 3D-DS0-CS6,3D-DS1-CS6, 4D-DS1-CS3, 4D-DS0-CS6. Bottom row from left to right:4D-DS1-CS6, 5S-DS0-CS7, 5D-DS0-CS6, 6D-DS0-CS6. Lines indicate the outer bounds of tensile specimens for each laminate.

5.2.2 Pseudo-Woven Comparison Specimen Preparation

Tensile specimens are extracted from the panels using a water-cooled disk saw, sample dimensions vary depending upon tow mask. Samples with two adjacent active

channels in the tow mask are wider, approximately 2.5 inches, whereas samples with non-adjacent active channels are 1.25 inches wide. An example of these varying sample widths are shown in Figure 5.1. Due to constraints imposed by the size of the panels, sample length vary from 10-12 inches. All tensile samples are bounded by the outer edges of one set of parallel 0° tows is shown in Figure 5.1, samples with 3 plies were cut along parallel 60° tows.

5.2.3 Experimental methodology

Samples are subjected to tensile testing according to ASTM D3039. Testing is performed using a MTS Teststar II with hydraulic wedge grips. To counteract slippage between the testing specimens and wedge grips, 120 grit emery cloth is used to secure the ends of the tensile specimens in the grips. Samples are loaded at 2.0 mm/min as specified in ASTM D3039. Strain is recorded using an MTS extensometer whose data is output by the Teststar II. For this study each tested laminate except 4S-DS1-CS3 has three samples to be characterized, 4S-DS1-CS3 has only one sample tested at 0° and as such it is not included into the results and discussion.

5.2.4 Results and Discussion

Stress strain curves for all specimens are linear to failure, tensile data for each is presented as average stiffness, ultimate strength, extensometer strain, and crosshead strain with their respective dispersion values in Table 5.2 except for panel 4S-DS1-CS3 whose sample size was too small to include. Experimental data indicates that the behavior of the PW laminates does not show a large departure from the behavior of QI and ASYM panels. The 3 ply laminate 3D-DS1-CS6 exhibit the highest strength in the 0° direction which is to be expected as they do not include a 90° fiber orientation.

Table 5.2 Experimental data taken from tensile tests. Dispersion values are presented beside the experimental values

	Stiffness (GPa)	Ultimate Strength (GPa)	Extensometer strain	Crosshead Strain
3D-DS0-CS6	51.538 ± 2.788	0.967 ± 0.052	0.018 ± 0.001	0.023 ± 0.001
3D-DS1-CS6	47.018 ± 3.557	0.980 ± 0.024	0.020 ± 0.001	0.023 ± 0.001
4D-DS0-CS6	44.977 ± 7.138	0.834 ± 0.037	0.021 ± 0.009	0.024 ± 0.002
4D-DS1-CS6	58.207 ± 5.503	0.913 ± 0.021	0.015 ± 0.002	0.025 ± 0.001
ASYM	50.953 ± 4.421	0.627 ± 0.046	0.014 ± 0.007	-
5S-DS0-CS7	49.348 ± 1.890	0.745 ± 0.038	0.016 ± 0.004	0.020 ± 0.001
5D-DS0-CS6	46.809 ± 8.867	0.755 ± 0.028	0.016 ± 0.001	0.022 ± 0.001
6D-DS0-CS6	50.438 ± 2.920	0.660 ± 0.017	0.012 ± 0.005	0.022 ± 0.002
QI	51.730 ± 6.201	0.704 ± 0.135	0.013 ± 0.001	-

Failure patterns of 4 ply specimens are shown in Figure 5.2 and failure patterns of other selected architectures are shown in 0. Complex failure patterns with matrix cracks, fiber failure, intralayer and interlayer delamination are observed for the PW architectures. Interlaminar stresses are likely to occur at the discontinuities both through thickness due to ply migrations and in-plane due to changes in fiber orientations. In addition to matrix cracks in the 90° regions, matrix cracks appear to form at different angles as indicated by arrows in Figure 5.2 (b). Ultimate failure is thought to occur progressively due to a complex sequence of these mechanisms.

It should be noted that laminate strength for the conventional laminates is only experimentally determined for the 4 ply and 8 ply AS4/8552 laminates while the PW laminates were manufactured with T-800SC. Although these material types are not the

same the purpose of the comparison is to give an idea of the architecture's performance. The Tsai-Hill failure criterion in conjunction with total ply discounting method is employed to estimate the laminate strength of 3, 4, 5, and 6 conventional laminates. Tsai-Hill failure criterion, Equation (5.1), where $\sigma_{1,2,3}$ are the stresses along the 1,2,3 axes and τ_{12} is shear stress in the 1-2 plane, $X_{t,c}$ denotes fiber strength in tension or compression, $Y_{t,c}$ denotes transverse strength in tension or compression, S is the shear strength, is applied to ASYM and QI panels to predict first ply failure (FPF) [36,37].

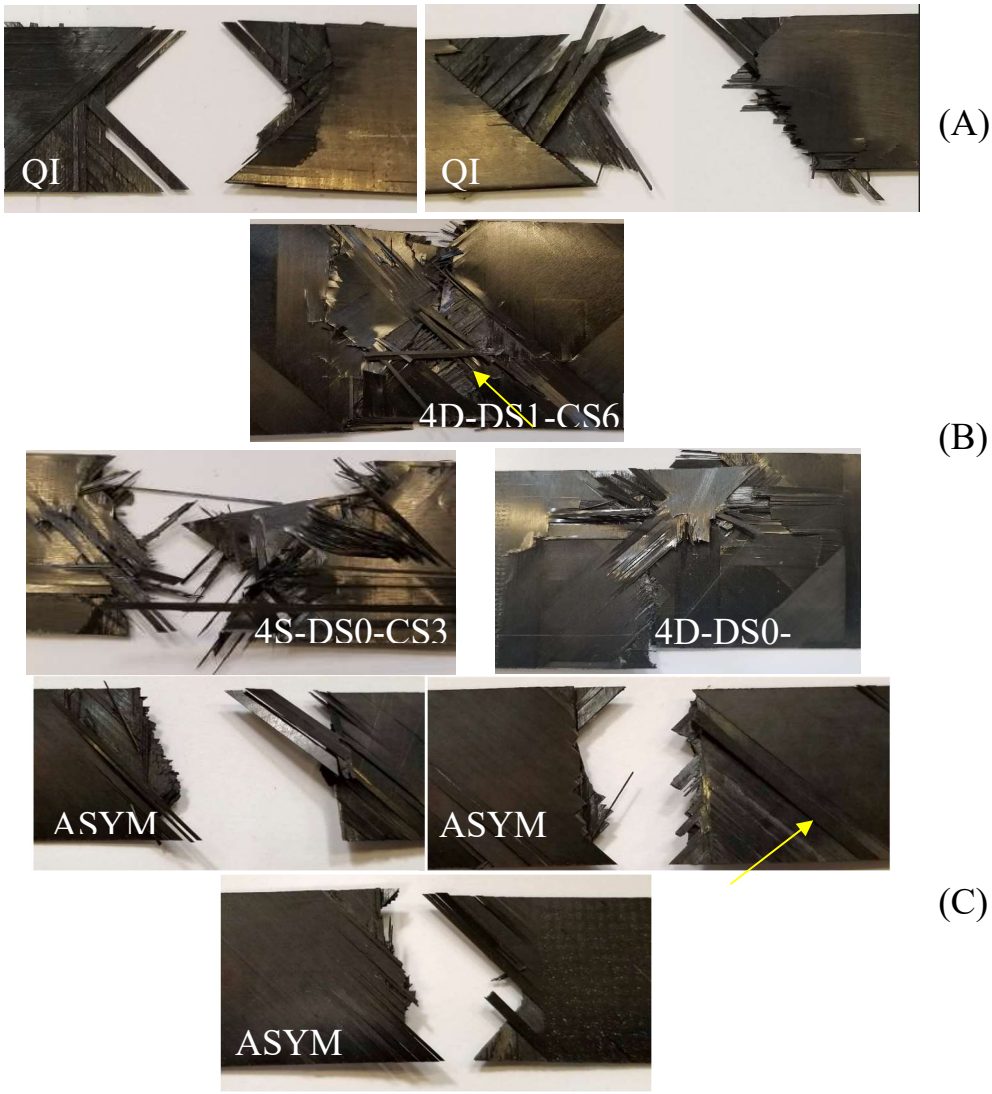

Figure 5.2 Failure patterns (A) QI tensile coupons (B) 4D-DS1-CS6 semi-woven tensile coupons (C) ASYM tensile coupons.

Tsai-Hill failure criterion predicts FPF in the 90° plies for both ASYM and QI panels. Following that failure is predicted to occur in the direction of loading, in the 0° fibers, the load then redistributes to the ± 45° fibers.

$$\left(\frac{\sigma_1}{X_{t,c}}\right)^2 + \left(\frac{\sigma_2}{Y_{t,c}}\right)^2 + \left(\frac{\tau_{12}}{S}\right)^2 - \frac{\sigma_1\sigma_2}{(X_{t,c})^2} = 1 \tag{5.1}$$

In Figure 5.3 the traditional laminate's strength is compared with the pseudo woven laminate strength. The points represent the extrema from plotting the highest and lowest predicted strengths from the analytical model. This is done by using CLT to predict the failure strengths of the different permutations possible in the stacking sequence. The stacking sequence for the extrema are below in Table 5.2. The boxed region shows the upper and lower bounds of experimental data for the PW laminates. All PW laminates except the 5 ply fall in the upper 50% of the conventional laminates' predicted strength.

Table 5.3 Stacking sequences of upper and lower bound laminate strength prediction

	3 Ply	4 Ply	5 Ply	6 Ply
Upper bound stacking sequence	[60/0/120]	[45/90/0/-45]	[72/36/0/-36/-72]	[30/60/0/90/120/150]
Lower bound stacking sequence	[0/60/120]	[90/45/-45/0]	[0/72/144/216/288]	[0/30/60/90/120/150]

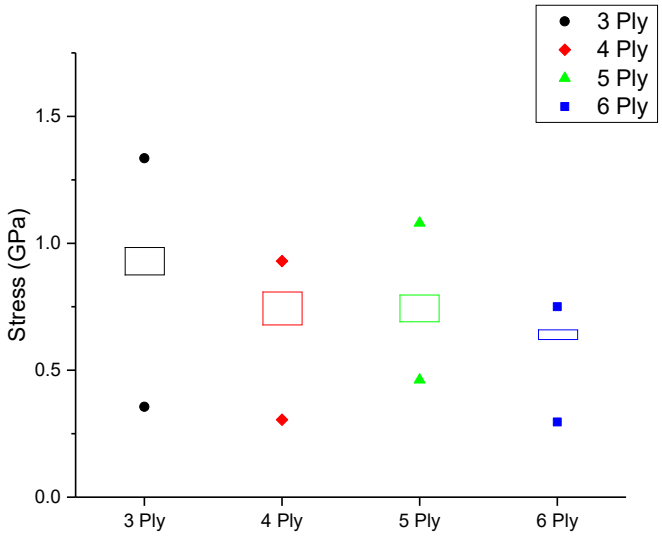

Figure 5.3. Comparison of predicted conventional laminate strength and experimental PW laminate strength

5.3 PSEUDO-WOVEN CHARACTERIZATION USING DIC STRAINS

5.3.1 Pseudo-Woven Control Comparison Specimen manufacturing

For this study two panels are made from ¼ inch IM7 G/8552-1 carbon/epoxy tows from Hexcel. A 8 Ply traditionally manufactured panel with a stacking sequence $[45/90/-45/0]_S$, and an 8 ply PW made from two mirrored 4 ply 4S-DS0-CS3 PWs whose AFP notation is shown in Table 5.4. A layer by layer breakdown of the manufacturing process of the 8 ply PW is shown in 0 . Both panels were intended to cured at 30 psi and 350°F for 5 hours, though due to mistakes were held at the dwell for a prolonged time, this may influence the performance of the laminates although because both were cured at the same time it is hypothesized that they will be comparable to one another.

Table 5.4 4S-DS0-CS3 AFP Notation

Laminate	AFP Notation		
4S-DS0-CS3	[45 90 -45 0]	[x000x000]n	[1/4"][0]

5.3.2 Pseudo-Woven Control Comparison Specimen Preparation

Tensile specimens made for the PW control comparison are extracted from panels using a waterjet. Specimens boundaries for the PW configuration are shown bounded by a yellow box in Figure 5.4. Specimens extracted are 1 inch x10 inches along the 45° fiber orientation. Specimen dimensions are selected to capture the full shift of the tows in the manufacturing process.

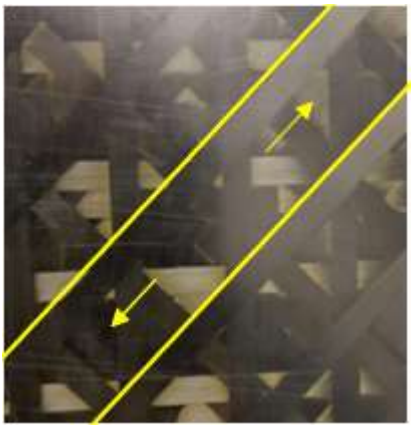

Figure 5.4 A boundary of tensile specimens extracted

The ends of the tensile specimens have glass fiber wedged end tabs applied to them to reduce slippage felt during tensile testing. The ends of the specimens are scored with emery cloth and end tabs are bonded onto the specimen using JB weld. A fine speckle pattern is applied to each specimen using spray paint for DIC.

Figure 5.5 A representative speckle pattern applied to tensile specimens

5.3.3 Experimental Methodology

Samples are subjected to tensile testing according to ASTM D3039. Testing is performed using a MTS Teststar II with hydraulic wedge grips. Samples are loaded at 2.0 mm/min as specified in ASTM D3039. Strain is recorded using a stereoscopic camera setup pointed at the face of the specimens and images are processed using VIC 3D. For this study the control and PW laminates have 10-12 specimens characterized each.

5.3.4 Experimental Results and Discussion

Stress vs time curves for the two laminate configurations are shown in Figure 5.6 laminates have similar stress values and loading rates as one another. It is important to note that while loading the load cell used was set to an improper range. Specimens that were subject to an improper load cell range have a failure load that has been approximated using a extrapolated linear line of best fit to the last few data points. Using this line an equation is generated, failure time is plugged in yielding the failure stress of the specimens

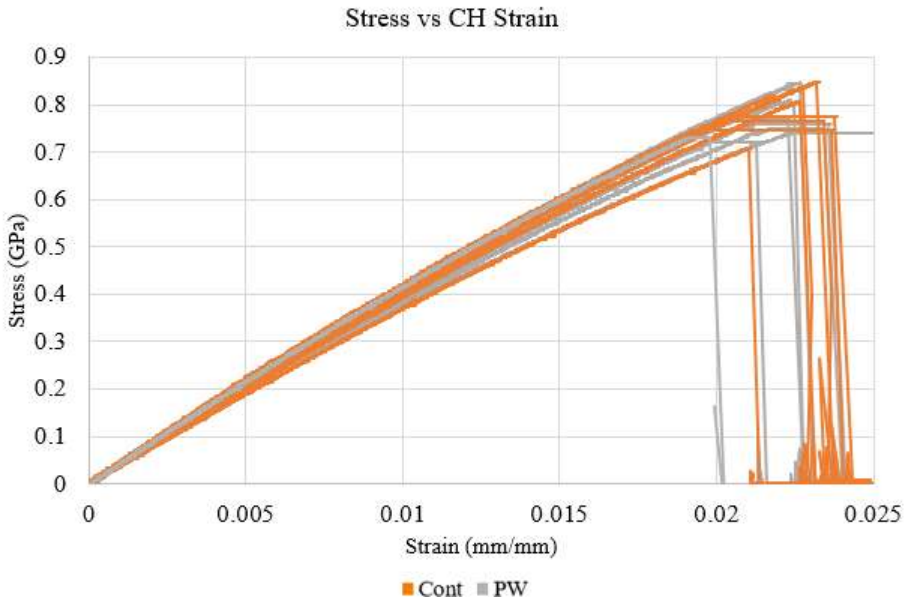

Figure 5.6 Superimposition of Stress vs Crosshead strain curves for 8 ply PW and Control specimens.

An average of the experimental results is shown in Figure 5.7. The percent differences between the average peak stress, average E_{yy} strain, average E_{xx} strain and average stiffness are 2.9 %, 0.9%, 10.6% and 2.6% respectively. Barring the difference between E_{xx} strain the values for peak stress, average E_{yy} strain, and average stiffness have similar values for both the 8 ply control specimen and the 8 ply PW specimens.

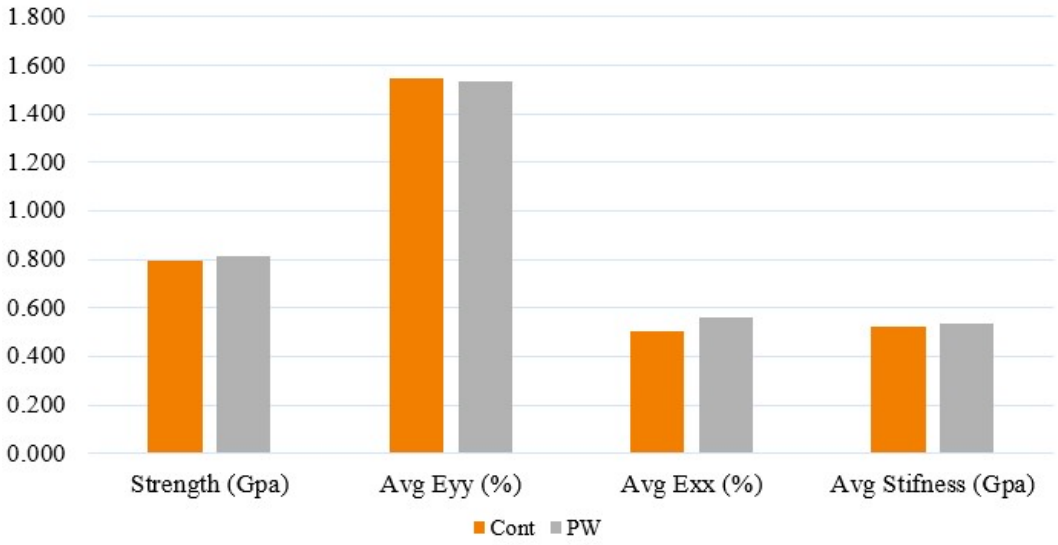

Figure 5.7 Average Strength, E_{yy}, $E_{xx,}$ and stiffness for 8 ply PW and Control laminates.

Failure patterns between specimens are also similar, the primary mode of failure is a mix of fiber pullout and interlaminar delamination when failure occurs towards the middle of the tensile specimens shown in the lower four figures of Figure 5.8. The failure that occurs at the end tabs can be seen in Figure 5.8, this failure is complex exhibiting a combination of fiber pullout, interlaminar and intralaminar delamination.

Results suggest that the 8 ply PW laminate exhibits similar uniaxial properties with the exception of E_{xx} strains when compared to an 8 ply conventional laminate. Failure mechanisms are observed to be similar between configurations.

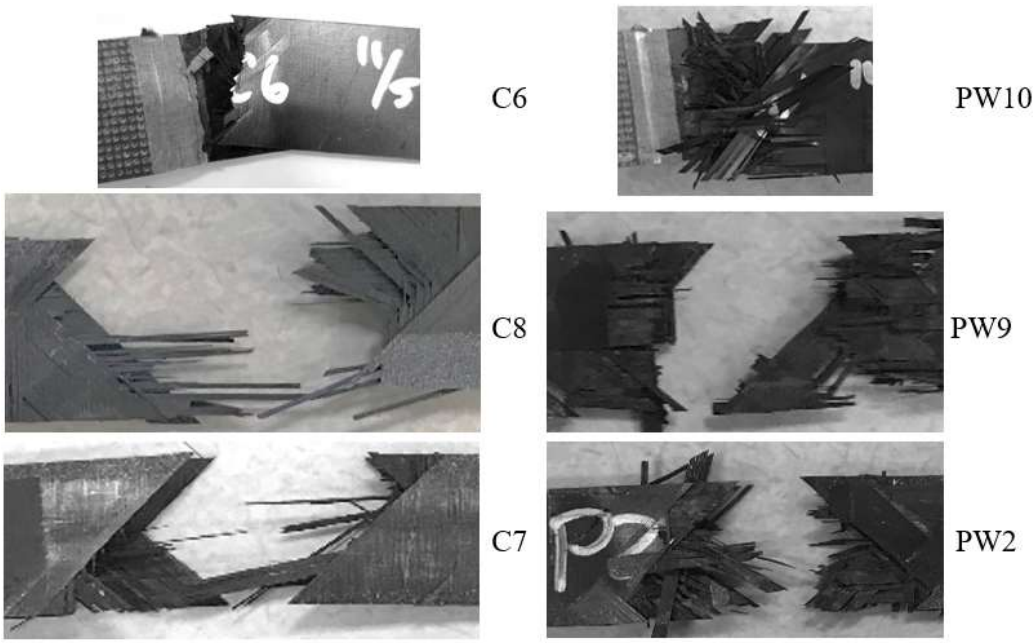

Figure 5.8 Examples of 8 ply laminate failure patterns. The right side is PW, the left control laminates.

5.4 SUMMARY AND CONCLUSION

This paper presented the manufacturing and characterization of novel fiber-reinforced composite laminate architectures enabled by AFP manufacturing. These laminates are heterogeneous due to variation of fiber orientation and therefore, the material properties vary as a function of in-plane spatial coordinates. They are manufactured through a fundamental change to the AFP manufacturing process utilizing tow skips to create woven like architectures. By changing the directional shifts and active channels between each pass in the AFP process, different PW laminate architectures were manufactured using 3, 4, 5 and 6 plies. These laminates exhibit complex tow migrations and resin rich regions due to the crossing of tows across the plies shown by microscopic images of cross sections shown in 0.

Average tensile stiffness, tensile strength and strain to failure of these laminates are experimentally characterized. The results indicate that these properties compare well to the

conventional QI and ASYM laminates since the **A** matrix remains largely unchanged. The 3, 4, and 6 ply PW laminates operate in the upper 50% of the predicted conventional laminate strength ranges. Complex failure patterns are observed for these architectures displaying matrix cracks, fiber failure, intralayer and interlayer delamination.

The results for the 8 ply PW and control demonstrate similar behavior between a 8 ply PW and 8 ply control panel manufactured using automated fiber placement. The percent differences between the average peak strength, average E_{yy} strain, average E_{xx} strain and average stiffness are 2.9 %, 0.9%, 10.6% and 2.6% respectively. The results shown here are from specimens that were not subject to the manufacturer recommended curing cycle potentially resulting in atypical laminate properties.

CHAPTER 6

LOW VELOCITY IMPACT CHARACTERIZATION

6.1 ABSTRACT

Fiber-reinforced composite laminate structures employed in aerospace applications can utilize both woven and unidirectional lamina. While the woven lamina allow for a higher degree of damage tolerance, unidirectional lamina allow for higher stiffness. The utilization of these two lamina types in a hybrid architecture allows the laminate to have high stiffness while also possessing higher damage tolerance. The hybridized configuration where PW laminates are on the outer surfaces, P2 - WTW, exhibited a smaller damaged area than both the P1 - TWT and P3 - Cont configurations at the 30 J and 55 J impact energies. In addition, P2 – WTW absorbed higher energy by 15-20% for 30 J impact compared to other panels. Highest absorbed impact energy for the 55J impact is shared equally between the P1 - TWT and P3 - Cont configurations.

6.2 SPECIMEN MANUFACTURING

Three laminates configurations are manufactured in this study, two structurally hybridized laminates, one with the PW laminates on the outer surfaces and the other with the PW laminate on the inside, and one control traditional laminate, these layups will be discussed in the coming sections. All laminates manufactured for this study are 24 plies thick and are made with Hexcel IM7G/8552-1 slit tapes cured at 176 °C and 6.2 Bar. The panels manufactured for these experiments are referred to as 4S-DS0-CS3 and INV4S-DS0-CS3.

Their AFP notations are [45, 90, -45, 0][x000x000]n[6.35mm][0] and [0, -45, 90, 45][x000x000]n[6.35mm][0] respectively.

6.2.1 Hybridized Structures

The manufacture of PW laminates is a time intensive process, skipping tows during manufacturing increases the time needed to lay up a single ply. For these PW laminates, each ply takes approximately four times longer to lay than a traditional ply because of the skipped tows. As such, hybridizing a traditional laminate structure with PW laminates is used to reduce manufacturing time while gaining insight on PW impact performance. In these experiments two hybrid structures are manufactured, one with the stacking sequence of $[(45/90/-45/0)_2/4S\text{-}DS0\text{-}CS3/INV4S\text{-}DS0\text{-}CS3/(0/-45/90/45)_2]$ where the PW laminates are on the inside, for simplicity, this panel is referred to as, Panel 1, or P1 - TWT. The other panel has the stacking sequence of $[4S\text{-}DS0\text{-}CS3_2/45/90/-45/0/0/-45/90/45/INV4S\text{-}DS0\text{-}CS3_2]$, this panel is referred to as Panel 2 or P2 - WTW. All panels manufactured for these tests are 24 plies thick including the control sample whose stacking sequence is $[45/90/-45/0]_{3s}$ this panel is referred to as Panel 3 or P3 - Cont.

6.3 EXPERIMENTAL METHODOLOGY

The experimental procedure for the low velocity impact tests is performed in accordance with the ASTM standard D7136. From the three manufactured panels, six 100 mm (4 inch) x 150 mm (6 inch) specimens were extracted from each panel using water jet cutting. To minimize delamination along the edges, panels were fixed onto a wood backing during water jet cutting to prevent vibration. To ensure good edge quality specimens were inspected using a Keyence optical microscope.

Specimens are impacted with a drop tower setup that complies to ASTM standard D7136. Samples were secured with Carr-Lane clamps rated at 1100 N per clamp and were impacted with an instrumented hemispherical impactor cap with a radius of 16 mm. The cart used had a mass of 6.25 kg, this was needed to reach the desired impact energies. Specimens were subjected to impact at15 J, 30 J, and 55 J, the height needed for the impact energies was calculated using Equation. (6.2). Where E is the energy level desired, m is the mass, and g is gravity.

$$H = \frac{E}{mg} \tag{6.2}$$

6.4 RESULTS AND DISCUSSION

6.4.1 Impact Metrics

The impact was quantified using several parameters ascertained from the experimental setup, velocity was obtained using Equation (6.3) where v is the impactor velocity, t is time and F is the impactor contact force at time t [38].

$$v(t) = v_i + g\,t\, - \int_0^t \frac{F(t)}{m}\,dt \tag{6.3}$$

Velocity is then used to find displacement using Equation (6.4) where δ is the impactor displacement at time t and δ_i is the impactor displacement from the reference location at time $t = 0$ [38].

$$\delta(t) = \delta_i + v_i\,t + \frac{g\,t^2}{2}\, - \int_0^t \left(\int_0^t \frac{F(t)}{m}\,dt\right)dt \tag{6.4}$$

Finally, velocity and displacement are used to find the energy absorbed in impact using Equation (6.5) where E_a is the energy absorbed [38].

$$E_a(t) = \frac{m(v_i^2 - v(t)^2)}{2} + m\,g\,\delta(t) \tag{6.5}$$

Metrics for the 30 J and 55 J tests will be discussed separately beginning with the discussion of the 30 J impact data. Figure 6.9 shows processed impact data for all 30 J impact experiments. Force Time data shows similar peak loads for all specimens.

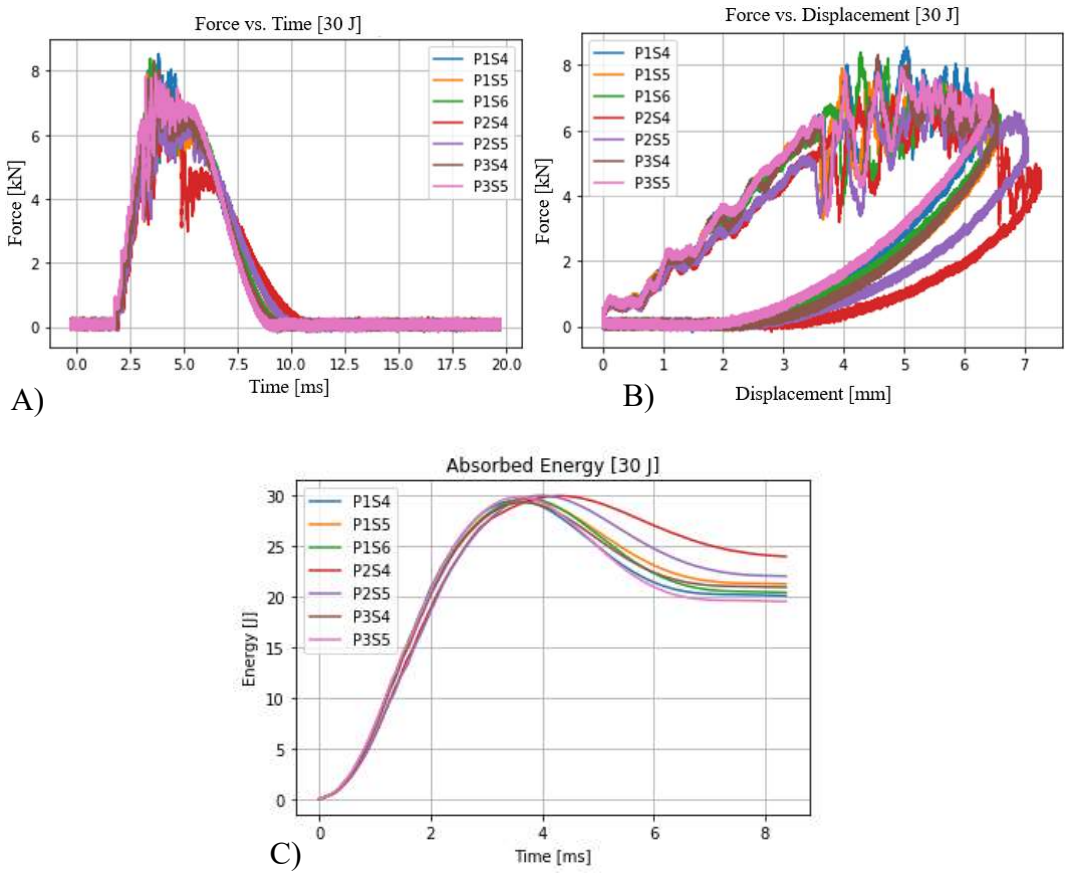

Figure 6.1 Processed impact data for 30 J impact specimens. A) Force vs Time B) Force vs Displacement C) Energy vs Time

Sample P2S4 shows a pronounced drop in force following the impactor event. This implies that the specimen experienced more damage than other specimens. This is also reflected in the Force Displacement, Figure 6.1 B), and Absorbed Energy plots Figure 6.1C). The higher energy absorption for P2S4 in Figure 6.1 C) supports the hypothesis that there is more damage in P2S4 than its counterparts. It can also be observed that P2S5 demonstrates

a higher displacement and higher energy absorption than both P1 - TWT or P3 - Cont specimens which follow similar trends. Surface level damage for these specimens will be discussed and further evaluated in Section Damage 6.4.2.

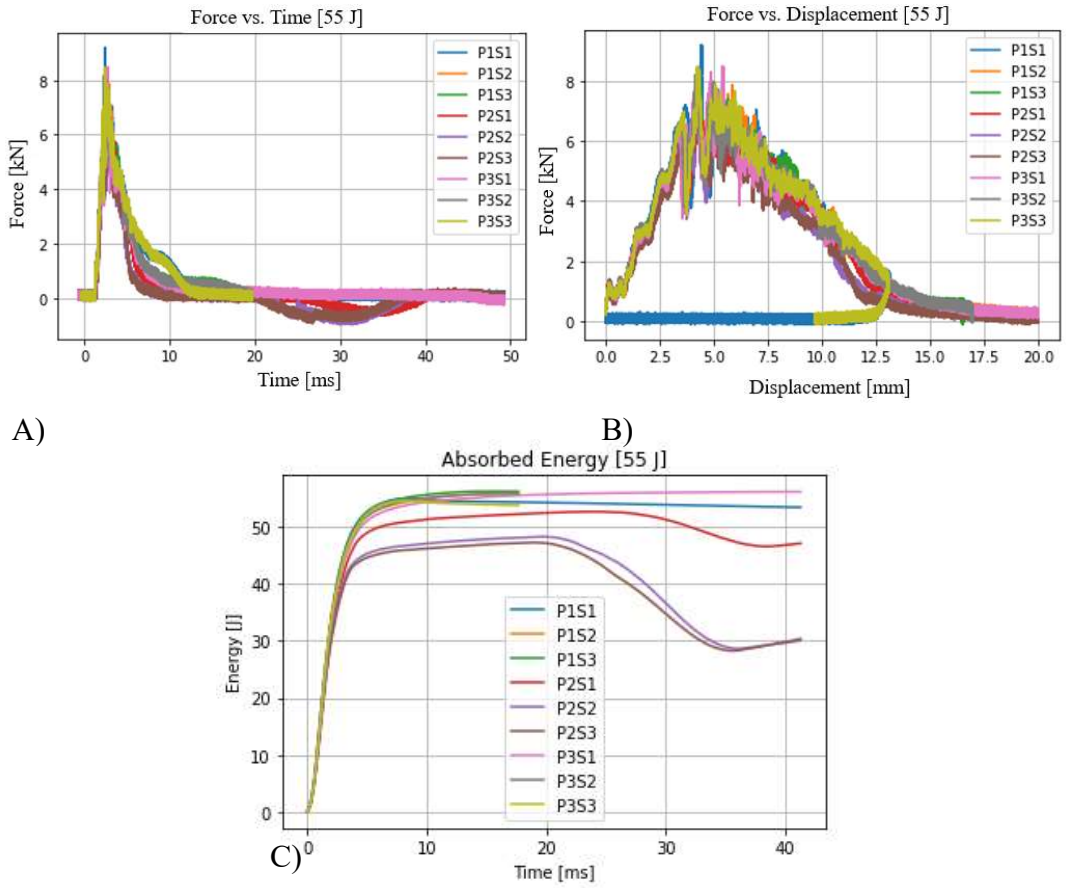

Figure 6.2 Processed impact data for 55 J impact specimens. A) Force vs Time B) Force vs Displacement C) Energy vs Time

Figure 6.2 exhibits processed impact data for the 55 J impacts. Similar to the 30 J impact data the P1 - TWT and P3 - Cont specimens performed similarly in force displacement, and absorbed energy. The P2 - WTW specimens demonstrated lower energy absorbed than both the P1 - TWT and P3 - Cont structures. All specimens experienced penetration at the 55 J energy level making conclusions on energy absorption curves difficult. But it can be hypothesized that the lower energy absorption of P2 - WTW suggests that the damage to

the P2 - WTW specimen is more localized when compared to P1 - TWT or P3 - Cont. A higher absorbed energy would correlate a greater extent of energy dispersal in the form of damage, which is evident in the impacted specimens and will be discussed in Section 6.4.2

6.4.2 Damage

Damage for composite specimens is a complicated matter, failure is progressive and evolves through many pathways. The primary causes of laminate failure are matrix cracking, delamination, and fiber breakage. Impact induced damage is dominated by fiber breakage and matrix cracking which is largely expressed as delamination between layers [3,5,7,9,12,14]. Pristine specimens for each panel type are shown in Figure 6.3.

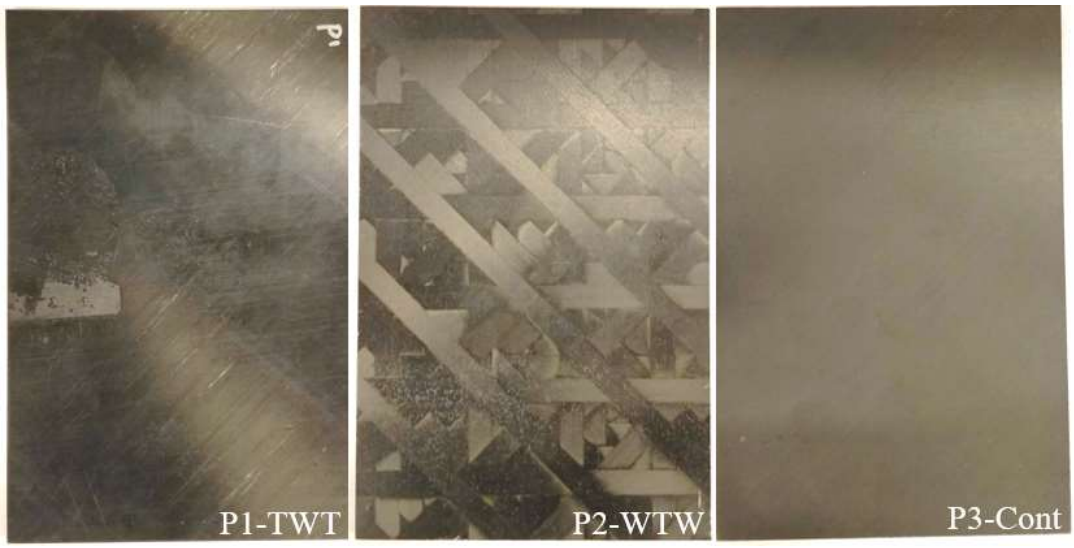

Figure 6.3 Pristine specimens, from left to right P1-TWT, P2-WTW, and P3-Cont

First 30 J impacted specimens will be discussed, impacted specimens shown in the figures below are formatted such that the image in the top left corner is the impact face, the bottom left is the back face, and the right is an angled view of the impacted specimen. Regions of surface damage are marked with a white outline to aid in identification. Comparing Figure 6.4 and Figure 6.6 it can be seen that surface level damaged areas are almost identical while P2 - WTW shows more localized damage with a smaller damaged footprint in Figure 6.5.

It is important to note that the response of the P2 - WTW configuration is dependent upon the impact location, Figure 6.7 shows a specimen from P2 - WTW subjected to a 30 J impact with a larger damage footprint. This is because the impactor struck in a region where a 45° tow was directly on the back face of the specimen, which resulted in a similar behavior to P1 - TWT and P3 - Cont which have the 45 layer unbounded, similar to what is seen in Figure 6.8. It is speculated that had the impact tip been larger the location dependent response would be mitigated. The current impactor tip is similar in size to the width of a tow, resulting in a strike that can be focused onto a single element, in this case a tow.

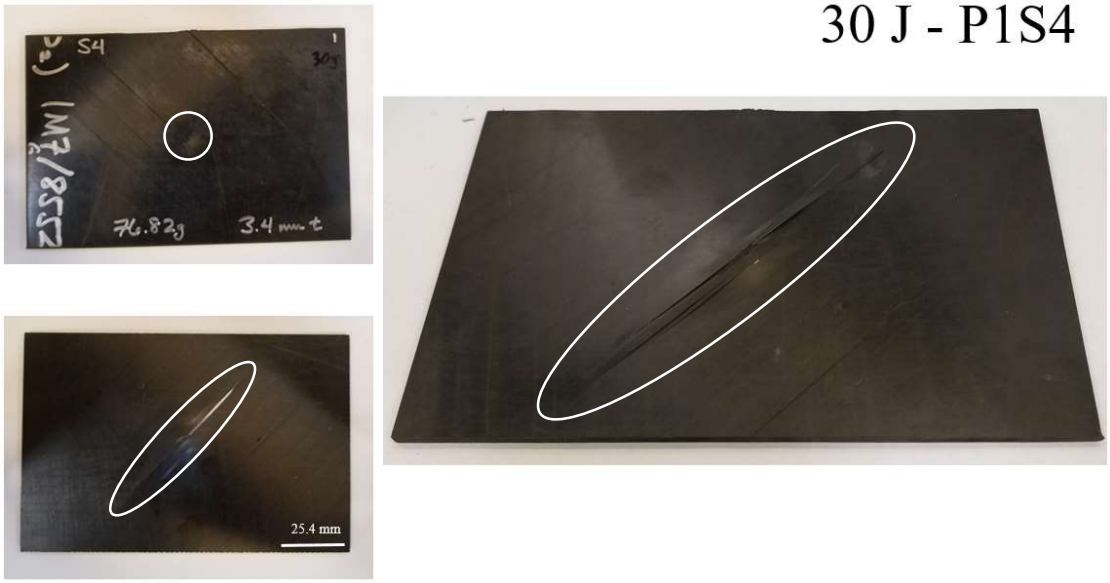

Figure 6.4 P1S4 30 J impacted specimen, top left: impact face, bottom left: back face, right side: angle view.

Figure 6.5 P2S4 30 J impacted specimen, top left: impact face, bottom left: back face, right side: angle view.

Figure 6.6 P3S4 30 J impacted specimen, top left: impact face, bottom left: back face, right side: angle view.

Figure 6.7 30 J impacted specimen, top left: impact face, bottom left: back face, right side: angle view.

The 55 J impact specimens suffered more damage than their 30 J counterparts, with most specimens experiencing penetration. Higher energy level impacts will result in a larger damage footprint until penetration or complete perforation occurs where fiber shearing will

occur which can potentially result in a smaller footprint depending upon the impact energy [3,5,7,9,12,14]. Comparing the 55 J impacted panels seen in the figures below it can be seen that the surface level damaged area of P2 - WTW is smaller than both P1 - TWT and P3 - Cont. It is difficult to breakdown the exact mechanisms of failure without further evaluation but the results shown here suggest that the P2 - WTW specimen has less of an ability to disperse the energies associated with impact. This potential lack may result in more extreme localized damage compared to the P1 - TWT and P3 - Cont setups which have a larger footprint inferring larger energy dispersal. Similar to what was seen in Figure 6.9 it is speculated that P2 - WTW would exhibit a similar response to both P1 - TWT and P3 - Cont had a tow been directly impacted.

Figure 6.8 P1S3 55 J impacted specimen, top left: impact face, bottom left: back face, right side: angle view.

Figure 6.9 P2S1 55 J impacted specimen, top left: impact face, bottom left: back face, right side: angle view.

Figure 6.10 P3S1 55 J impacted specimen, top left: impact face, bottom left: back face, right side: angle view.

6.4.3 Compression After Impact

Impacted specimens for the 30 J impact energy have been subjected to compression after impact testing to determine the compressive residual strength of an impacted specimen. This demonstrates the effect of an impact on the strength of a laminate. The panels are set

into a fixture and loaded as per ASTM standard D7137 at 1.25 mm/min. Failed specimens can be seen in Figure 6.10, they are oriented such that the bottom edge is the loading end. End crushing occurs at the unsupported loading end in all specimens except for the P3 30 J specimen where the specimen fails at the impact site. Pristine specimens were evaluated first and can be seen in Figure 6.11 with the 30 J impact specimens, the percent differences between impacted specimens and pristine specimens for P1, P2, and P3 are 0.5%, 20.6%, and 11.9% respectively. Tested coupons can be seen below, the 30 J specimen for the P3 – Cont configuration is the only specimen that failed at the location of impact damage.

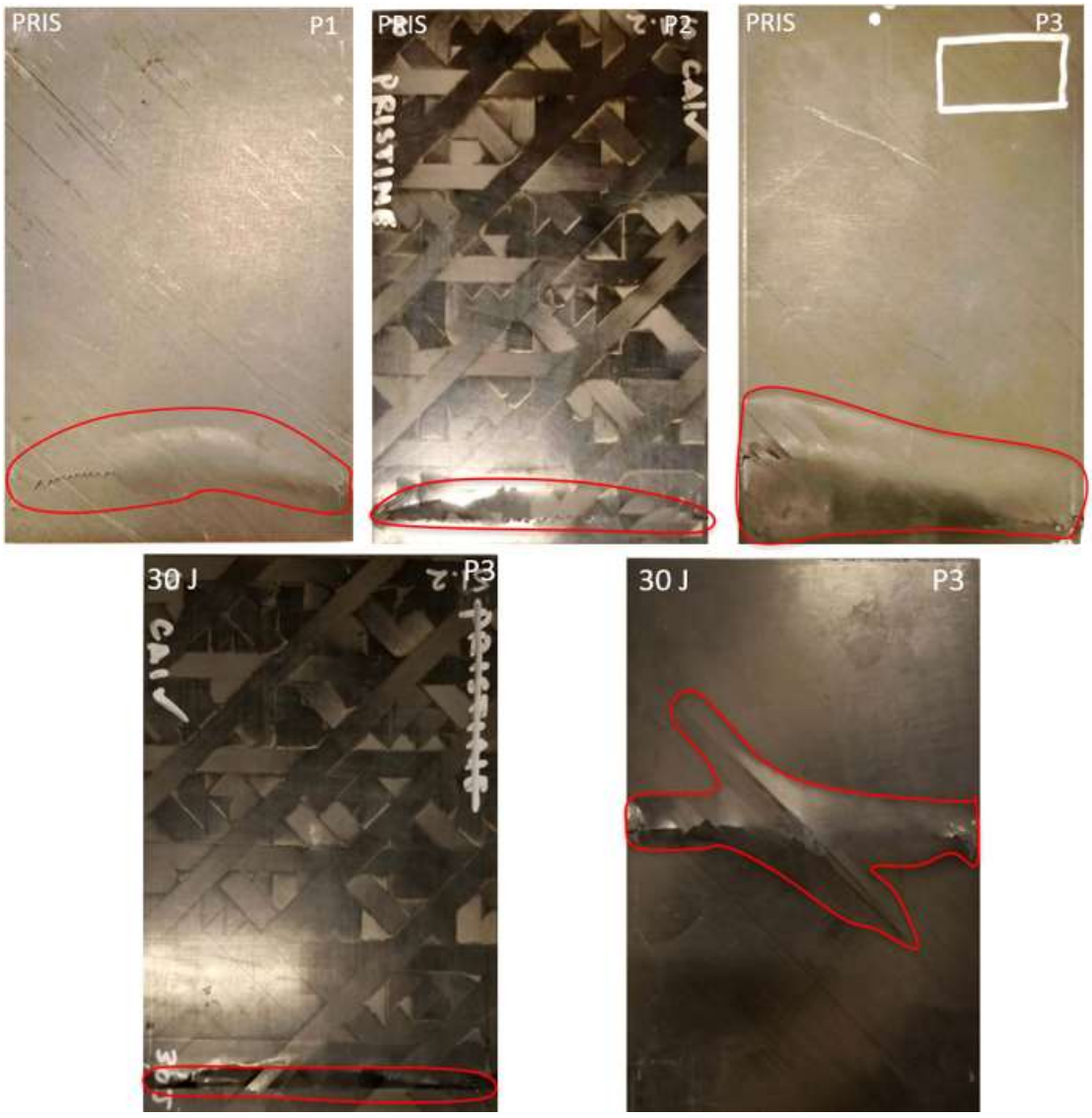

Figure 6.11 Compressive failure specimens. PRIS represents pristine specimens. The loading end is the bottom most edge of each specimen.

Because of restrictions on the quantity of samples used for this test all results should be taken as preliminary and should not be used to draw conclusive results as such, information will be presented, and no speculative conclusions will be made as to their results. The data shown in green in Figure 6.12 is pulled from a NIAR study on the properties of IM7/8552 Materials. The CAI results from the NIAR study are presented as a single averaged data point from 10 specimens [39].

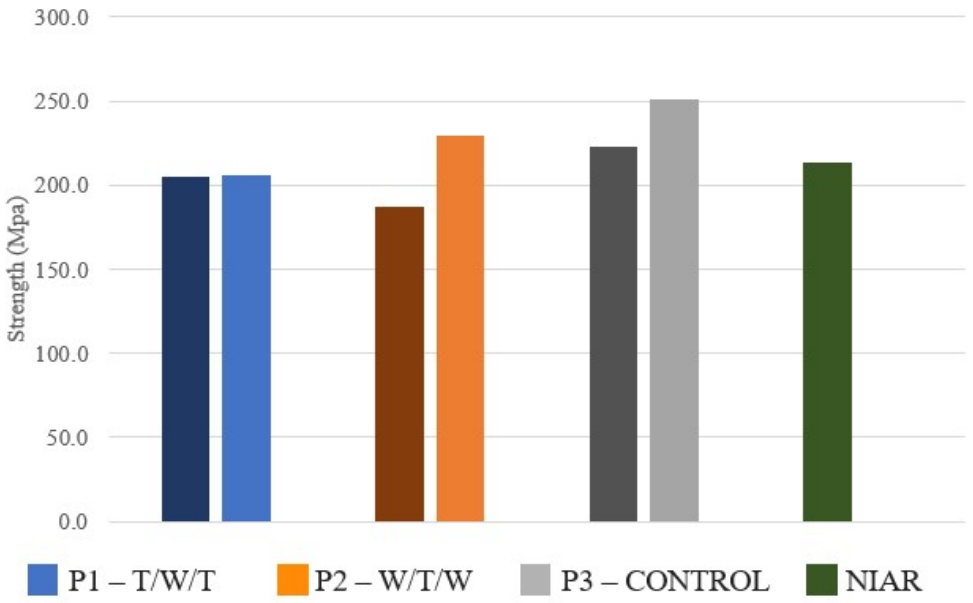

Figure 6.12 Compressive failure strength of pristine specimens (lighter) and 30 J impacted specimens (darker).

The compressed panels show regions on the side of the failed specimens as shown in Figure 6.13, while failure locations vary the overall the failure modes for each laminate are similar with some nuances. The P1 – TWT and P2 – WTW configurations seem to exhibit delamination at about roughly a third through the laminate. This could be due to the interface region but further analysis needs to be done with a larger sample size before definitive conclusions can be drawn on the performance and damage mechanisms associated with compression after impact failure modes.

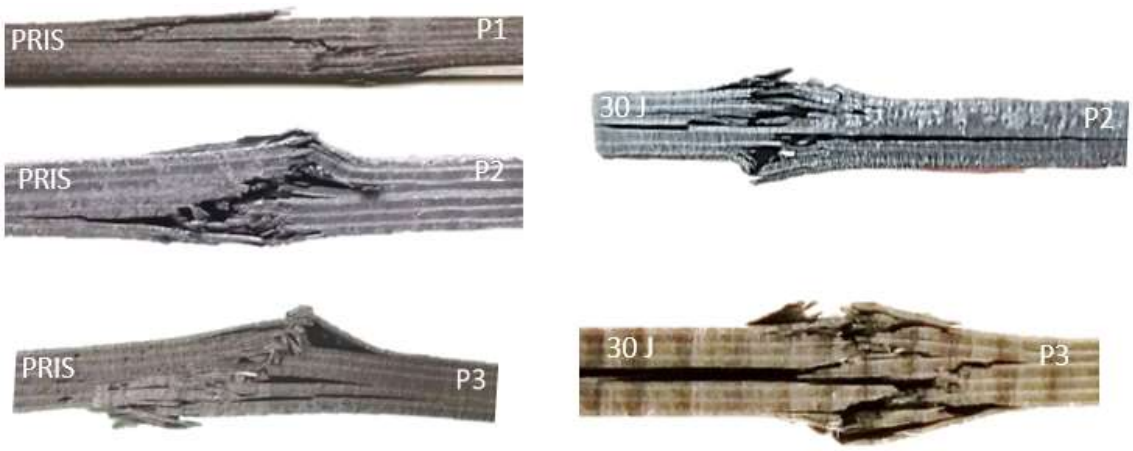

Figure 6.13 Failed specimens for compression testing.

6.5 SUMMARY AND CONCLUSION

The incorporation of pseudo-woven laminates with traditional laminates are used to significantly reduce the manufacturing time compared to producing fully pseudo-woven laminates. Low-velocity impacts are performed on two hybridized specimens and a control specimen. The hybridized configuration where PW laminates are on the outer surfaces, P2-WTW, exhibited a smaller damaged area than both the P1 - TWT and P3 - Cont configurations at the 30 J and 55 J impact energies. In addition, the laminates with PW on the outer surfaces absorbed higher energy by 15-20% for 30 J impact compared to other panels. Highest absorbed impact energy for the 55J impact is shared equally between the P1 - TWT and P3 - Cont configurations. Imaging techniques are needed to accurately quantify damage for impacted specimens and help to provide insight for damage mechanisms for the different configurations.

CHAPTER 7

HIGH VELOCITY IMPACT CHARACTERIZATION

7.1 ABSTRACT

An intermediary architecture of woven laminates and unidirectional laminates, referred to as pseudo-woven laminates, is proposed as an alternative hybridized structure to improve impact properties of composite laminates. Pseudo-woven laminates make use of an automated fiber placement (AFP) manufacturing process to produce a unique laminate architecture. These laminates are heterogeneous with spatially defined features where elasticity tensor is spatially variable unlike traditional composites. The heterogeneity is associated with interply locking and topological variations in the fiber orientations within individual layers resulting in multiple interfaces and an expanded design space.

In this study, carbon/epoxy pseudo-woven subassemblies are hybridized with traditional unidirectional layups to enhance impact and damage tolerance. Three different laminate configurations are assessed under high velocity impact according to ASTM D8101. During the experiments digital image correlation (DIC) and high-speed video were employed to evaluate the laminate's response.

7.2 SPECIMEN MANUFACTURING

In this study three 24 ply laminate configurations were manufactured using Hexcel IM7 G/8552-1 slit tapes, cured at 350 °F and 90 psi. Two of the laminates manufactured are a hybrid of traditionally manufactured laminates and PW laminates, one with PW laminates on the outer surfaces, P1, the other with PW laminates on the inside, P2. The other laminate is a traditionally manufactured control. The PW laminate components manufactured are 4S-DS0-CS3 and INV 4S-DS0-CS3. Their AFP notations are [45, 90, -45, 0][x000x000]n[1/4"][0] and [0, -45, 90, 45][x000x000]n[1/4"][0] respectively.

The first hybrid configuration, P1 – TWT, is a panel with two PW laminates sandwiched by two traditional laminates on each side. P1 has a stacking sequence of $[(45/90/-45/0)_2/4S\text{-}DS0\text{-}CS3/INV4S\text{-}DS0\text{-}CS3/(0/-45/90/45)_2]$. The other hybridized PW panel, P2 – WTW, is 2 traditional laminates sandwiched by 2 PW laminates on each side, called P2 – WTW. The stacking sequence for P2 – WTW is $[4S\text{-}DS0\text{-}CS3_2/45/90/-45/0/0/-45/90/45/INV4S\text{-}DS0\text{-}CS3_2]$. The control laminate's stacking sequence is $[45/90/-45/0]_{3s}$ and is referred to as P3 – CONT.

Panels made for this study were constructed using two different AFP machines, multiple panels of P1 - TWT, P2 - WTW, and P3 - CONT were made at the McNAIR Center University of South Carolina while one P1 - TWT panel was made at the NASA Langley Research Center.

7.2.1 Specimen Preparation

Laminates were laid up into oversized sheets and trimmed to the 12" by 12" specimen dimensions specified in ASTM Standard D8101 using a waterjet. Edges were

finished with hand sanding to reduce edge effects resulting from waterjet cutting. A circular hole pattern was added using a 4 flute carbide endmill with a CNC machine to ensure a proper fit on the test fixture. Care was taken as to not overheat the specimen during milling and degrade the matrix. After specimens were trimmed and brought into specifications a coarse speckle pattern, Figure 7.1, was added onto the backside of the laminate. The speckle pattern was applied with spray paint using a stencil for each specimen.

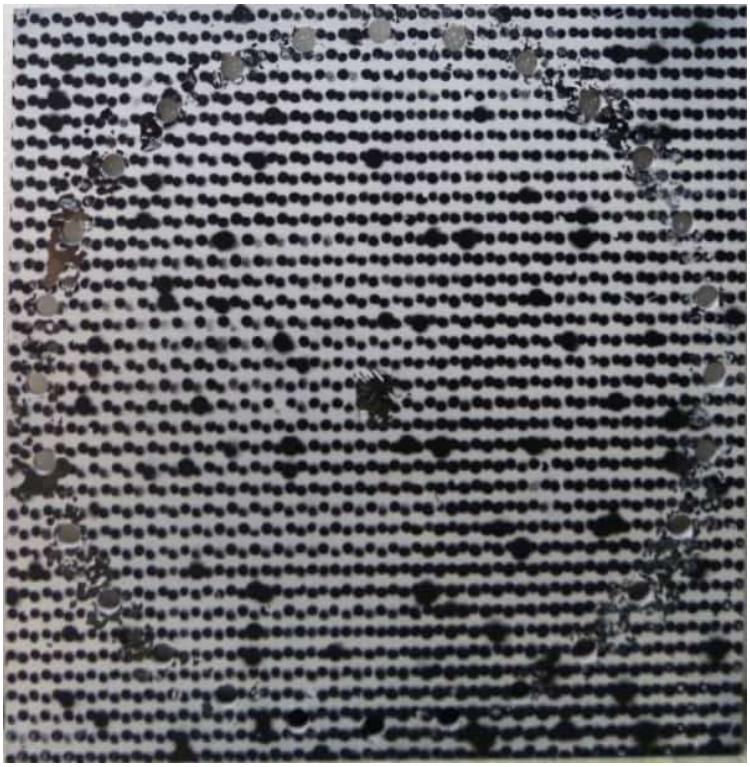

Figure 7.1 A typical example of the speckle pattern used in experimentation.

7.3 EXPERIMENTAL METHODOLOGY

Impact tests were performed in accordance to the ASTM Standard D8101 at the NASA Glenn Research Center Ballistic Impact Lab. In this experiment, composite flat panels were impacted in the normal direction with hemispherical aluminum projectiles, technical drawing shown in Figure 7.2, weighing approximately 51 g each. Specimens were

clamped to the rear frame of the test fixture seen in Figure 7.3 by a circular frame to ensure a rigid connection with the rear frame [40].

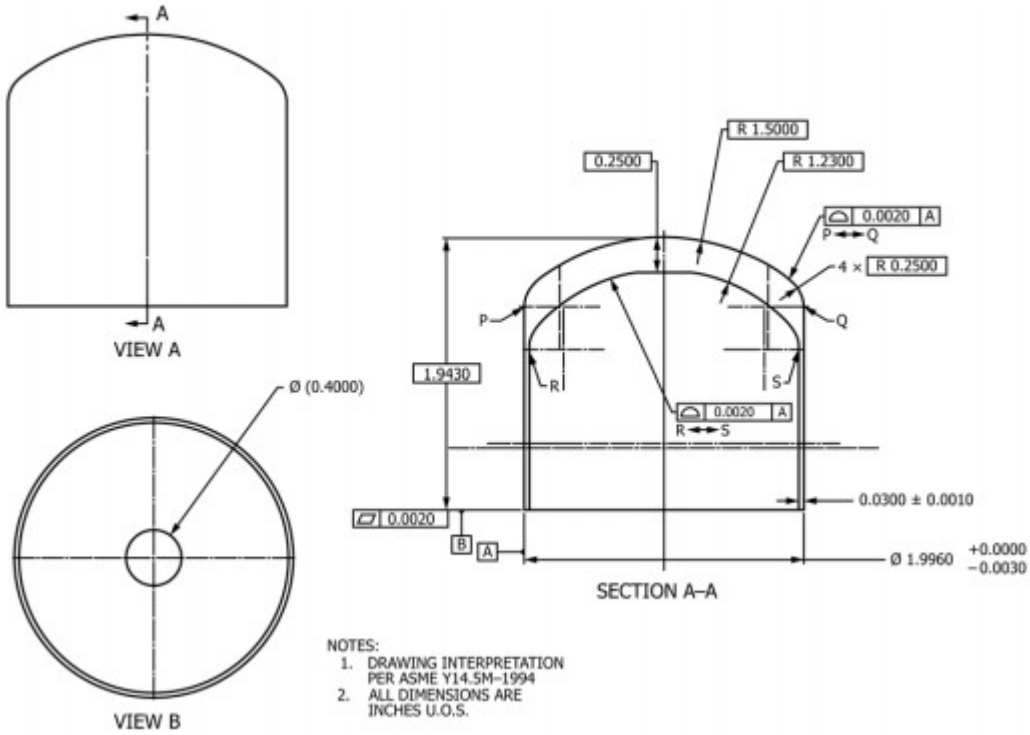

Figure 7.2 The technical drawing of the impactor used [40].

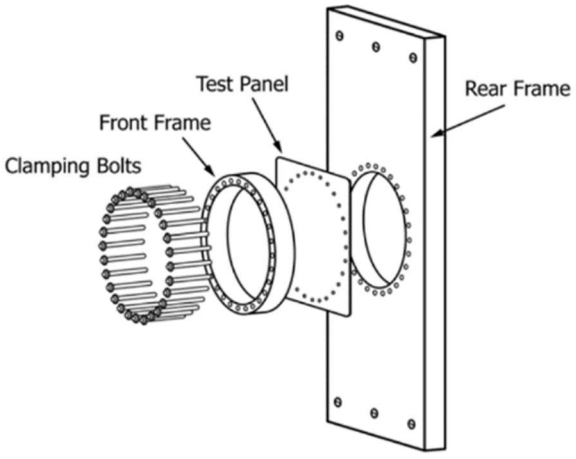

Figure 7.3 Exploded view of the test fixture [40].

Projectiles were fired at the panel using a single stage gas gun, impactor velocities were determined using a high speed camera setup and TEMA motion analysis software by

tracking a speckle pattern on the impactor. The camera setup used for data acquisition is shown in Figure 7.4. Multiple cameras were used to collect data from different viewpoints each with a different purpose. A single camera on the side of the test housing was used to capture projectile's impact and rebound velocity. A Camera at the front of the impact housing, above the projectile barrel, was used to record the strike face. Camera pairs on the backside of the test housing were used to capture backside displacement by acquiring stereoscopic videos of the speckle pattern used to derive displacement using ARAMIS.

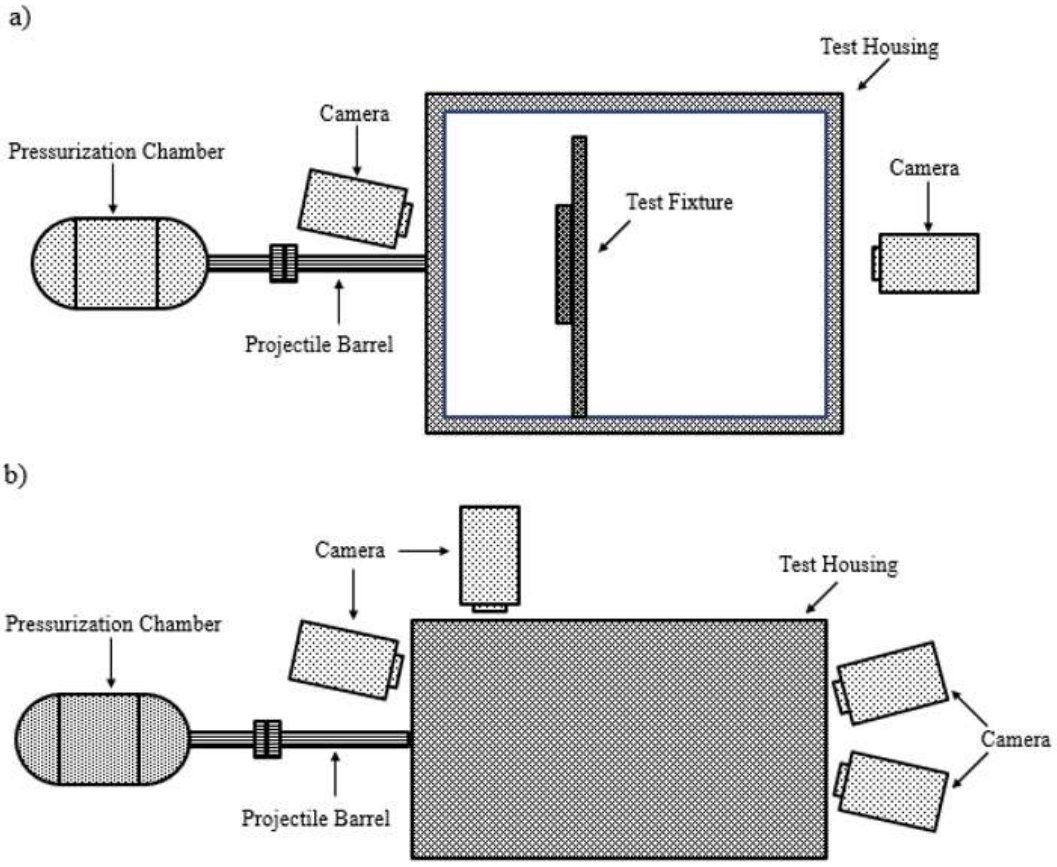

Figure 7.4 Multiple angles of the experimental camera setup. a) side view b) top view.

7.4 RESULTS AND DISCUSSION

In this section, kinetic energy loss, $V_{50,}$ and displacement are used to assess the impact response of the laminate configurations. Due to the costs associated with manufacturing the sample size for the impacted specimens is low, this results in one sample per target impact velocity. Five velocities were targeted for this series of tests, 250 ft/sec, 300 ft/sec, 350 ft/sec, 375 ft/sec, and 400 ft/sec. Table 7.1 shows a summary of unprocessed test results. This data is used to tabulate data discussed in the sections below.

Table 7.1 A table including the target impact velocities, test IDs, panel descriptions, projectile masses, impact velocities, rebound velocities, exit velocities, and results. 'Con' means that the projectile was contained while 'pen' means that the projectile penetrated the specimen.

Targeted Impact Velocity	Test	Panel Description	Projectile Mass (g)	Impact Vel (ft/s)	Rebound Vel (ft/s)	Exit Vel (ft/s)	Result
250	LVG1305	P1 - TWT	51.89	233.9	-100.7	-	con
	LVG1301	P2 - WTW	49.84	256.1	-102.7	-	con
	LVG1326	P3 - CONT	52.16	257.3	-109.0	-	con
300	LVG1302	P1 - TWT	52.03	307.8	-133.8	-	con
	LVG1297	P2 - WTW	51.87	292.5	-94.0	-	con
	LVG1306	P3 - CONT	52.02	298.5	-115.3	-	con
350	LVG1303	P1 - TWT	51.99	352.7	-114.1	-	con
	LVG1298	P2 - WTW	52.22	359.2	-96.4	-	con
	LVG1307	P3 - CONT	52.15	351.6	-109.3	-	con
375	LVG1304	P1 - TWT	51.94	369.9	-123.0	-	con
	LVG1300	P2 - WTW	52.29	367.7	-102.6	-	con
	LVG1308	P3 - CONT	52.05	372.3	-	129.8	pen
400	LVG 1327	P1 - TWT	50.33	395.9	-151.0	-	con
	LVG1299	P2 - WTW	51.8	392.2	-	78.3	pen

7.4.1 V_{50} velocity

The V_{50} for the different composite configurations is calculated with Equation (7.1). Where V_{RM} is the maximum impact velocity at which the laminate still rebounded the projectile. The variable V_P is the lowest velocity at which penetration occurred.

$$V_{50} = \frac{V_{RM} + V_P}{2} \tag{7.1}$$

Table 7.2 shows the computed V_{50} values, with P1 - TWT being greater than 392.2 ft/s as the laminate did not penetrate at that impact velocity. The V_{50} of P1 - TWT is approximately 8.5% higher than the V_{50} of P3 – CONT. The V_{50} of P2 - WTW configuration is 5.5% higher than P3 - CONT. This would suggest that the incorporation of PW laminate architecture increases the velocity required to cause penetration.

Table 7.2 Calculated V_{50} data

Laminate	V_{50} m/s (ft/s)
P1 – TWT	> 392.20
P2 - WTW	381.05
P3 - CONT	361.95

7.4.2 Kinetic energy loss

Residual kinetic energy was calculated following with Equation (7.2) where E_r is the residual kinetic energy, computed from projectile mass, M, and the residual velocity, V_r.

$$E_r = \frac{MV_r^2}{2} \tag{7.2}$$

Impact Kinetic energy was calculated using Equation (7.3) from ASTM standard D8101. Impact kinetic energy, E_i, is computed from the projectile mass, M, and the projectile impact velocity, V_i.

$$E_i = \frac{MV_i^2}{2} \tag{7.3}$$

Kinetic energy loss was calculated as demonstrated in ASTM standard D8101 with Equation (7.4) where loss in kinetic energy of the projectile as a result of impact is computed.

$$E_a = E_i - E_r \tag{7.4}$$

Specimens were impacted at 5 velocities resulting in clusters around the 150 J, 220 J, 300 J, 330 J, and 360 J impact kinetic energy levels. Loss in kinetic energy and impact kinetic energy are plotted against one another in Figure 7.5. Overall, P2 - WTW shows the highest loss in kinetic energy at each impact kinetic energy. The P1 – TWT and P3 – Cont configurations exhibit similar losses in kinetic energy for all clusters except the 150 J cluster where P1 absorbs the least. It is important to note that penetration occurs at higher impact kinetic energies than the control specimen.

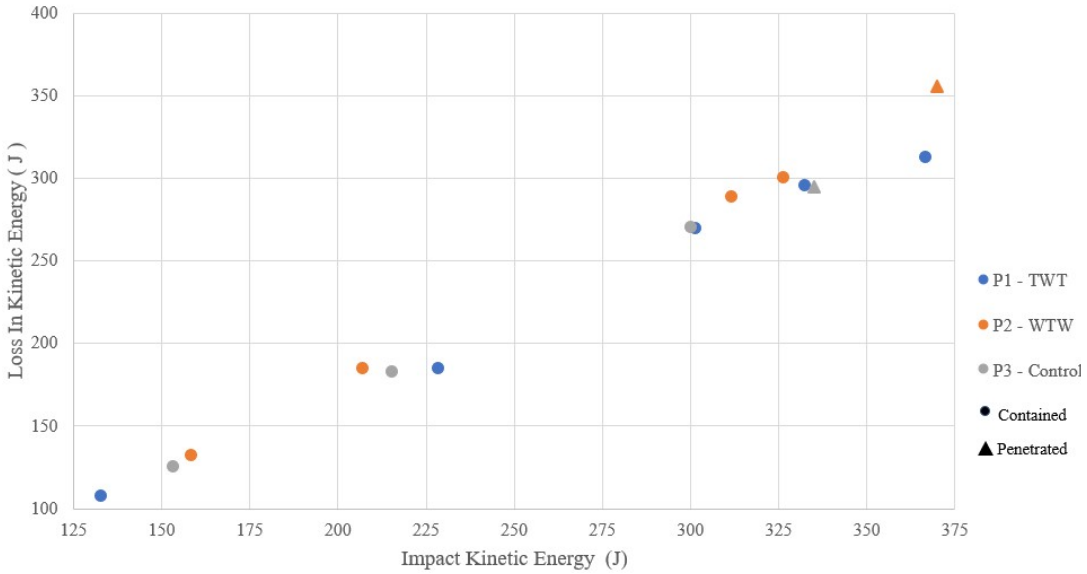

Figure 7.5 Residual Kinetic Energy vs Impact Kinetic Energy.

To reduce the variation of the energy absorbed due to discrepancies in impact kinetic energies E_a/E_i is used to normalize absorbed kinetic energy. Normalized absorbed

kinetic energy is shown for different target impact velocities in Figure 7.6, and supports the takeaways stated above. P2 – WTW shows higher normalized absorbed kinetic energy than the two other configurations at all energy levels. The P3 – Cont has higher energy absorption than P1 – TWT until it experiences penetration at the 375 ft/sec band. The low normalized absorbed kinetic energy for the P3 – Cont specimen and high V_{50} would imply that the P1 – TWT specimen is redirecting the impactor without taking on damage. To draw a conclusive result imaging needs to be used to see the extend of damage in the specimens, without it statements made are merely speculation.

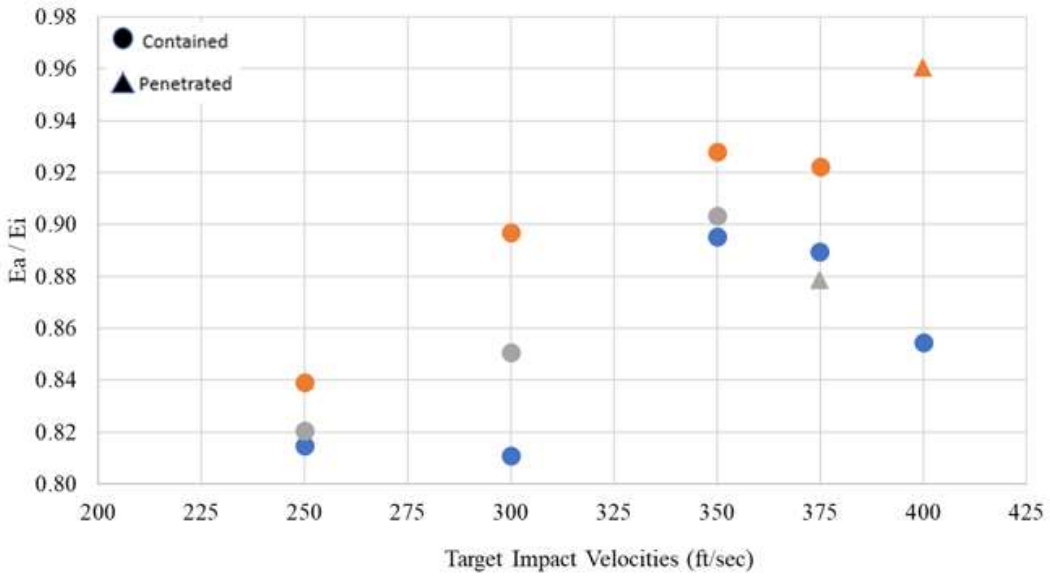

Figure 7.6 Ea/Ei for different target impact velocities.

Peak displacement is represented in the impact event in Figure 7.7. Peak displacement was determined using a displacement plot output in ARAMIS, seen in Figure 7.8. This plot uses points along a line drawn through the center of the specimen, this line can be seen in Figure 7.7. When all points show peak displacement, as shown by the red x's in Figure 7.8, the corresponding video frame is extracted and used as peak displacement. Discontinuities in the displacement data are due to the paint breaking from

the backside of the specimen during the impact event. The breakage of the speckle pattern reduces the accuracy of displacement data making it difficult to truly draw a conclusion on displacement because of the nature of impact some of the contours have an artificially high displacement due to specimen and paint breakage. This value does not represent the behavior of the laminate but rather a small failed portion skewing the data.

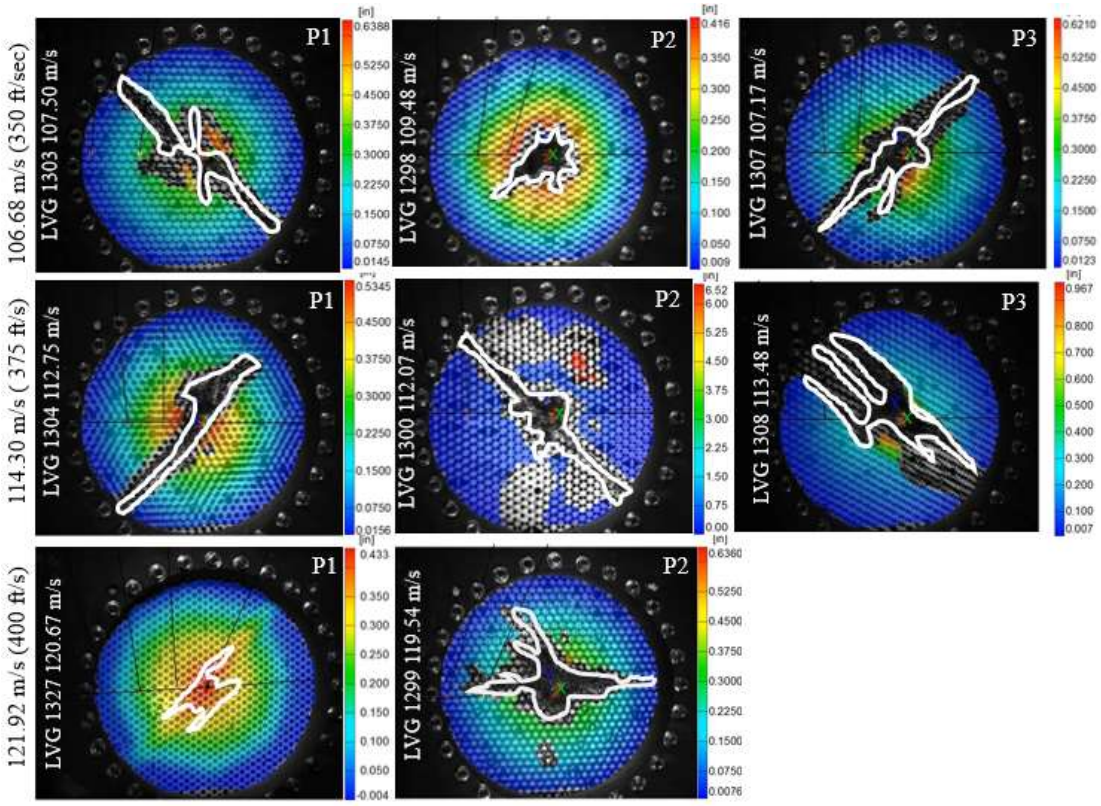

Figure 7.7 DIC contours and outlined backside surface damage for three different target impact velocities. Displacement contour units are in inches.

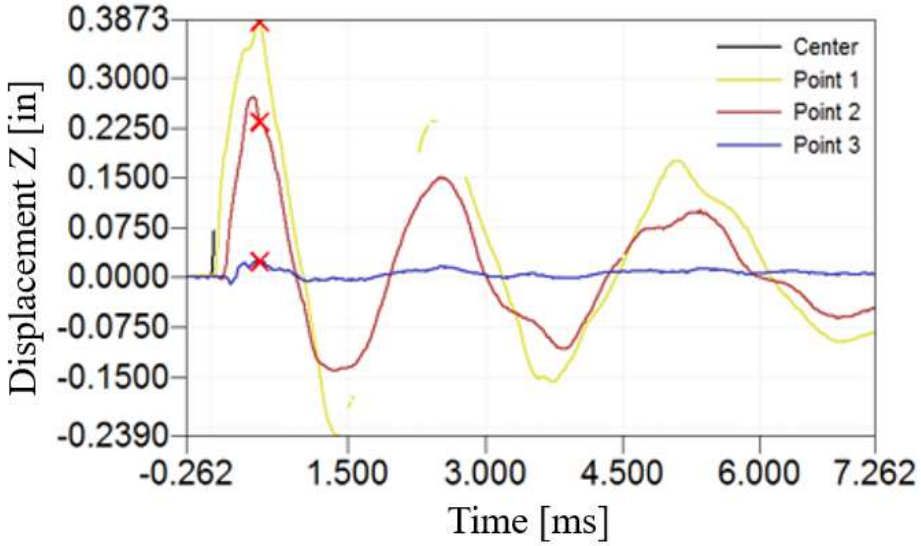

Figure 7.8 The points used to map displacement and detect peak displacement, shown by red x's, for test LVG 1297

The displacement along the cross-sectional area of specimens at peak displacement at the 300 ft/sec impact velocity are given in Figure 7.9. Displacement data was taken from the line discussed previously in this section, referred to as section 0. Displacement cross sections all exhibit similar behavior for different target impact velocities. Figure 7.9 shows the displacement section for a 300 ft/sec impact. Displacement along the section 0 at peak displacement shows P3 - CONT with the highest displacement while P1 - TWT has the lowest. All specimens show a gap where displacement data was lost due to the impactor breaking the speckle pattern from the backside of the specimen. Experimental data suggests that the back face deflection of PW hybridized configurations are lower than the P3 – Control.

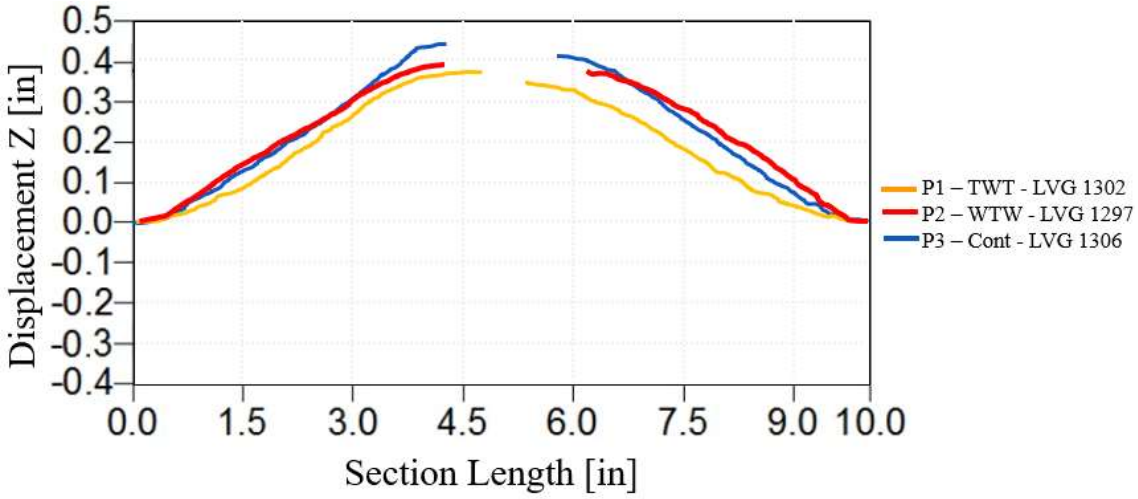

Figure 7.9 A superimposed image of displacement along the section 0 taken from the 300 ft/sec impact velocity. The orange, red, and blue lines represent P1 – TWT, P2 – WTW, and P3 – CONT respectively

7.4.3 Damage footprint

Superimposed onto the displacement contours given in Figure 7.7 is a white outline indicating surface damage on the back face of the specimen. From this it can be said that hybridized PW laminates sustain a smaller damaged surface area at each impact velocity.

It is interesting to note that both the P1 - TWT and P2 - WTW configurations demonstrate smaller damaged surface area than the traditional configuration for each impact velocity. Typical failure modes for these laminates can be seen in Figure 7.10, independent of laminate architecture the back face damage of each specimen for the different impact velocities are similar. Delamination on the backside manifests in the 45° layers in each of the configurations, damage becomes more pronounced in the form of the extent of back face delamination as the impactor velocity increases.

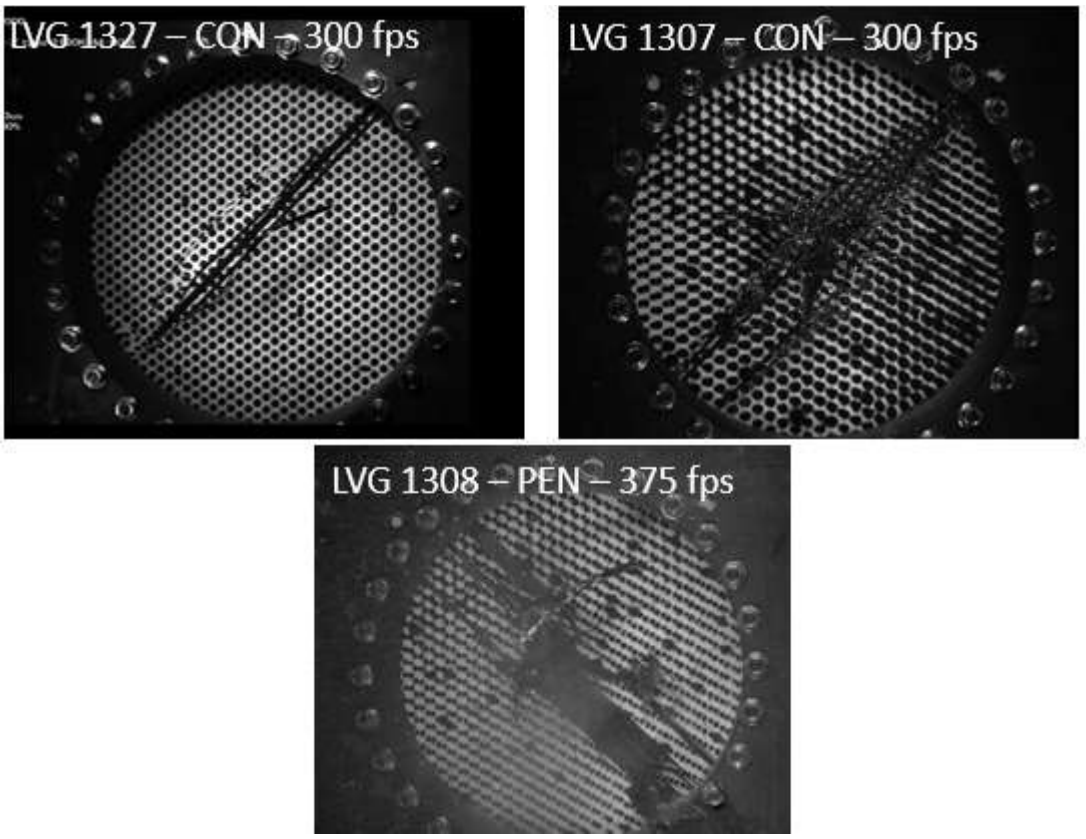

Figure 7.10 Typical damage modes for HVI specimens

7.5 SUMMARY AND CONCLUSION

Three 24 ply carbon/epoxy hybrid pseudo-woven laminate configurations are manufactured in this study using automated fiber placement. One with semi-woven

laminate on the inside (named as P1-TWT), second with semi-woven laminate on the outer surfaces (named as P2-WTW) and third quasi-isotropic control laminate $[45/90/-45/0]_{3s}$ named as P3-CONT. High velocity impact tests are conducted according to the ASTM D8101 standard. The hybridized configuration P1-TWT show a V50, 8.5% greater than the control. Results suggest that the P2 – WTW absorbs the most energy for different impact velocities shown in both normalized and non normalized absorbed kinetic energy calculations. Experimental results indicate reduction in back face damage and back face deflection for the hybridized laminates compared to the control layups. Further investigation using nondestructive evaluation is required to better understand the damage mechanisms experienced by the different laminate configurations.

CHAPTER 8

CONCLUSIONS AND FUTURE WORK

Traditionally, composite structures are made utilizing one or both of two material types, unidirectional and woven materials. These different material types are the fundamental building block of composite manufacturing with each holding their own benefits. PW laminates are manufactured through a fundamental change to the AFP manufacturing process, moving away from the ply-by-ply manufacturing concept where tows are laid adjacent to one another to a manufacturing technique that skips tows to make a woven like structure using unidirectional materials. This thesis focuses on the characterization of pseudo-woven laminates through experimental methods. Warpage, uniaxial tension, low velocity impact, and high velocity impact are used for the characterization of these pseudo-woven laminates. Experimental results indicate that Pseudo-woven laminates, due to their unique fiber architecture, show a reduction of hygrothermally induced warpage by up to 58% when compared with traditional asymmetrical laminates. This is likely caused by spatial variations in the stacking sequence resulting in variation in the **B** matrix components of the ABD matrix.

A variety of PW laminate configurations are manufactured and subjected to uniaxial tension for this study, results suggest that PW laminates perform comparably to conventionally manufactured composite laminates possessing similar strength and similar and often show higher strains compared to conventional laminates. While strength remains

the same the difference in strains appear to diminish with increasing PW laminate thickness where stacked PW laminates are shown to have small percent differences when compared to traditionally manufactured laminates with the exception of E_{xx} strains. The variation in average peak stress, average E_{yy} strain, average E_{xx} strain and average stiffness between the PW and control configuration is 2.9 %, 0.9%, 10.6% and 2.6% respectively.

The utilization of these traditionally manufactured composite architectures and PW laminates in a hybrid architecture allows the laminate to have high stiffness while potentially possessing higher damage tolerance and reducing manufacturing time compared to a wholly PW structure. Two structurally hybridized PW configurations are subjected to low velocity impact. The second hybrid configuration where PW laminates are on the outer surfaces, P2 - WTW, exhibited a smaller damaged area than both the P1 - TWT and P3 - Cont configurations at the 30 J and 55 J impact energies. In addition, the P2 -WTW configuration absorbed higher energy by 15-20% for the 30 J impact compared to other panels. Highest absorbed impact energy for the 55J impact is shared equally between the P1 - TWT and P3 – Cont configurations. These results suggest that the incorporation of PW laminates into a structure can improve impact properties with respect to surface level damaged area and energy absorption.

High velocity impact tests have shown that the hybridized configuration P1 - TWT show a V50, 8.5% greater than the control. Results suggest that the P2 – WTW absorbs the most energy for different impact velocities shown in both normalized and non-normalized absorbed kinetic energy calculations. Experimental results indicate reduction in back face damage and back face deflection for the hybridized laminates compared to the control layups.

Pseudo-woven laminates show promise, exhibiting similar strength compared to traditional laminates while demonstrating reduced hygrothermal warpage. Impact studies suggest that the incorporation of the PW laminate architectures can reduce surface level damage footprint while increasing the energy absorbed during impact as shown in low velocity experiments. High velocity experiments suggest that the incorporation of PW laminates into a composite structure can increase V_{50}, and effect kinetic energy absorption while slightly reducing overall deflection compared to the control layup. Future works would benefit from revisiting these experiments presented in this thesis with a larger sample size to provide statistically significant results and accurately assess the effect of the incorporation or sole use of PW laminates in uniaxial tension and impact scenarios.

REFERENCES

[1] Vakili Rad C, Thomas FD, Seay B, van Tooren MJL, Sockalingam S. Manufacturing and characterization of novel clutch non-conventional fiber-reinforced composite laminates. Compos Struct 2019;215. https://doi.org/10.1016/j.compstruct.2019.02.018.

[2] Cantwell W, Curtis P, Morton J. Post-impact fatigue performance of carbon fibre laminates with non-woven and mixed-woven layers. Composites 1983;14:301–5. https://doi.org/10.1016/0010-4361(83)90020-4.

[3] Cantwell WJ, Morton J. The impact resistance of composite materials - a review. Composites 1991;22:347–62. https://doi.org/10.1016/0010-4361(91)90549-V.

[4] Aktaş M, Atas C, Içten BM, Karakuzu R. An experimental investigation of the impact response of composite laminates. Compos Struct 2009;87:307–13. https://doi.org/10.1016/j.compstruct.2008.02.003.

[5] Cantwell WJ, Morton J. Detection of impact damage in CFRP laminates. Compos Struct 1985;3:241–57. https://doi.org/10.1016/0263-8223(85)90056-X.

[6] Xu S, Chen PH. Prediction of low velocity impact damage in carbon/epoxy laminates. Procedia Eng 2013;67:489–96. https://doi.org/10.1016/j.proeng.2013.12.049.

[7] Damage in Laminated Composites Due to Low Velocity Impact-1998-Naik-1232-63.pdf n.d.

[8] Wehbe R. Modeling Of Tow Wrinkling In Automated Fiber Placement Based On Geometrical Considerations. Theses Diss 2017:121.

[9] Evci C, Gülgeç M. An experimental investigation on the impact response of composite materials. Int J Impact Eng 2012;43:40–51. https://doi.org/10.1016/j.ijimpeng.2011.11.009.

[10] Rozant O, Bourban PE, Månson JAE. Drapability of dry textile fabrics for stampable thermoplastic preforms. Compos Part A Appl Sci Manuf 2000;31:1167–77. https://doi.org/10.1016/S1359-835X(00)00100-7.

[11] Ansar M, Xinwei W, Chouwei Z. Modeling strategies of 3D woven composites: A review. Compos Struct 2011;93:1947–63. https://doi.org/10.1016/j.compstruct.2011.03.010.

[12] Delfosse nonpenetrating impact behavior of CFRP at low and intermediate velocites.pdf n.d.

[13] Lopes CS, Seresta O, Coquet Y, Gürdal Z, Camanho PP, Thuis B. Low-velocity impact damage on dispersed stacking sequence laminates. Part I: Experiments. Compos Sci Technol 2009;69:926–36. https://doi.org/10.1016/j.compscitech.2009.02.009.

[14] Sebaey TA, González E V., Lopes CS, Blanco N, Costa J. Damage resistance and damage tolerance of dispersed CFRP laminates: Effect of ply clustering. Compos Struct 2013;106:96–103. https://doi.org/10.1016/j.compstruct.2013.05.052.

[15] Wang SX, Wu LZ, Ma L. Low-velocity impact and residual tensile strength analysis to carbon fiber composite laminates. Mater Des 2010;31:118–25. https://doi.org/10.1016/j.matdes.2009.07.003.

[16] Aluko O, Gowtham S, Odegard GM. The effect of chirality and strain rate on mechanical properties of carbon nanotube (CNT) and CNT/epoxy composite. 33rd Tech Conf Am Soc Compos 2018 2018;2:780–91. https://doi.org/10.12783/asc34/31365.

[17] Saleh MN, Yudhanto A, Lubineau G, Soutis C. The effect of z-binding yarns on the electrical properties of 3D woven composites. Compos Struct 2017;182:606–16. https://doi.org/10.1016/j.compstruct.2017.09.081.

[18] Potluri P, Hogg P, Arshad M, Jetavat D, Jamshidi P. Influence of fibre architecture on impact damage tolerance in 3D woven composites. Appl Compos Mater 2012;19:799–812. https://doi.org/10.1007/s10443-012-9256-9.

[19] Chou S, Chen HC, Chen HE. Effect of Weave Structure on Mechanical Fracture-Behavior of 3-Dimensional Carbon-Fiber Fabric Reinforced Epoxy-Resin Composites. Compos Sci Technol 1992;45:23–35.

[20] Greenhalgh E, Hiley M. The assessment of novel materials and processes for the impact tolerant design of stiffened composite aerospace structures. Compos Part A Appl Sci Manuf 2003;34:151–61.

[21] Greenhalgh E, Hiley M. The assessment of novel materials and processes for the impact tolerant design of stiffened composite aerospace structures. Compos Part A Appl Sci Manuf 2003;34:151–61. https://doi.org/10.1016/S1359-835X(02)00188-4.

[22] Mouritz AP. Review of z-pinned composite laminates. Compos Part A Appl Sci Manuf 2007;38:2383–97. https://doi.org/10.1016/j.compositesa.2007.08.016.

[23] Francesconi L, Aymerich F. Effect of Z-pinning on the impact resistance of composite laminates with different layups. Compos Part A Appl Sci Manuf 2018;114:136–48. https://doi.org/10.1016/j.compositesa.2018.08.013.

[24] Zhang X, Hounslow L, Grassi M. Improvement of low-velocity impact and compression-after-impact performance by z-fibre pinning. Compos Sci Technol 2006;66:2785–94. https://doi.org/10.1016/j.compscitech.2006.02.029.

[25] Apichattrabrut T, Ravi-Chandar K. Helicoidal composites. Mech Adv Mater Struct 2006;13:61–76. https://doi.org/10.1080/15376490500343808.

[26] Ginzburg D, Pinto F, Iervolino O, Meo M. Damage tolerance of bio-inspired helicoidal composites under low velocity impact. Compos Struct 2017;161:187–203. https://doi.org/10.1016/j.compstruct.2016.10.097.

[27] Cheng L, Thomas A, Glancey JL, Karlsson AM. Mechanical behavior of bio-inspired laminated composites. Compos Part A Appl Sci Manuf 2011;42:211–20. https://doi.org/10.1016/j.compositesa.2010.11.009.

[28] Grunenfelder LK, Suksangpanya N, Salinas C, Milliron G, Yaraghi N, Herrera S, et al. Bio-inspired impact-resistant composites. Acta Biomater 2014;10:3997–4008. https://doi.org/10.1016/j.actbio.2014.03.022.

[29] Nagelsmit MH, Kassapaoglou C, Gürdal Z. Executive summary A New Fibre Placement Architecture for Improved Damage Tolerance. 2010.

[30] Nagelsmit MH. Fibre Placement Architectures for Improved Damage Tolerance. 2013. https://doi.org/http://doi.org/10.4233/uuid:f8c8ad4e-5d52-4bfd-8449-2748bad26673.

[31] Zheng W, Kassapoglou C, Zheng L. Tailoring of AP-PLY composite laminates for improved performance in the presence of delaminations. Compos Struct 2019;211:89–99. https://doi.org/10.1016/j.compstruct.2018.12.015.

[32] Nagelsmit MH, Kassapaoglou C, Gurdal Z. AP-PLY: A New Fibre Placement Architecture for Fabric Replacement, SAMPE Journal; 2011, p. 36–45.

[33] 3D Systems. Sense 3D Scanner | Technical Specifications 2017.

[34] Soltani SA, Vali H, Bhasin A, Vo D, Nguyen T, Rao AK, et al. Effect of nonwoven fabric type and stacking sequence on distortion of flat panels made of out-of-autoclave carbon-fiber epoxy prepreg. SAMPE Tech Conf Proc 2013.

[35] Soltani SA, Keshavanarayana S, Bhasin A, Krishnamaraja MT, Saremi F. Effect of fabric weave type on distortion of flat panels made of out-of-autoclave carbon-fiber epoxy prepreg. SAMPE Tech Conf Proc 2013.

[36] HexPly 8552 Product Data Sheet 2016:1–6.

[37] Marlett K, Ng Y, Tomblin J. Hexcel 8552 AS4 Unidirectional Prepreg at 190 gsm & 35 % RC Qualification Material Property Data Report. Niar 2011.

[38] D7136 A. Standard Test Method for Measuring the Damage Resistance of a Fiber-Reinforced Polymer Matrix Composite to a Drop-Weight Impact Event. ASTM Int Des D 2005;i:1–16. https://doi.org/10.1520/D7136.

[39] Marlett K, Ng Y, Tomblin J. Hexcel 8552 IM7 Unidirectional Prepreg 190 gsm & 35%RC Qualification Material Property Data Report. NCAMP Test Rep Number CAM-RP-2009-015 Rev A 2011:1–238.

[40] Materials C. Standard Test Method for Measuring the Penetration Resistance of Composite Materials to Impact by a Blunt Projectile 1 2017:1–14. https://doi.org/10.1520/D8101.

APPENDIX A

PLY BOOK

	Material: P2362W-19			AFP Operator: Chase Murray			Date: 7/26/2019					
		General			Environment		Machine		Heater			
Ply Number	Tow #	Orientation	Start Time	End Time	Temperature (F)	Humidity (rel. %)	Compaction (lbs)	Feed Rate (%)	Pulse Duration (min/max) (ms)	Frequency (Hz)	Voltage (v)	Notes
Date Started: 5/24/2019												
1.1	13,17	45	2:00	2:17	73.5	67.7	100	-------	2	60	150	
1.2	13,17	90	2:18	2:24	73.8	70.7	100	30,50	2	60	150	
1.3	13,17	M45	2:47	2:52	74.1	65.2	100	20,50	2	60	150	
1.4	13,17	0	3:01	3:16	74.6	64.4	100	20,40	2	60	150	
2.1	14,18	45	3:16	3:19	74.8	64.6	100	20,40	2	60	150	
2.2	14,18	90	3:24	3:28	74.8	64.3	100	20,40	2	60	150	
2.3	14,18	M45	3:31	3:36	74.9	64	100	20,40	2	60	150	
2.4	14,18	0	3:38	3:42	75	64.2	100	20,60	2	60	150	
3.1	15,19	45	3:44	3:59	75.1	63.3	100	-------	2	60	150	
3.2	15,19	90	4:04	6:29	75.3	63.2	100	-------	2	60	150	
New Day: 5/25/2019												
3.3	15,19	M45	10:00	10:06	67	76	100	20,40	2	60	150	
3.4	15,19	0	10:10	10:16	67.6	76.1	100	20,70	2	60	150	
4.1	16,20	45	10:25	10:33	67.9	76.1	100	20,40	2	60	150	
4.2	16,20	90	10:35	10:40	68.3	75.8	100	20,40	2	60	150	
4.3	16,20	M45	10:44	10:50	68.7	75.8	100	20,40	2	60	150	
4.4	16,20	0	10:50	10:53	68.9	75.6	100	30,70	2	60	150	
5.1	16,20	0	11:17	11:21	69.6	76.7	100	30,70	2	60	150	
5.2	16,20	M45	11:26	11:31	70	75.8	100	20,40	2	60	150	
5.3	16,20	90	1:58	2:02	71.6	75.9	100	20,40	2	60	150	Tow Failure
5.4	16,20	45	2:03	2:08	72.3	75	100	40	2	60	150	
6.1	15,19	0	2:15	2:35	73.6	72.7	100	40,70	2	60	150	
6.2	15,19	M45	2:37	2:45	73.8	72.4	100	20,50	2	60	150	
6.3	15,19	90	2:57	3:03	74	70.7	100	30,40	2	60	150	
6.4	15,19	45	3:05	3:11	74.2	70.7	100	20,40	2	60	150	
7.1	14,18	0	3:17	3:24	74.5	70.1	100	50,75	2	60	150	
7.2	14,18	M45	3:26	3:31	74.7	69.5	100	40	2	60	150	
7.3	14,18	90	3:48	3:52	74.8	69.6	100	40	2	60	150	
7.4	14,18	45	3:55	3:59	74.9	69.5	100	30,40	2	60	150	
8.1	13,17	0	4:13	4:30	75.3	68.3	100	75	2	60	150	Tow Failure
8.2	13,17	M45	4:41	4:45	75.6	68	100	30,40	2	60	150	
8.3	13,17	90	5:00	5:04	68	68	100	40	2	60	150	
8.4	13,17	45	5:05	5:09	67.3	67.3	100	30,40	2	60	150	
Total Manufacturing Hours: 5 Hours 50 Minutes												
Average Time per Ply: 10.9 Minutes												
Dimension of Panel: 27" x 27"												

Figure A.1 A representation of a ply book used for manufacturing. PW layers are broken down into sub plies designated by #.1 to #.4 as these utilize 4 fiber angles.

APPENDIX B

FAILED SPECIMENS

Figure Failed Specimens 1 Fractured Tensile Specimen of 3D-DS1-CS6

Figure Failed Specimens 2 Fractured Tensile Specimen of 5S-DS0-CS7

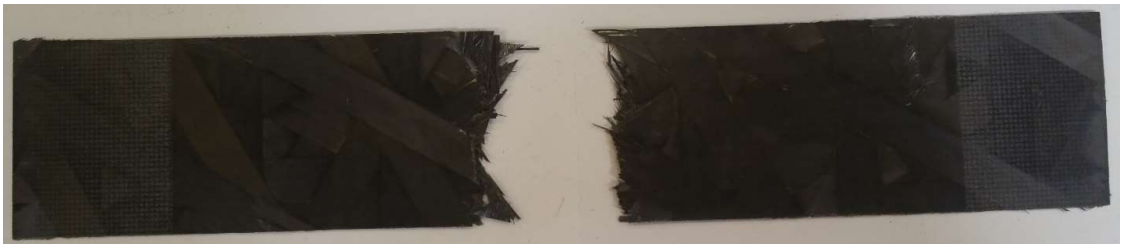

Figure Failed Specimens 3 Fractured Tensile Specimen of 6D-DS0-CS6

APPENDIX C

PW LAYUP

Figure C.1 Layup 1 45

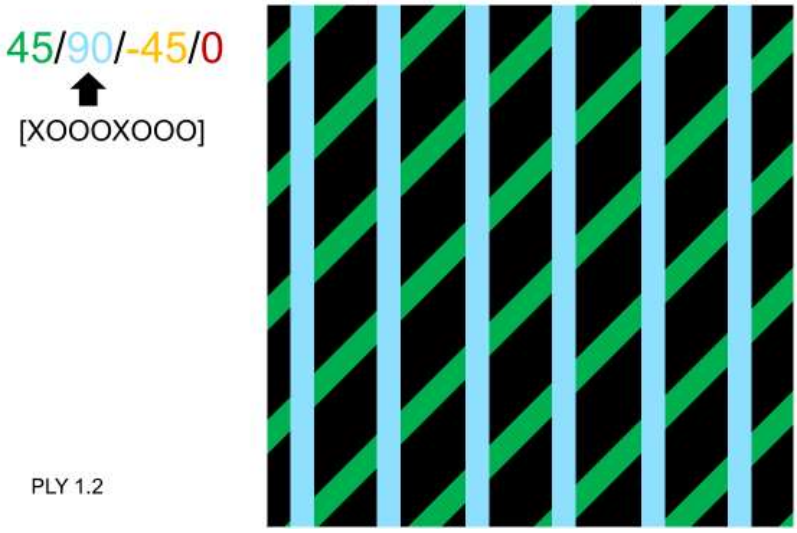

Figure C.2 Layup 2 90

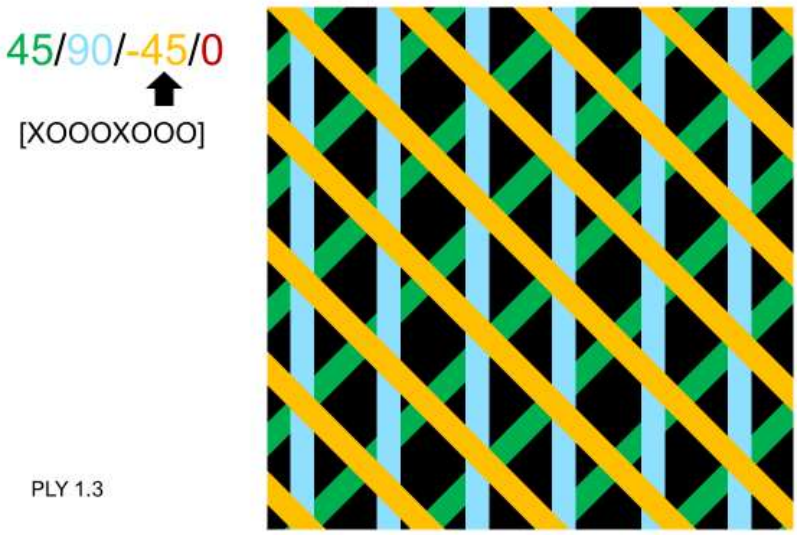

Figure C.3 Layup 3 M45

`

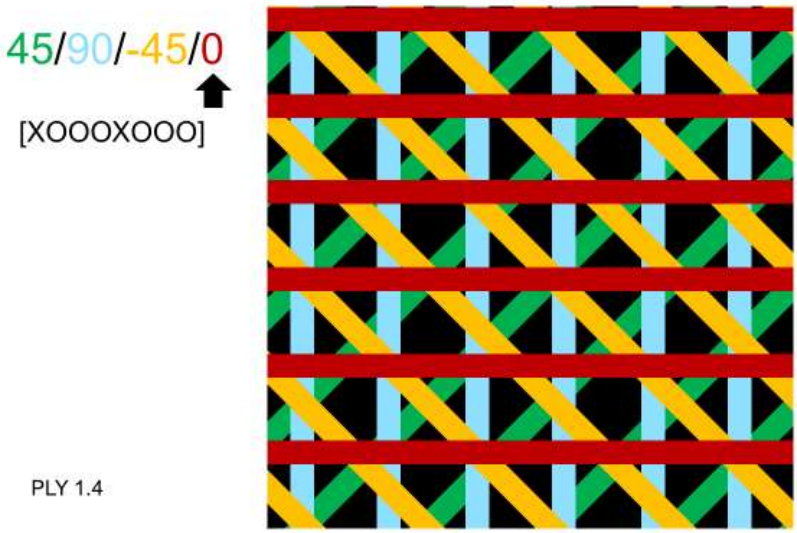

Figure C.4 Layup 4 0

`

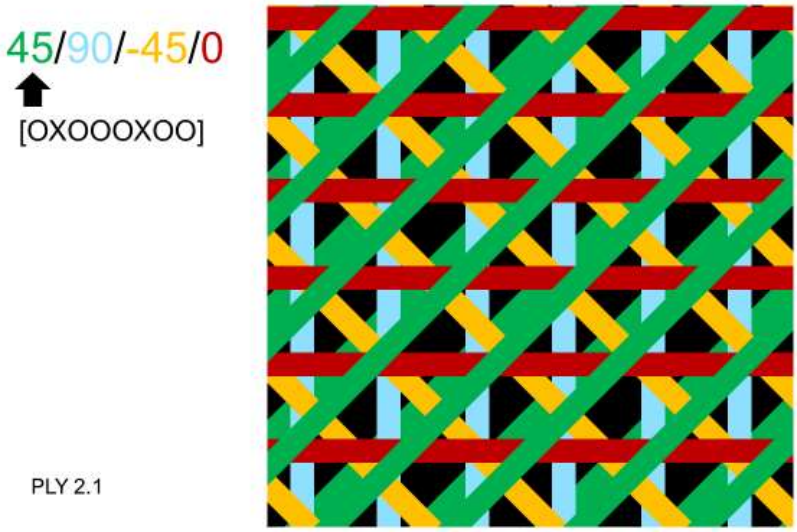

Figure C.5 Layup 5 45

`

Figure C.6 Layup 6 90

`

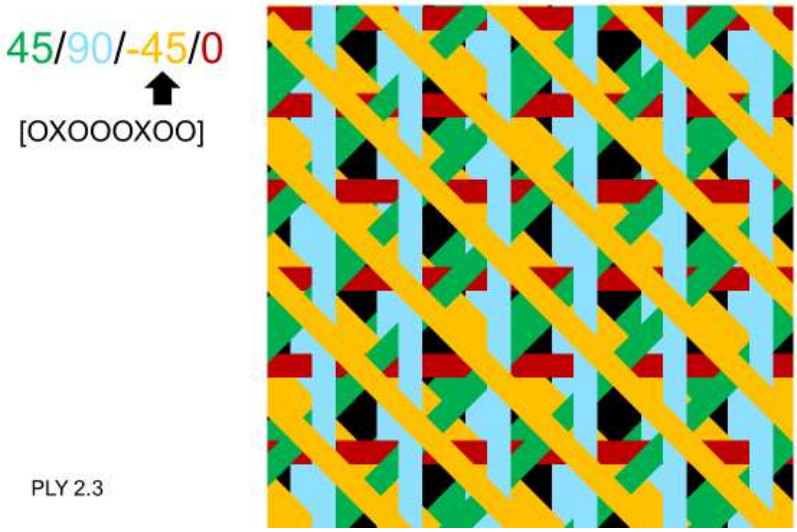

Figure C.7 Layup 7 -45

`

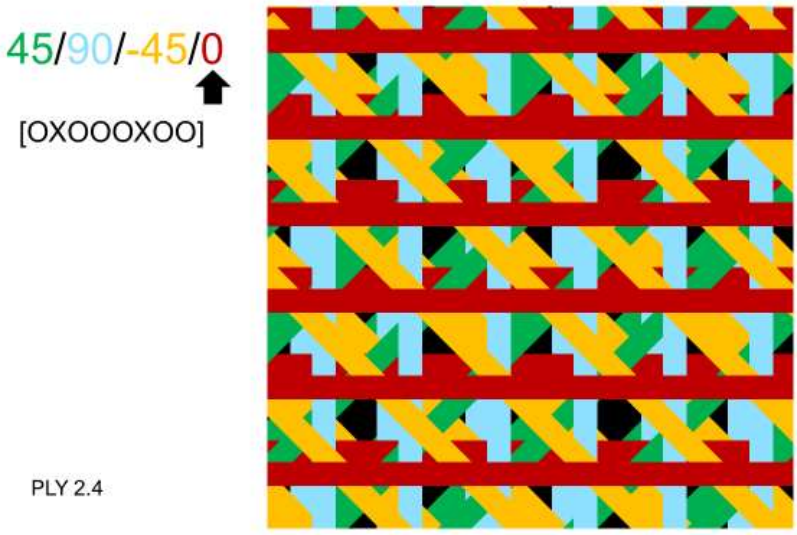

Figure C.8 Layup 8 0

`

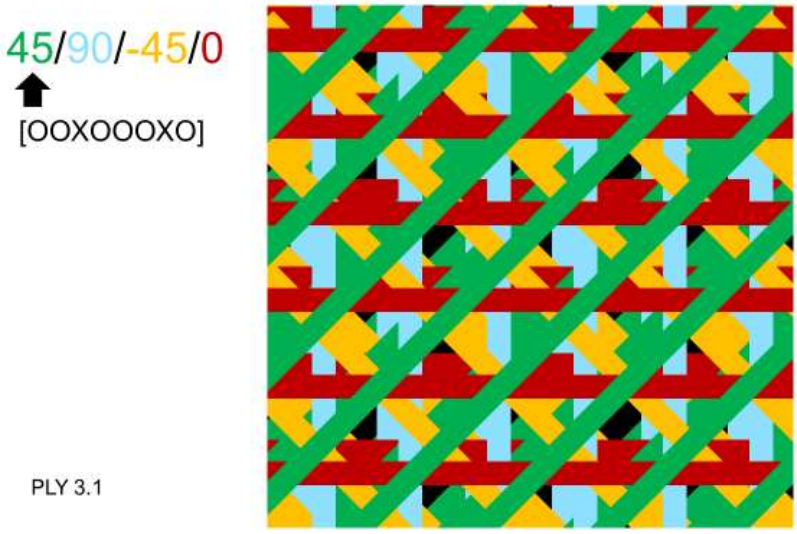

Figure C.9 Layup 9 45

`

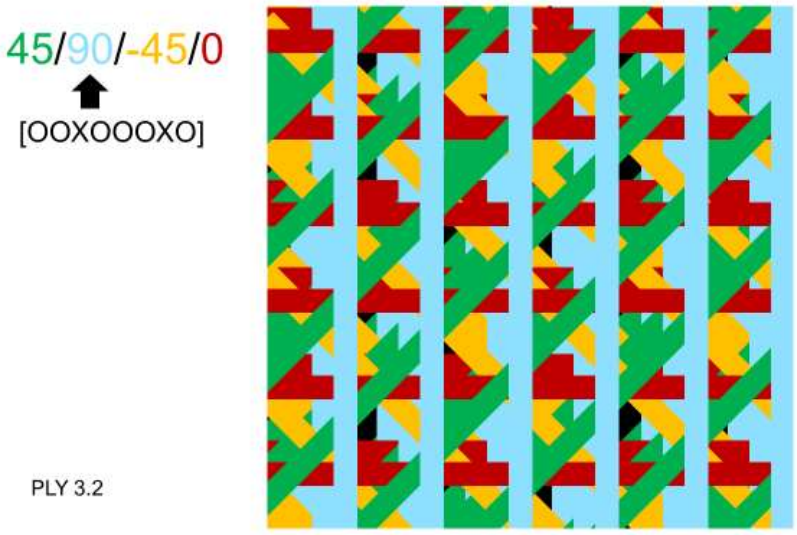

Figure C.10 Layup 10 90

`

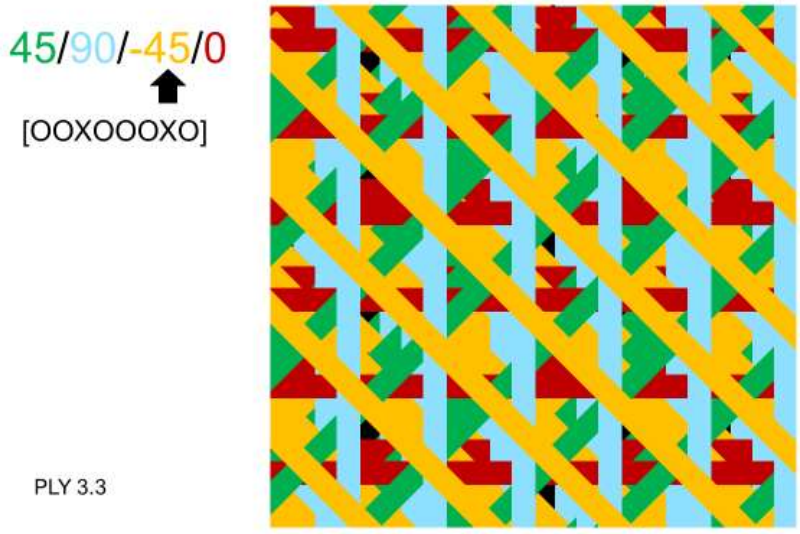

Figure C.11Layup 11 -45

`

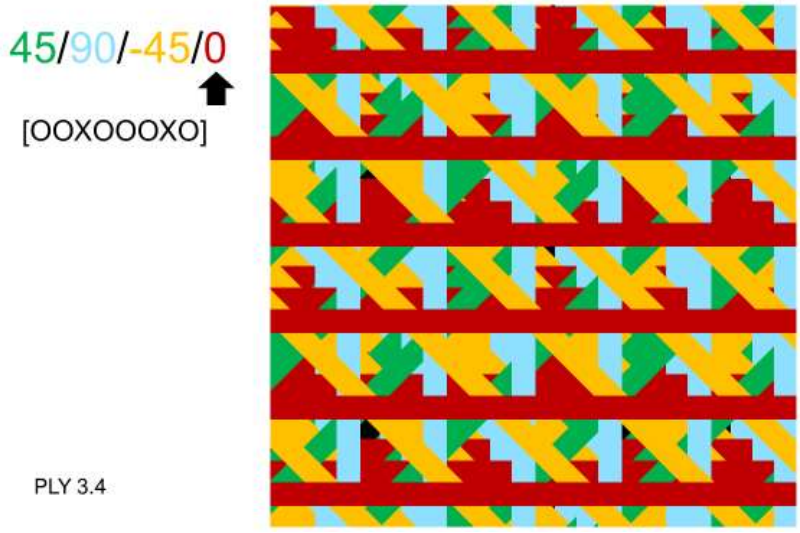

Figure C.12 Layup 12 0

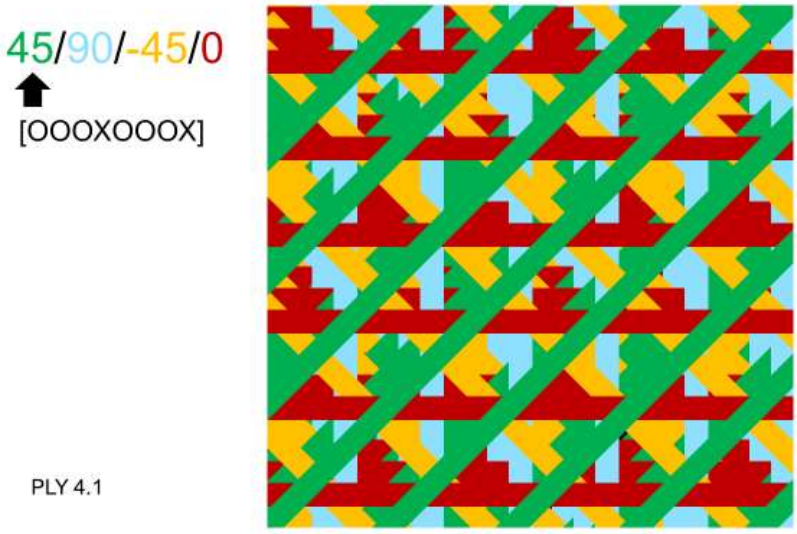

Figure C.13 Layup 13 45

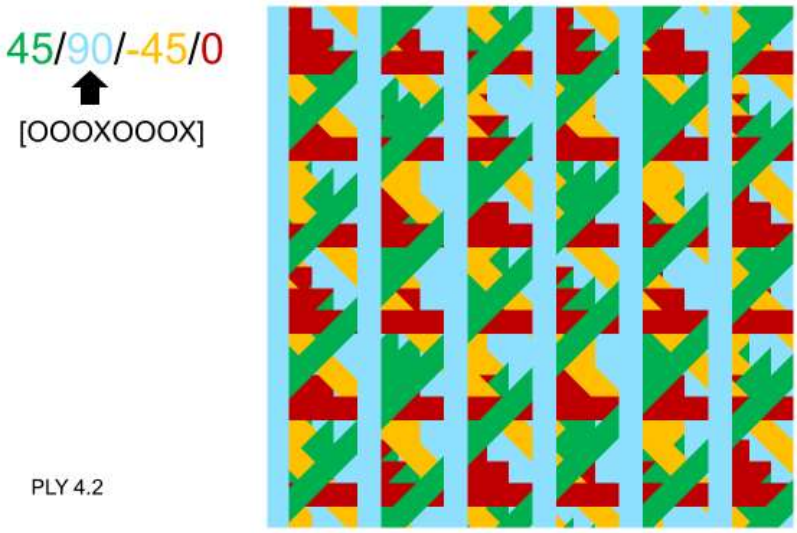

Figure C.14 Layup 14 90

`

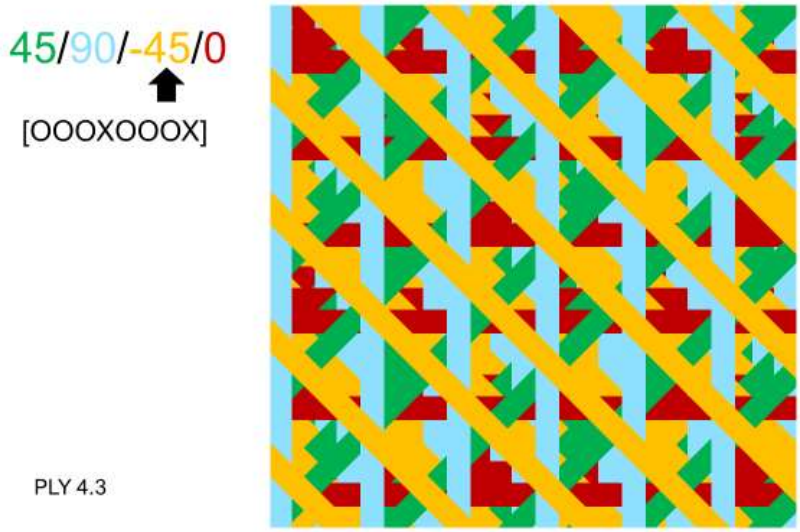

Figure C.15 Layup 15 -45

`

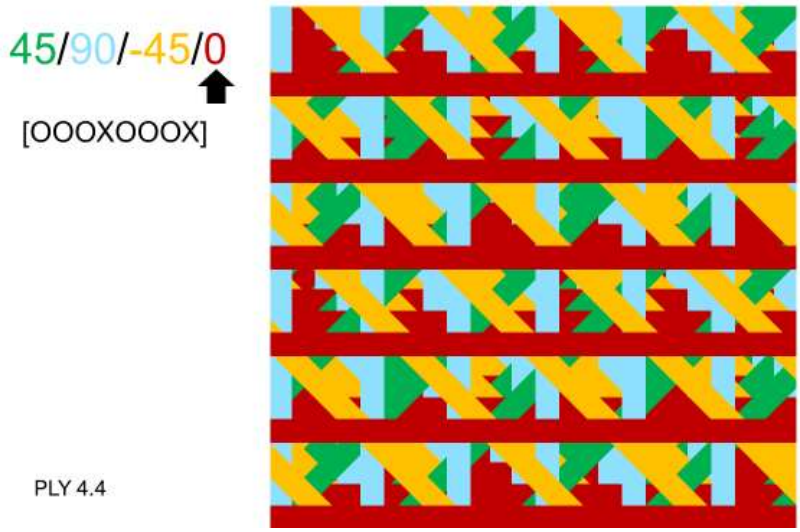

Figure C.16 Layup 16 0

`

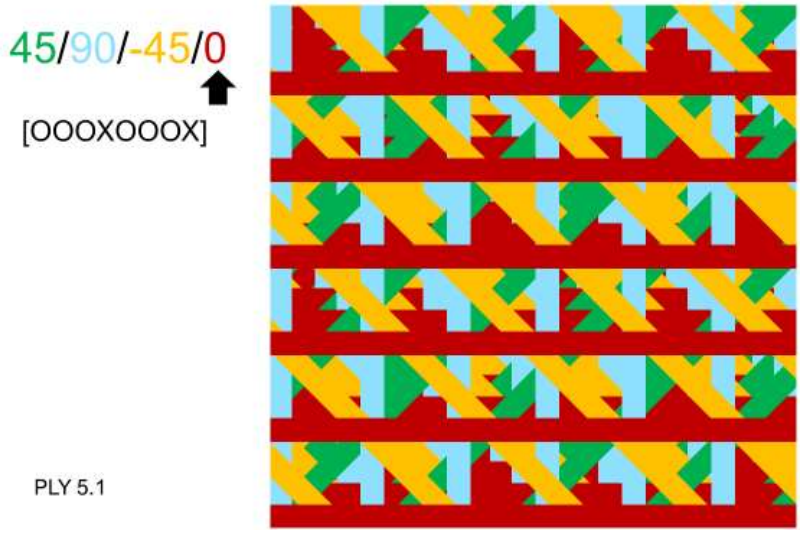

Figure C.17 Layup 17 0

`

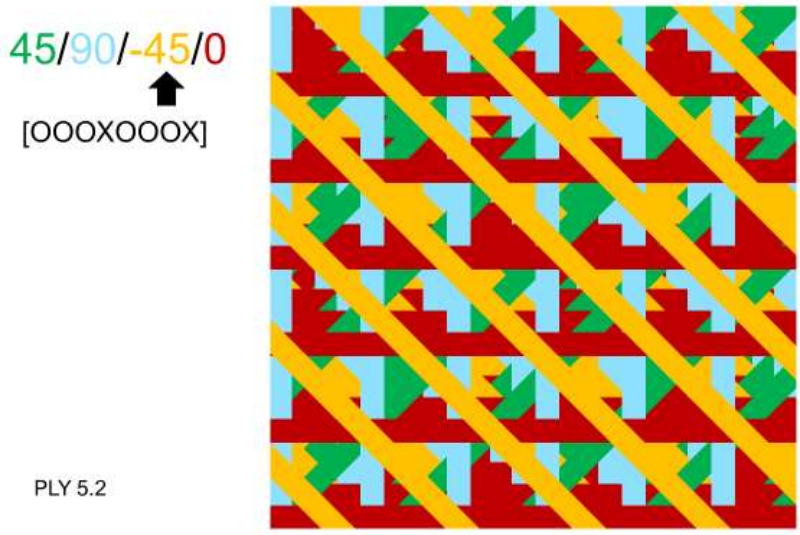

Figure C.18 Layup 18 -45

`

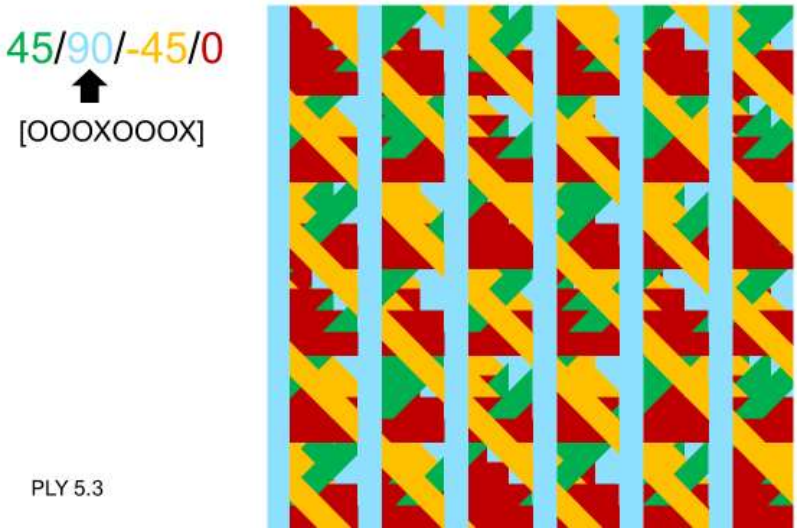

Figure C.19 Layup 19 90

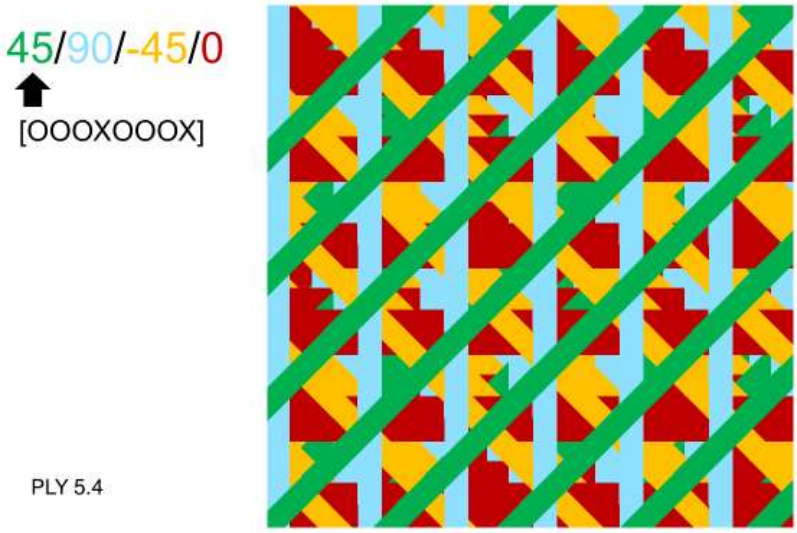

Figure C.20 Layup 20 45

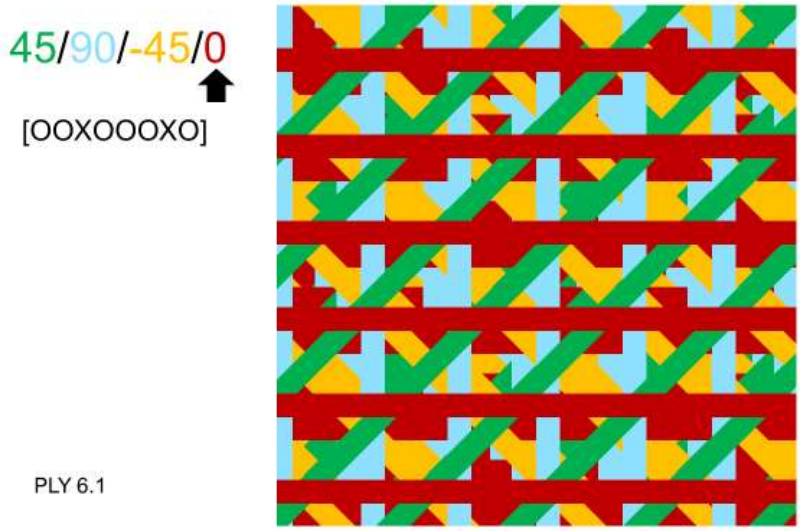

Figure C.21 Layup 21 0

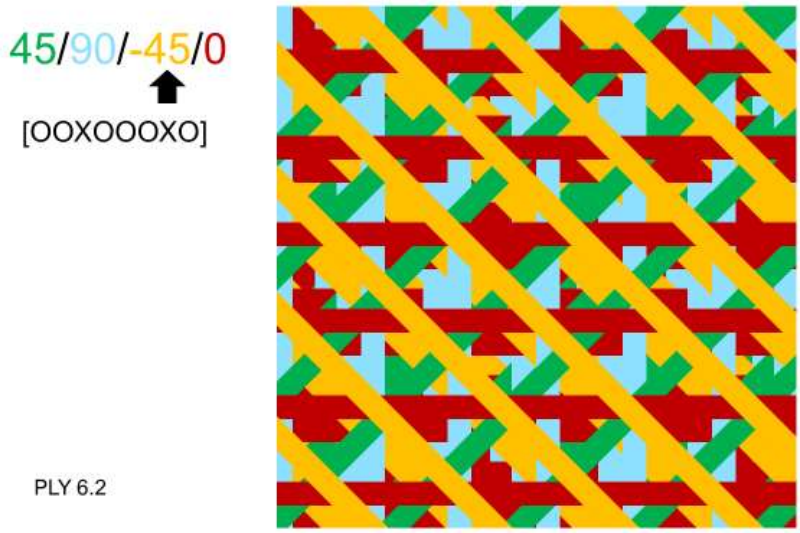

Figure C.22 Layup 22 -45

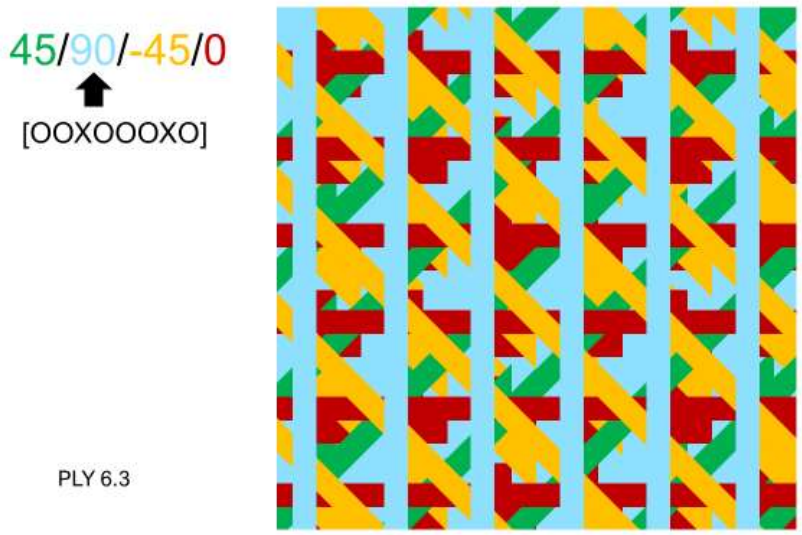

Figure C.23 Layup 23 90

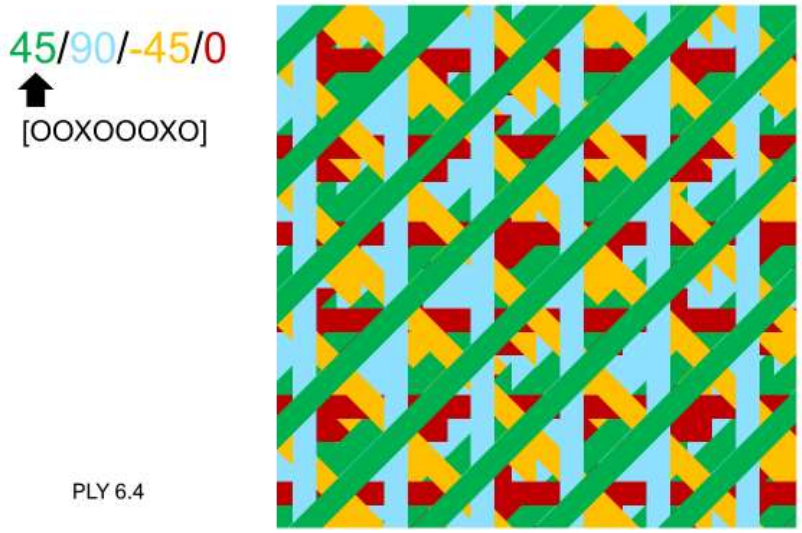

Figure C.24 Layup 24 45

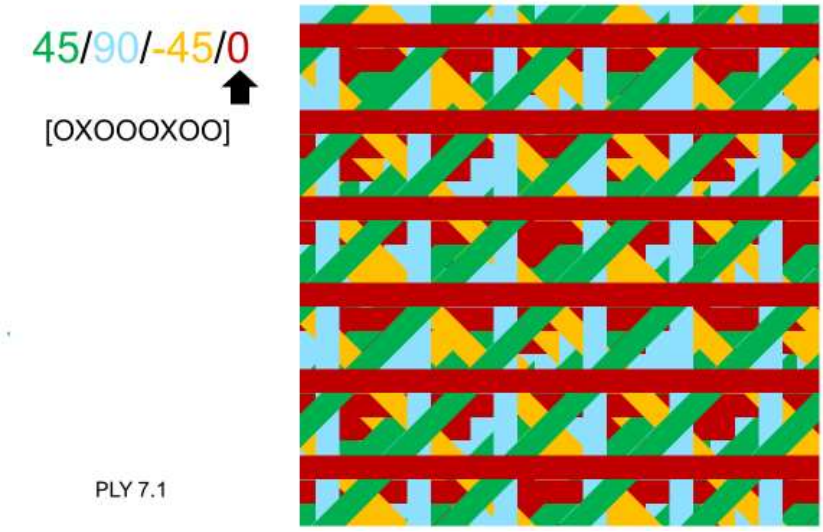

Figure C.25 Layup 25 0

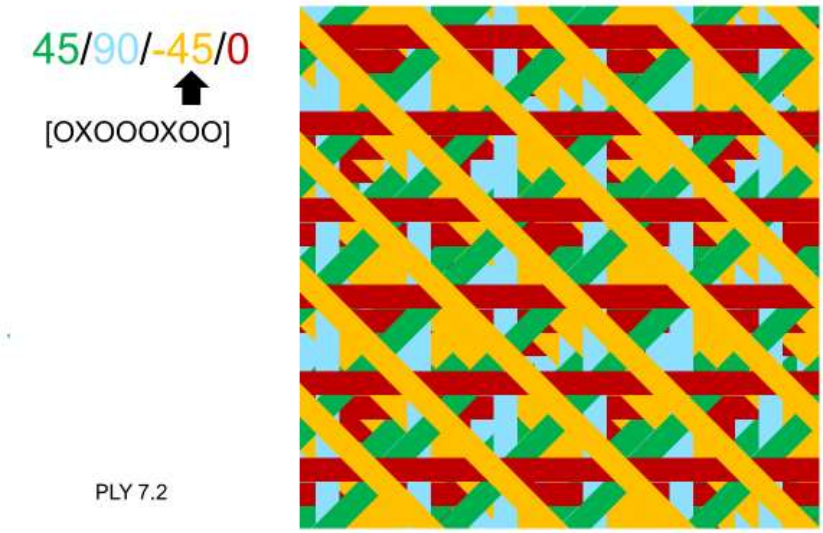

Figure C.26 Layup 26 -45

Figure C.27 Layup 27 90

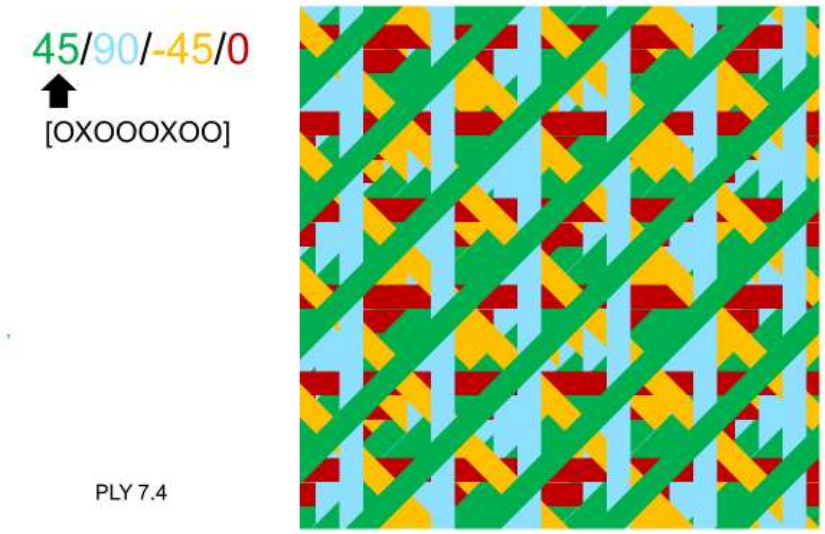

Figure C.28 Layup 28 45

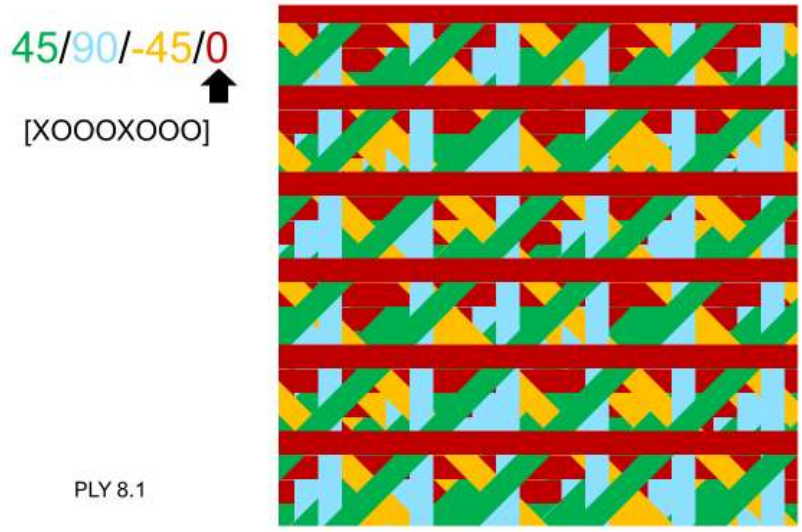

Figure C.29 Layup 29 0

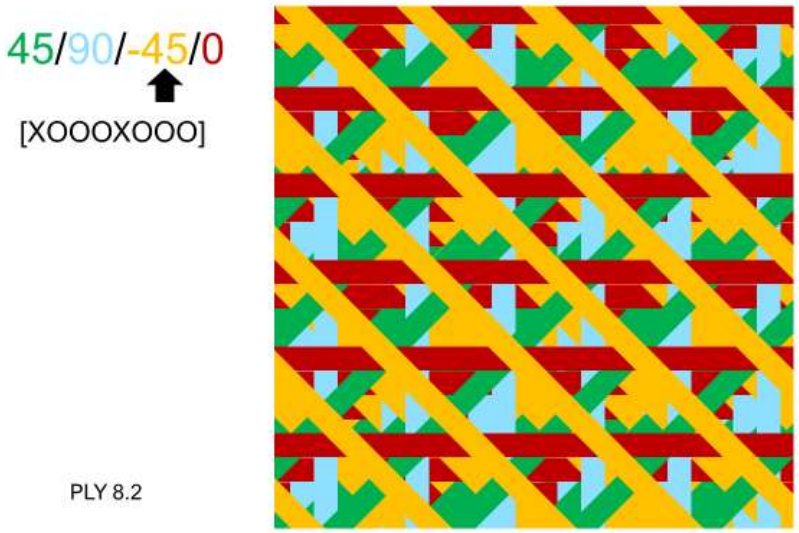

Figure C.30 Layup 30 -45

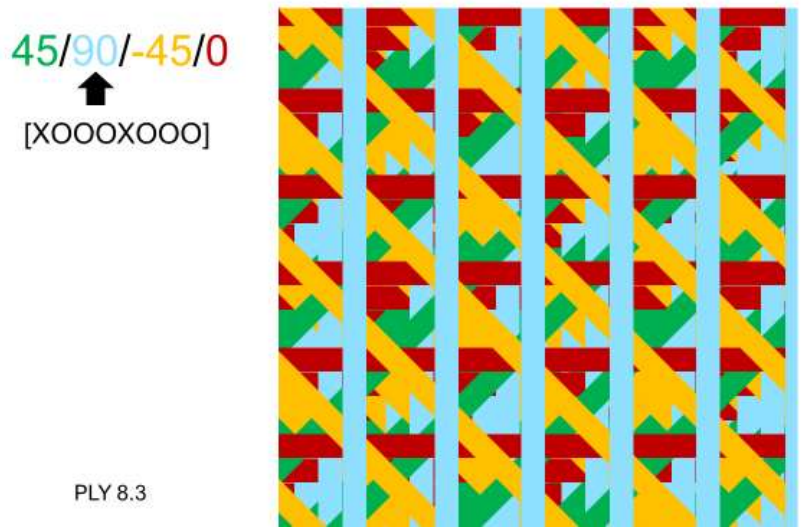

Figure C.31 Layup 31 90

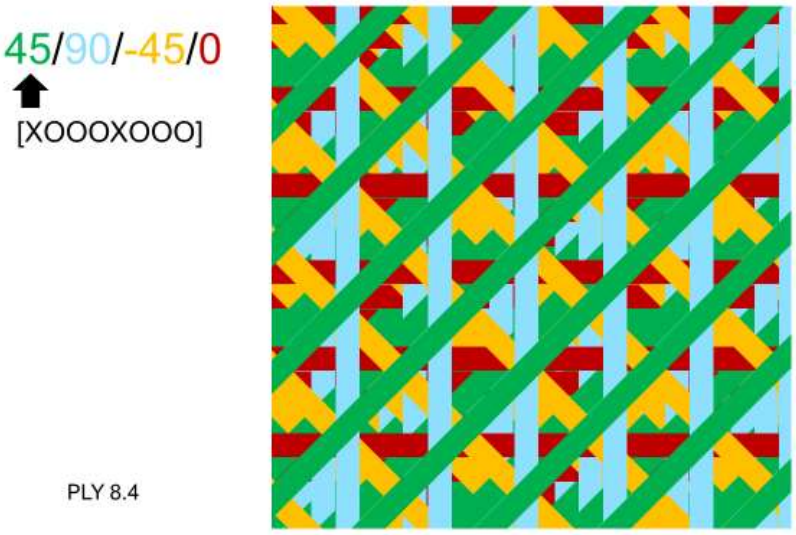

Figure C.32 Layup 32 45

APPENDIX D

MICROSCOPE IMAGES

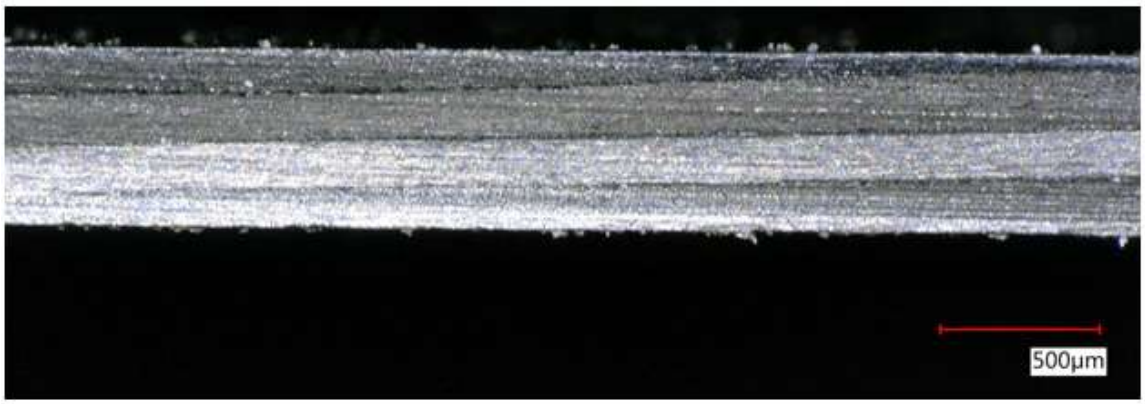

Figure D.1 A cross-sectional image of 3D-DS0-CS6

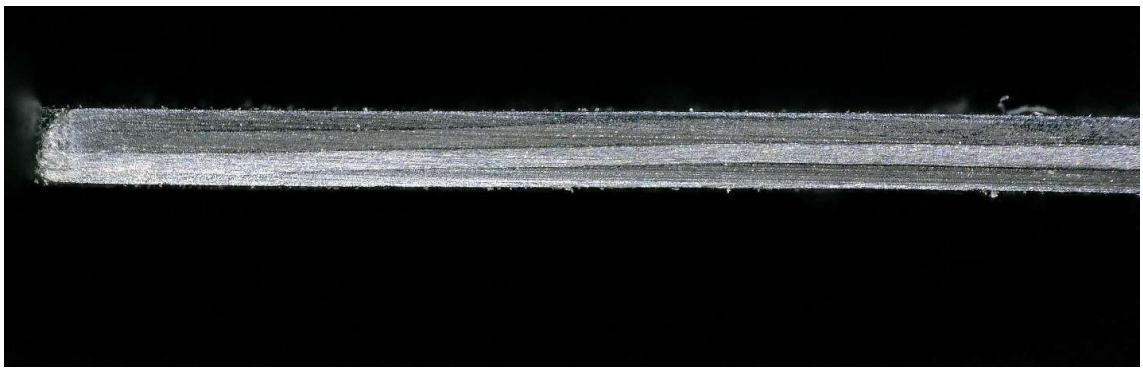

Figure D.2 A cross-sectional image of 3D-DS0-CS6

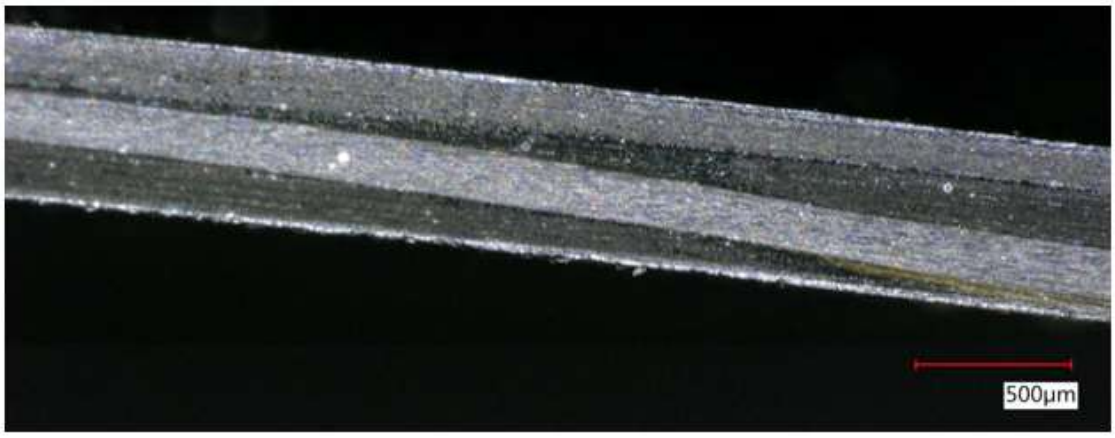

Figure D.3 A cross-sectional image of 3D-DS0-CS6

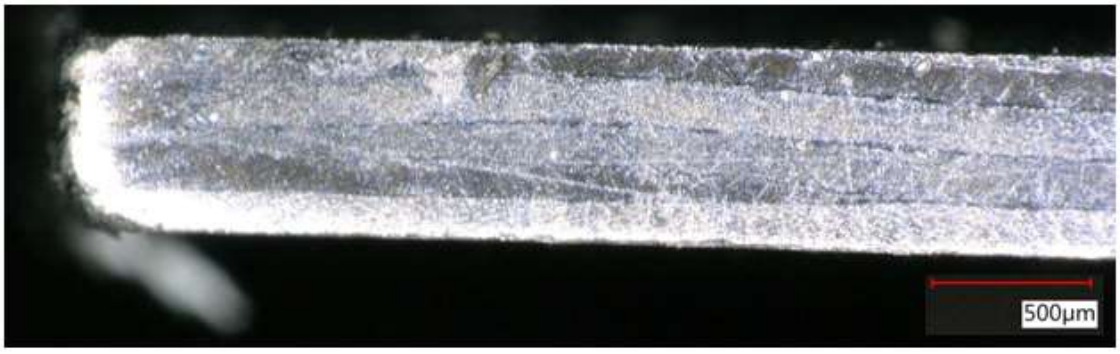

Figure D.4 A cross-sectional image of 4S-DS1-CS3

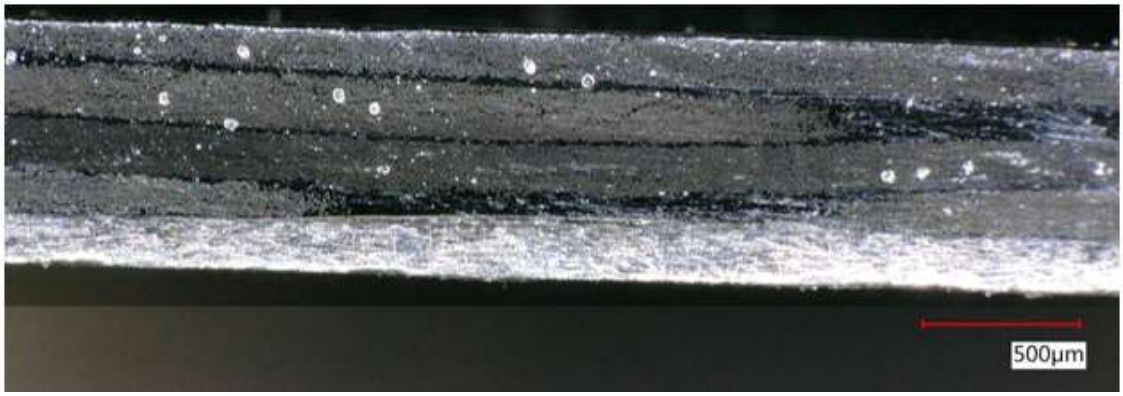

Figure D.5 A cross-sectional image of 4S-DS1-CS3

Figure D.6 A cross-sectional image of 6D-DS0-CS6

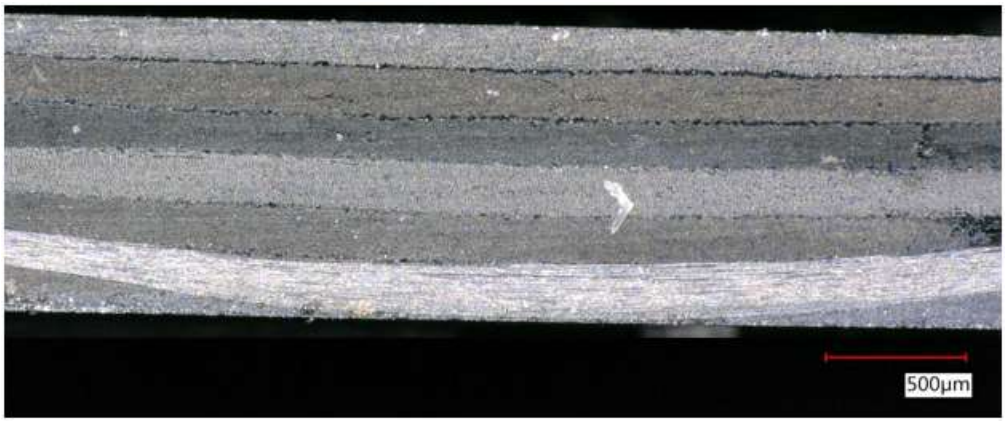

Figure D.7 A cross-sectional image of 6D-DS0-CS6

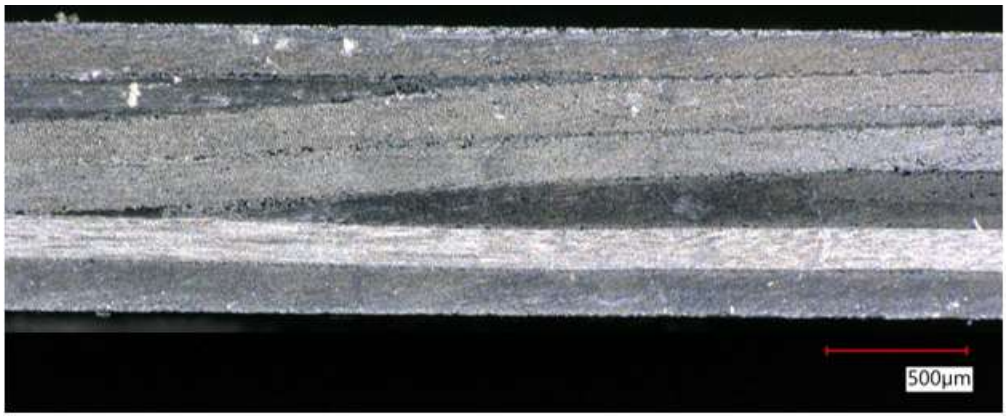

Figure D.8 A cross-sectional image of 6D-DS0-CS6

Figure D.9 A cross-sectional image of 6D-DS0-CS6